THE ROLE OF DIATOMS IN THE GLOBAL CARBON CYCLE

BY

SOPHIE FRANÇOISE CHOLLET

FOR THE DEGREE OF

DOCTOR OF PHILOSOPHY

THESIS PRESENTED TO THE

UNIVERSITY OF EAST ANGLIA,
SCHOOL OF ENVIRONMENTAL SCIENCES

31ST OCTOBER 2011

© This copy of the thesis has been supplied on condition that anyone who consults it is understood to recognise that its copyright rests with the author and that no quotation from the thesis, nor any information derived there from, may be published without the author's prior, written consent.

UNIVERSITY OF EAST ANGLIA, SCHOOL OF ENVIRONMENTAL SCIENCES

ABSTRACT

DOCTOR OF PHILOSOPHY

THE ROLE OF DIATOMS IN THE GLOBAL CARBON CYCLE

SOPHIE FRANÇOISE CHOLLET

2011

The Dynamic Green Ocean Model PlankTOM5.3 is a global ocean biogeochemical model representing interactions between planktonic organisms, ocean and atmosphere. The plankton is divided into five Plankton Functional Types (PFTs), each playing a specific role in carbon and nutrient cycling and in the trophic chain. The growth parameters for each PFT are now being derived in order to represent their dependence on environmental conditions, including climate change. Here we present our work on diatoms, a phytoplankton group of major importance.

We reviewed published data on the temperature dependence of diatom growth rate. By applying a quantile regression we calculate the upper-edge of the maximum growth rate. Exponential and optimal curves both have a higher intercept (0.99 and 0.96 d^{-1}) than Eppley's (1972) curve (0.59 d^{-1}). However, the rates at high temperature are over-estimated by the exponential function. Both average and maximal diatom community growth rate up to 37°C are better represented by an optimal function.

Photosynthesis experiments were carried out with an Oxygraph on four diatom species acclimated to different irradiances. PI curve parameters α^{Chl}, θ_m, P_m and R_d were calculated. Compared to the literature, θ_m values are low, resulting in high α^{Chl} values. Values for α^{Chl} and θ_m differs also between polar and temperate species. Optimisation of the model (Buitenhuis and Geider, 2010) give similar θ_m and lower α^{Chl} values than those we calculated.

Finally, we applied the optimal temperature-dependence function and our values of α^{Chl} and θ_m to the model PlankTOM5.3. The sensitivity of the ecosystem to each parameter is studied by changing one parameter at a time, in eight different simulations. Primary production varies from 47.28 to 50.44 Pg C yr^{-1}. Changes of PFTs abundance are highest for mixed-phytoplankton and coccolithophores. Meso-zooplankton, mixed-phytoplankton and diatom abundances are more sensitive to changes in temperature-dependence, while coccolithophores respond more to photosynthesis parameters.

TABLE OF CONTENTS

LIST OF TABLES

LIST OF FIGURES

ACKNOWLEDGEMENTS

I would like to acknowledge the very good supervision of Dr Erik Buitenhuis. I am very grateful to him for his support, his availability and his patience in teaching me how to run the model. I am as well very grateful to Corinne Le Quéré, a very much appreciated team-leader, for her constructive and pragmatic comments.

Thank you to Géraldine Sarthou and Jan Bissinger for providing data on diatom growth rate, as well as to Klaas Timmermans for giving me some polar diatom living cultures.

I would like to thank Gill Malin for her support in the laboratory work. Thank you to Jackie Heath from the School of Biology, for lending me the Oxygraphs. The laboratory work would not have been the same without the dedicated help of Rob Utting and Gareth Lee.

The support from the ENV PGR director was very much appreciated. A big thanks to Dr Sue Jickells and the officers of the Dean of Students for their support and help in writing. I would like to thank my friends and office-mates, I am thinking especially to Amandine Caruana, Marie-Fanny Raccault, Alba (Gonzales-Posada-Martinez-Franco) and Michal Bolchenek. Their support was very valuable, and their encouragement a precious help during the final year.

I would like to thank the examiners for their patience and for constructive and encouraging comments after my re-submission.

Finally, how not to mention those who made my time in Norwich a pleasant, enjoyable and rich experience, the start of a new path… So long, and thanks for all the fish.

CHAPTER 1

INTRODUCTION

Since early civilisations developed, humans have affected their environment, as any living being affects its ecosystem, in a short or long term. Starting in early 19th century, the industrial revolution led to major economical, demographical and societal changes. Among the many transformations the world has gone through over the last 200 years, one is to impact our lives as we had never imagined, in a scale current scientists are still trying to estimate. I mean of course the climate change we are experiencing.

Industrial, mechanical, economical and societal progresses of the last century that led to improvements of our standard of living would not have been possible without an affordable source of energy for transport, industry and homes: fossil fuels. First, coal became commercially used in the mid 18th century, followed by oil and later supplemented by natural gas. In the late 19th century, the shortage of whale oil brought the USA to extract petroleum (Energy Information Administration, 2012). Since then, the use of fossil fuel burning has been in constant increase (Prentice *et al.*, 2001).

The main effect of fossil fuel burning is the release of CO_2 and other green-house gases into the atmosphere. Measurements of atmospheric CO_2 concentration show a dramatic increase since the 19th century (Petit *et al.*, 1999). Although fossil fuel burning is the main con-tributor to the rise of atmospheric CO_2 concentration (Marland *et al.*, 2000), other changes like deforestation add to the effect. Consequences on the Earth are such that the period starting from the industrial revolution in late 18th century and going on until now has been suggested to be called the “anthropocene” (Crutzen and Stoermer, 2000).

Other gases such as methane, nitrous oxide and chlorofluorocarbons (CFCs) are released from human activities. Like carbon dioxide, they have the property to absorb energy at long-wavelength, i.e. energy radiated from the earth to the atmosphere. Because they contribute to the absorption of energy by the atmosphere, those gases are called green-house gases. Although methane, nitrous oxide and CFCs have a higher energy-absorption capacity per mol, the release of CO_2 has been so large that it accounts for 60% of the green-

house effect (Rasmawany *et al.*, 2001). It is carbon that most importantly matters in the present study.

1.1 Carbon Cycle

To understand the consequences of CO_2 release in the atmosphere, one should understand the repartitioning of carbon in the Earth system. We distinguish three reservoirs: atmospheric, terrestrial and oceanic (Fig. 1.1). The atmosphere is a thin layer in contact with both ocean and land and contains a minor part of the total carbon. Although the atmospheric storage is small, fluxes of carbon between it and the oceanic or terrestrial reservoirs are high. The green-house gases it contains play an important role in the radiative heating of the Earth. The two major reservoirs, terrestrial (including underground) and oceanic, host most of the carbon (6000 and 38000 Pg C, respectively). They contain six and 36 times the amount present in the atmosphere, respectively. Their carbon turn-over are slow (hundreds to thousands of years). As a consequence of this disproportion, small changes in the oceanic or land reservoir can lead to large changes in the atmospheric carbon, as in the case of fossils fuels burning. On the contrary, changes in atmospheric carbon concentration will impact the oceans slowly. Because the atmosphere is the smallest reservoir and is more homogenous than the other reservoirs, any changes in the carbon cycle will first be noticed by variations of the atmospheric CO_2 concentration.

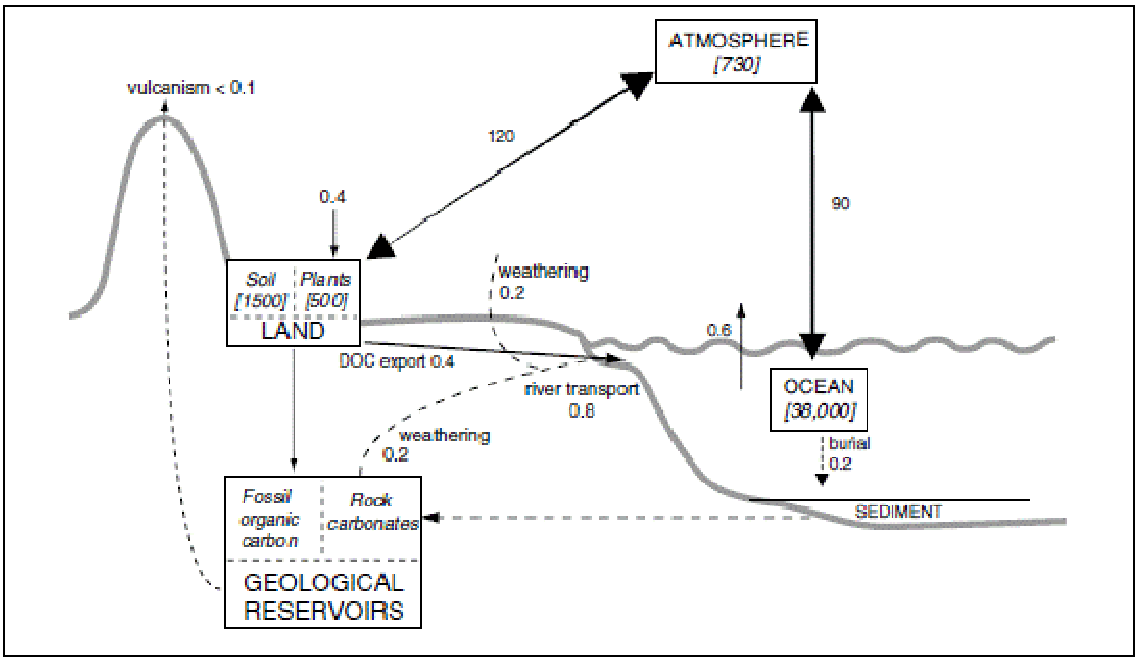

Fig. 1.1: Main components of the carbon cycle: reservoirs (Pg C) and fluxes (Pg C per year) as in the 1980s. From Prentice et al., 2001.

1.2 ATMOSPHERIC CO_2 ON THE GEOLOGICAL SCALE

Atmospheric CO_2 concentration has been subjected to large variations on geological scale. It was up to 6000 ppm 200 million years ago. The general trend between 60 and 40 million years ago is a decrease, leading to a concentration during the past 20 million years of 100-400 ppm (Pearson and Palmer, 2000).

Regular variations over the last 400 000 years are associated with glacial/interglacial cycles, during which CO_2 concentrations ranged from 180 ppm to a maximum of 280 ppm (Petit *et al.*, 1999) (Fig.1.2.D). This was also the atmospheric CO_2 concentration before the beginning of the industrial revolution in the 19th century (Indermuhle *et al.*, 1999, 2003; Etheridge *et al.*, 1996). Since then the atmospheric CO_2 concentration has been in constant increase. While this level of CO_2 concentration is comparable with previous glacial to interglacial changes, the time-scale is not. Whereas the glacial to interglacial transition took about 15000 years, the anthropogenic carbon was released over less than 200 years.

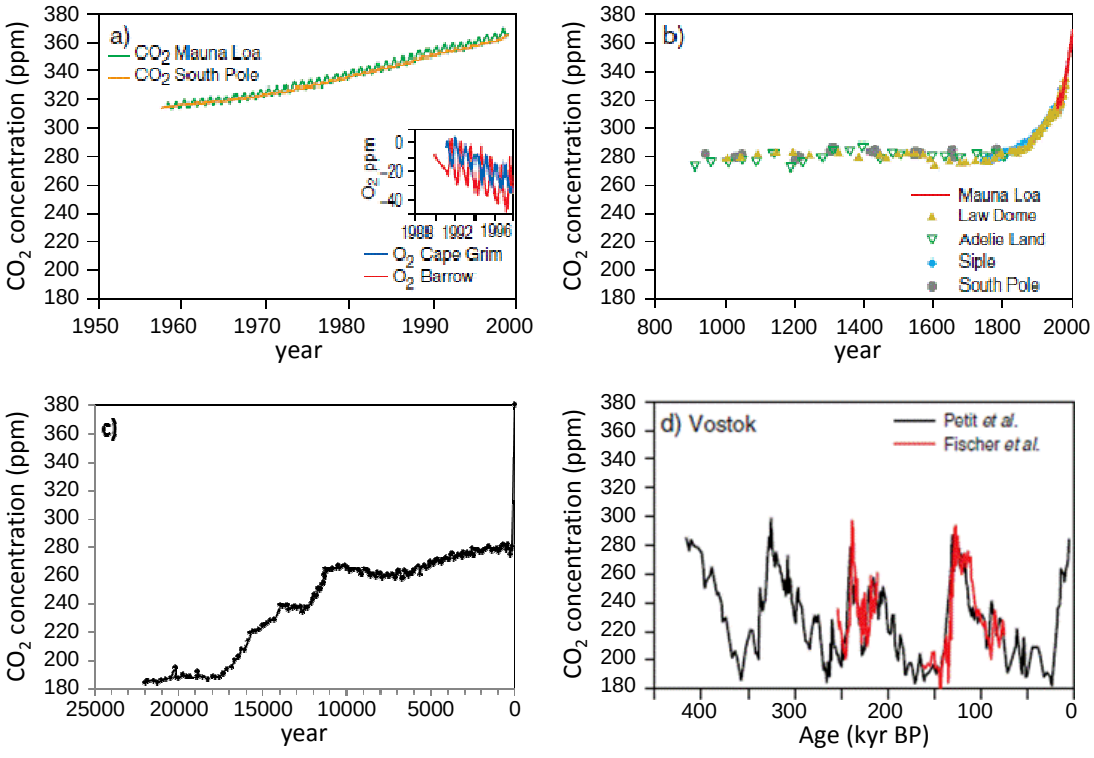

Fig. 1.2: Variation of the atmospheric CO_2 concentration on different time-scales. a) based on direct observations, b, c and d) CO_2 concentration in Antarctic ice-core. c: Monnin *et al.* (2001), a, b and d: Prentice *et al.* (2001).

In the 10 000 years of the current interglacial period and before the start of the industrial revolution in the mid 18th century, the atmospheric CO_2 was relatively stable (Fig. 1.2.C), and net fluxes between the atmosphere, land and ocean are estimated to have been small (about 20 ppm) (Smith *et al.*, 1999; Indermuhle *et al.*, 1999). The use of fossil fuel and the changes in land-use led to an increase of carbon flux from the land to the atmosphere. Because of its large surface area and a high absorption capacity, the ocean is affected by changes in atmospheric carbon. It is estimated that a third of human-released CO_2 has been taken up by the ocean. Only the part of CO_2 remaining in the atmosphere contributes to green-house warming. Therefore to be able to predict future atmospheric concentration and its effect on climate change and feedbacks with both land and ocean, we need to understand and quantify the oceanic absorption.

1.3 THE CARBON CYCLE DURING THE ANTHROPOCENE

The carbon released during the anthropocene (1800-1994) is estimated between 340 and 420 Pg C (Sabine *et al.*, 2004), coming from fossil fuel combustion, cement production and land-use change. Most of it remained in the atmosphere, leading to an increase of the atmospheric carbon concentration of about 30%, from 280 ppm in 1800 to 360 ppm in 1994.

Emissions have increased over the 20th century, from 3.92 Pg C per year in 1950 to 9.28 Pg C in 2009 (Le Quéré, 2010) (Fig. 1.3). During those sixty years, absorption by oceans decreased: during the sixties 39% remained in the atmosphere, while oceans absorbed 33% and the land 28%; in 2000-2009, 46% of the emissions remained in the atmosphere, while oceans absorbed only 27%.

Although oceans have had a major role of buffer by absorbing the atmospheric carbon, this capacity is limited. Furthermore, the absorption of carbon by the oceans is modifying seawater properties. Understanding the response of the ocean to the rise of atmospheric CO_2 concentration is necessary to estimate the amount of carbon the ocean will be able to absorb. This includes understanding the biochemistry behind CO_2 dissolution as well as the effect of CO_2 rise on organisms.

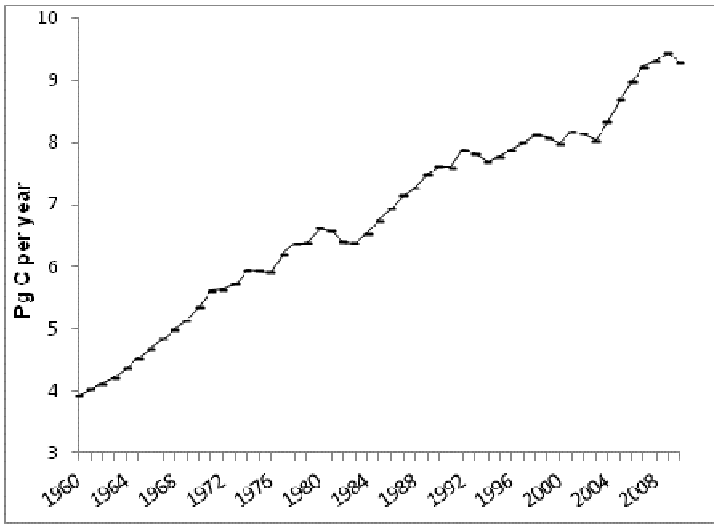

Fig. 1.3: Global carbon emission from fossil fuel combustion and cement production from 1960 to 2009 (Le Quéré *et al.*, 2010).

1.4 CO_2 ABSORPTION BY THE OCEANS

Ocean absorption of CO_2 is a physical, chemical and biological process.

The great capacity of the ocean to store carbon first comes from the chemical dissolution of CO_2 in seawater. Like every gas, CO_2 diffuses from high to low-concentration compartments. Dissolution increases in colder water. Most of the CO_2 reacts with seawater to form bicarbonate and carbonate ions while about 1% remains in dissolved CO_2. The sum of bicarbonate, carbonate and CO_2 is called dissolved inorganic carbon (DIC). The concentration of DIC is about 40 times larger than of organic carbon.

The atmospheric CO_2 absorbed by the ocean does not remain in the surface: the DIC concentration increases with depth. This is the result of physical processes which contribute to the vertical repartitioning of the DIC by transporting cold and carbon-rich waters to the deep ocean. Moreover, carbon is more soluble in the cold water of the deep ocean layer. Biological processes are also responsible for a large part of the transport of DIC in the ocean deep-layer.

1.4.1 Biological pump

Phytoplankton are the main actor of the biological pump, responsible for the direct export of carbon from the surface to the deep-ocean. Those photosynthetic organisms use dissolved inorganic carbon as a source of CO_2 for photosynthesis. The global oceanic

primary production of organic carbon has been estimated at 36 to 47 Pg C yr^{-1} (Behrenfeld & Falkowski, 1997; Behrenfeld *et al.*, 2005; Antoine *et al.*, 1996). Most of this organic matter is consumed by zooplankton or remineralised by bacteria in the surface layer. The organic matter that is not recycled within the surface layer sinks to deeper layers, contributing to the increase of DIC in the water column. Around 10 Pg C yr^{-1} escapes the grazers and reaches the deep-layer (Schlitzer, 2004), where they are also consumed by deep organisms or respired by bacteria into inorganic carbon and nutrients. Only about 1% is transferred to the sediments.

Many observations, in the field or *in vitro*, show organisms can react differently to changes in surrounding conditions. While the oceanic environment is thought to have been stable in the last 2000 years, we are now witnessing effects of anthropogenic carbon emissions on the ocean chemistry. The behaviour of phytoplankton cells in future marine ecosystems will influence the absorption of the excess atmospheric carbon by the ocean. This is why understanding the key features of the different types of phytoplankton and the main drivers of their growth is essential to predict tomorrow's climate.

1.4.2 Phytoplankton

Life exists around the entire ocean. Single cells, following the current, are spread over all fresh and seawater. They are called "plankton", from the greek "*planktos*" meaning "wanderer" or "drifter". Phytoplankton, including cyanobacteria and algae, are unicellular organisms with a volume from less than $1\,\mu m^3$ to a few mm^3. They are the photoautotrophic part of the plankton and perform 98% of the primary production of organic carbon in the oceans (Falkowski and Raven, 1997). Like plants in terrestrial ecosystems, phytoplankton are the base of the food chain in oceans: organisms in higher trophic levels are directly dependent on their abundance.

Light, temperature and nutrient concentration are the major factors influencing primary production. The light constrains phytoplankton growth to the upper layer, called the euphotic zone. The more productive waters are also rich in nutrients. They are situated near the continental shelves, where tidal mixing, direct contact with remineralised nutrients from the sediments and river input provides them with nutrients, or in upwelling regions, where nutrient-rich deep water is transported to the surface.

Some general features of the phytoplankton distribution across the ocean are well known. For example, open ocean areas, poor in nutrients, are dominated by small

organisms. They grow relatively fast and recycle efficiently the nutrients within the surface layer. By contrast, coastal ecosystems rich in nutrients are dominated by bigger organisms that also export organic matter in the deep layers by forming aggregates.

Phytoplankton cells interact with their environment, taking from it the elements required for growth and, in exchange, releasing organic or inorganic matter. Their growth depends on and affects the chemical, physical and biological characteristics of the medium and of the entire water-column. The interaction of phytoplankton communities with their environment has shaped the geochemical features of the oceans. Physical water circulation tends to distribute homogeneously over the ocean nutrients like nitrate, phosphate and silicate. It enhances the absorption of atmospheric CO_2 by surface seawater and transports carbon-rich cold water to the deep ocean. The presence of phytoplankton has a major influence on nutrient distribution and on carbon dissolution, working against the physical homogenisation. As phytoplankton grows, mainly in the surface mixed layer, nutrients tend to be depleted. A part of the nutrients contained in cells are recycled within the surface layer. Another part forms aggregates that are exported to deeper layers, increasing the nutrient concentration in the deep ocean. Bacteria and zooplankton are responsible for the remineralisation of the organic matter. Therefore, phytoplankton has a major influence on global elemental cycles.

The many different ecosystems found in the ocean have permitted the co-existence of much diversity, in which each group of plankton has developed a strategy to compete with others. Thanks to their different adaptations, plankton species have conquered the entire surface ocean. Phytoplankton community is diverse and can be classified, for instance, by phylogeny, size or by metabolic pathway, as we detail below.

Because of their different metabolism and chemical composition, the numerous types of plankton affect differently the nutrient and DIC concentrations. In this study we are particularly interested in the carbon export from the surface to the deep ocean, at present time and in the future. This factor will be determining in the regulation of oceanic, and indirectly atmospheric, CO_2 concentrations.

The carbon export varies among phytoplankton species, depending on grazing and bacterial degradation rates and on sinking speed. Mineral components such as calcite ($CaCO_3$) and opal (SiO_2) are particularly important in the determination of carbon export

(Klaas and Archer, 2002). According to Armstrong *et al.* (2002), the flux of organic carbon depends on the mineral ballast of the cell, calculated as the concentrations in silica, calcite and dust. These authors conclude carbonate is the more efficient transporter of particulate organic carbon to 2000m.

Some organisms affect the sinking rate through particle aggregation (Alldredge and Gotschalk, 1989). Diatom cells are known for forming post-bloom large aggregates of high density. They tend to aggregate faster than coccolithophores (Iversen and Ploug, 2010), though aggregates from coccolithophores are more compact and denser, so they have higher sinking velocity. As a consequence, diatoms tend to be respired by bacteria deeper than smaller phytoplankton cells.

Another factor influencing carbon export is the formation and sinking of fecal pellets by zooplankton. Diatoms play again a role here, often associated with meso-zooplankton, like copepods, which leads to formation of pellets rich in silica. Therefore diatoms tend to dominate the export of carbon from the surface layer to the sediment (Buesseler, 1998).

Among the large diversity of planktonic organisms, calcifiers (coccolithophores) and silicifiers (diatoms) play an important role in exporting carbon from the surface layer to the sediment. In the following section we focus on diatoms, their characteristics and role in marine ecosystem.

1.4.3 Diatoms

Diatoms are found all around the world, from sea-ice to warm waters, in fresh and seawater, in benthos or in the water column. The number of living marine diatom species has been estimated between 1400 and 1800 species (Sournia *et al.*, 1991). Diatoms are unicellular, chain-forming yellow-brown algae with numerous discoid plastids, containing chlorophyll a, c1, c2 and the accessory pigment fucoxanthin. They are characterised by their siliceous frustules (or exoskeleton). There are 2 large orders: centric diatoms (valves usually cylindrical, making a frustule resembling a traditional pill box) and pennate diatoms (valves elongate but the girdles are short, having the appearance of the halves of a date box).

Diatoms are one of the major phyla of algae, not only by their abundance but by their importance in biogeochemical cycles. They account for about 40% of the total primary

production in the ocean (Nelson *et al.*, 1995). Diatoms are a key component of global marine ecosystem models, playing an important role in primary production (Uitz *et al.*, 2010) and in carbon export to the deeper layers of the ocean (Egge and Jaconsen, 1997). They are known to be highly competitive in nutrient-rich waters, where they form blooms. They are dominant in nutrient-rich surface waters at high latitudes and the tropics, as well as in coastal or upwelling waters (Nelson *et al.*, 1995). They are also found in high-nutrient low-chlorophyll (HNLC) regions, where iron concentration limits phytoplankton growth. Because of their requirement for silicic acid to build their frustules, they have a strong impact on the global silicate cycle (Tréguer *et al.*, 1995). They require more iron and phosphorus than most of the small phytoplankton (Sarthou *et al.*, 2005). However, their ability to store nutrients in vacuoles enables them to grow well in turbulent water with irregular daylight and nutrient supply, unlike coccolithophores, dinoflagellates and diazotrophs. Diatoms respond quickly to iron fertilisation experiments (Boyle *et al.*, 2000).

1.5 BIOGEOCHEMICAL MODELLING

The need to understand marine ecosystems and to predict and quantify the impact of climate change has led to the development of marine ecosystem models. Modeling tight links between living organisms and their immediate environment impose a coupling of the physical, chemical and biological dynamics of the ocean.

Physical oceanographic models are well developed and include for instance coastlines and bottom topography, fluid dynamic, diffusion, viscosity and mixed-layer depth. Their mathematical representation follows known first principles. Atmospheric conditions such as pressure, temperature, light and wind are often represented by an atmospheric model, independently parameterised and coupled to the oceanic model. To this already complex figure is added a biological model compiling biological variables. Numerous biological models exist, more or less complex, depending on which questions they aim to answer.

Modellers face several issues:

- How to represent the complexity of the marine ecosystem? What criteria should be considered to represent the phytoplankton?

Modellers are constantly confronted by a trade-off between computational cost and modelling complexity, good representation of known processes and fit to observational

data. However, none of the models aim to represent the whole ecosystem complexity, for (1) it is beyond our knowledge and (2) it has been assumed there is an optimum level of complexity beyond which higher complexity would bring more deviation or uncertainty than it would improve the model accuracy (Anderson and Totterdell, 2004).

- How to parameterise the model?

Unlike physical phenomena, that follow known first principles, biological growth depends on many variables that are not always described by mathematical functions. Even a simple model such as cellular growth as a function of the temperature cannot be described with metabolic parameters. Cellular growth depends on the activity of several enzymes, on the cell respiration and on the photosynthesis performance. Modeling each of those processes would be far too complex. Instead we simply find the mathematical function fitting the best to the observations of growth as a function of temperature (see Chapter 2). The same principle can be applied to higher level of complexity, for instance the growth of the whole marine phytoplankton as a function of the nutrient concentration (as in a nutrient-phytoplankton model). Instead of modelling all the processes involved, such as considering all the cellular processes involved as well as the different species and their specific needs, a solution is to represent the growth as a function of the nutrient uptake, the maximal growth rate and a term for loss, summing respiration, mortality and grazing. Although those parameters can eventually be estimated from field measurements, they can also be tuned for the model output to show agreement with observational data.

However, tuning is not the optimal solution. A “tuned” model performing well in certain conditions of the ecosystem may not give realistic output in a changing environment. In other words, the ideal model would show accuracy under a range of environmental conditions.

To summarise, the challenge is to find the simplest function and parameters that would represent well the observations in different conditions. Previous efforts were made to come up with parameters defining plankton physiology in a context that can be used in global biogeochemical model. Literature reviews of experimental studies on plankton physiology (for diatoms: Sarthou *et al.*, 2005) provide an estimation of physiological parameters that can be applied in a model. Geider’s work on photosynthesis and photo-acclimation (Geider, 1997) is an example of plankton parameterisation as a function of physical parameters (irradiance, day-length, temperature and nutrient availability) and using measurable

physiological variables. Chapters 2 and 3 of the thesis examined the temperature and light-dependence, respectively, of diatom growth rate.

- The last task, but not the least important, is the validation of the model.

Model outcomes are compared to observational data. Regarding plankton, those are often Chlorophyll concentration, biomass or density obtained from the field, or observation of sea surface colour by satellite (converted to Chlorophyll concentration). Validation remains a key issue as modellers often lack field data for comparison. In some cases, the same data are used for parameterisation and validation. Moreover, in order to use a model as a tool to predict future changes in the ocean, the model should not only return results close to current observations, but also model any changes in ecosystem caused by variations of the environment.

1.5.1 NPZ models

A simplification of the lower food web is an NPZ model, for nutrient- phytoplankton-zooplankton. The three components of this type of model are considered as boxes through which is transferred a flux of matter, e.g. nitrogen or carbon. For example, nitrogen input to phytoplankton is a function of the nitrogen concentration, the light intensity and the maximum growth rate. The output will depend on respiration, grazing and mortality. NPZ models can be used to assess our knowledge of nutrient cycling or to simulate chlorophyll, primary production or the timing of phytoplankton blooms (Olascoaga *et al.*, 2005). It does not take into account the diversity of plankton but may provide a relatively good representation of general nutrient dynamics, Chlorophyll concentration (Fasham, 1995) or dimethyl sulphate (DMS) distribution (Aumont *et al.*, 2002).

Representation of the various marine ecosystem specificities requires more complex models, including for instance the possibilities of iron limitation, grazing preference of zooplankton or a specific requirement, e.g. silicate for diatoms. More complex models either use multiple boxes, like the dynamic green ocean models (Le Quere *et al.* 2005), or represent ecological shifts within each trophic level, like the multiple size class model by Armstrong (1994), differentiating the role of phyto- and zooplankton depending on their size.

Fundamental biologically mediated processes of the ocean have been identified, such as denitrification and nitrogen fixation, dissolved CO_2 fixation by autotrophs, calcification and silicification. Those processes are essential to certain organisms and require specific metabolic pathways that are not present in all organisms (Falkowski and Raven, 1997).

Moreover, we know from observation of nutrient concentrations in the global ocean that phytoplankton is one of the drivers of the global nutrient distribution. Furthermore, biochemical processes are linked together. For instance diatoms influence dissolved silicate distribution and also, as autotrophs, play a role in dissolved carbon concentration and carbon export. Therefore, the study and modelling of one biogeochemical cycle cannot be done without taking the links to other biogeochemical cycles into account.

1.5.2 Biogeochemical models

As we explained above, grouping organisms into black boxes for zooplankton or phytoplankton does not allow representation of specific biochemical functions. Global biogeochemical models have been built in order to characterise the functioning of the carbon cycle (Najjar 1992) and other nutrient cycles (Aumont and Bopp, 2006). Recent models are based on the differentiation of biogeochemical characteristics of the phyto- and zooplankton, grouped into Plankton Functional types (PFTs). PFTs are composed of organisms with a common metabolic pathway or ecological role. Those models allow changes in biogeochemical cycles caused by a change in ecosystem variables. The first were developed to represent the seasonal succession of plankton species at the regional scale (Van den Berg, 1996; Allen *et al.*, 2004; Lancelot *et al.*, 2000). Only dominant species were represented, like diatoms and *Phaeocystis* in the North Sea (Lancelot *et al.*, 2000) or diatoms, dinoflagellates, flagellates and the coccolithophore *Emiliania Huxleyi* in the Bering Sea (Merico *et al.*, 2004). Agreement with data was generally achieved, though some PFTs, like diatoms, are easier to constrain than others.

Then PFTs were implemented in global studies. Moore *et al.* (2002) included small phytoplankton, diatoms and nitrogen fixers; Gregg *et al.* (2003) used diatoms, chlorophytes, coccolithophores and cyanobacteria. In a Dynamic Green Ocean Model (DGOM), Le Quéré *et al.* (2005) define ten PFTs chosen regarding the following criteria: they have an explicit biogeochemical role as well as a specific physiology or metabolism; their behaviour affects other PFTs, e.g. by grazing or nutrient competition; they are of quantitative importance, in at least some region of the ocean. Phytoplankton is divided in

six PFTs: silicifiers, mixed-phytoplankton, calcifiers, pico-autotrophs, N_2-fixers and DMS-producers.

It is worth mentioning an alternative approach to the ecosystem complexity. While biogeochemical models emphasis the diversity of physiological traits among various PFTs, dynamic energy budget (DEB) models tend to simplify the ecosystem biodiversity and focus on the common traits of individual life's cycle (Kooijman, 2000). DEB models specify the uptake of energy from the environment and its use by the organism, either for maintenance, reserve or reproduction. First applied to single species, the DEB theory has been used to describe ecosystems, including photo-adaptation and nutrient-limitation. They have successfully described individual growth, inter-species interactions as well as marine ecosystem dynamic. As in Bruggeman and Kooijman (2007), every species are modelled with the same equations; the interspecific differences reside in differences in values of key parameters. This type of model could be used to quantify the impact of climate change on the marine ecosystem.

1.5.3 PlankTOM

The objective behind a DGOM is to predict the effects of climate change on the marine ecosystem and their feedbacks. Therefore it is necessary to represent PFTs by mechanistic parameters controlled by the environment rather than empirical values. Parameters should give the average value for the group considered, hence not focus on only one main species. In fact, the most abundant species could disappear with climate change, while others would thrive.

Although we understand well phytoplankton cells physiology, largely studied in the laboratory, we are still at the stage of identifying and quantifying the links connecting PFTs to each other and to their environment. Some PFTs are not easy to constrain, like for instance coccolithophores. Effectively, a valid model should not only represent accurately plankton production in the conditions considered, but also give accurate output in the case of changes in the environmental conditions. This shows the importance of well-chosen mechanistic parameters that will describe PFTs behaviour and subsequent effects on other types. It has been shown that if PFT representations are based on observed physiology and

ecological interactions, this results in a closer match to observed PFT distributions and biogeochemical cycles (Buitenhuis *et al.* 2006, 2010).

The model PlankTOM (Le Quéré *et al.* 2005) is under constant development. Based on PISCES (Aumont *et al.*, 2003), it has been modified to include more PFTs or to match observational data. The latest version is PlankTOM5.3, used in the present study. PlankTOM5.3 includes five PFTs, within which three phytoplankton groups (silicifiers, mixed-phytoplankton, and calcifiers) and two zooplankton groups (proto-zooplankton and meso-zooplankton). PlankTOM10, where five PFTs are added (pico-heterotrophs, pico-autotrophs, DMS-producers, N2-fixers and macro-zooplankton), is under development.

The Dynamic Green Ocean Project (Le Quéré et al., 2005 or http://lgmacweb.env.uea.ac.uk/green_ocean/index.shtml) brings together biologists and modellers to improve our understanding of marine ecosystems and develop the PlankTOM models. The present study is part of a series of five projects, each one aiming to improve the modelling of one PFT. It focuses on a particular PFT of PlankTOM5.3: the silicifiers, represented by diatoms. Other projects focusing on calcifiers (coccolithophores, Heinle, subm.), non-calcified nanophytoplankton (Foch-Gatrell, PhD ongoing), picophytoplankton (Stawiarski, PhD ongoing) and mesozooplankton (Nobili, 2013), were initiated afterward.

Several reasons justify the choice of diatoms as a PFT:

- they require silicate and by consequence influence significantly the silicate cycle (Treguer *et al.*, 1995),
- they play a major role in carbon export (Buesseler, 1998),
- they are one of the most abundant marine plankton types (LeBlanc *et al.* 2012),
- they require more iron and phosphate than smaller phytoplankton (Sarthou *et al.*, 2005).

1.5.4 The current state of diatom growth modelling

Diatoms are generally represented in models which contain more than one phytoplankton group. This is probably a consequence of several factors. The fact that diatoms require silica makes them a particular PFT that researchers have widely studied.

Diatoms tend to dominate phytoplankton community in nutrient-rich areas like coastal waters. Hence they have been included in early models of regional ecosystems (Van der Berg *et al.*, 1996; Lancelot *et al.*, 2000, 2005). Because of their major contribution in primary production and organic matter export, biogeochemical modellers have often included them as a specific functional group. The silica cycle in the ocean is much simpler than the cycle of other elements like nitrogen and iron, and is relatively well understood (Brzezinski, 1985; Nelson *et al.*, 2005; Tréguer and De La Rocha, 2013). The numerous studies of silica assimilation brought insights on elemental composition and particularly the flexible composition of diatoms, e.g. under nutrient limitation.

As for other phytoplankton groups, diatom growth depends on temperature, light and macronutrient and trace metal concentrations.

The response to temperature is often represented by an exponential function, as in Eppley (1972). Several models suggest a relationship between growth and light intensity. Among the most used are the exponential function of Webb *et al.* (1974), Smith (1936) and the tangent function of Jassby and Platt (1976). The nutrient uptake is often a Monod function, defined by the half-saturation concentration and the maximum uptake rate (Monod, 1949).

However, those relations do not take into account the acclimation of the cell to the light intensity. Changes in light intensity, e.g. through the mixed-layer or over light: dark periods, affect the cell's ability to absorb light and lead to an acclimation of the cell to the new irradiance.

A large part of the literature concerns the acclimation of phytoplankton cells to nutrients, iron and/ or light limitation. Although diatoms are dominant in nutrient-rich waters, they can also survive under Si-, Fe- or N-limitation, reaching a large range of Si:N or Fe:C ratios.

A significant progress has been made recently in modelling flexible elemental composition where, instead of having a fixed biomass composition (e.g. constant C: N: Si: P ratio), cells are allowed to incorporate C, N, Si and Fe independently, resulting in changes in elemental composition depending of the local nutrient conditions (Moore *et al.*, 2002a, b). This way, diatoms are able to maintain their high growth rate under N, Si or Fe limitation. This feature is essential to represent the adaptability of diatoms to Fe and Si limitation. The PlankTOM 5.3 model includes a constant cellular O: C: N: P ratio whereas

Fe: C and Si: C ratios are variable. Fe and Si uptake rates depend on the external and cellular concentrations.

If diatoms are relatively well represented in current models (Moore et al., 2002, a b; Aumont et al., 2003), the prediction of their behaviour under future climate requires a better understanding and modelling of their growth under nutrient and light limitation. In particular, progresses are yet to be done in modelling dark uptake of silicate, silicate and iron co-limitation and iron-light co-limitation. An iron-light co-limitation model for the photosynthesis (Buitenhuis and Geider, 2010) was incorporated into the PlankTOM 5.3 model. Experimental data on diatom growth and photosynthesis under iron-light co-limitation are needed to improve the parameterisation of this model. This study aims to answer a part of the question by providing data on growth rate as a function of temperature and on light-limitation.

1.6 OBJECTIVES

This study aims:

- to implement the best relationship of diatom growth rate as a function of temperature, based on growth experiment data,

- to obtain physiological data on photosynthesis of several diatom species under light limitation and fit the results to a dynamic photosynthesis model,

- to evaluate the effects of variation in growth parameters on the model outputs, such as primary production (PP), PFT distribution and carbon export,

- and to estimate the uncertainty of the model associated with the measurement errors of the parameters.

As we underline above, we aim to represent PFTs by few state variables that will enable the representation of physiological responses to variations in environmental conditions.

Up to now, growth rate as a function of temperature is calculated from Eppley's relation calculated for all phytoplankton types (Eppley, 1972). The specificity of diatoms imposes a

study of their growth rate in a temperature range adapted to the model application (Chapter 2).

Diatom photosynthesis is calculated in an iron-light co-limitation model (Buitenhuis and Geider, 2010). Diatom photosynthesis parameters in PlankTOM5.3 come from experimental data by Sunda and Huntsman (1995, 1997), who studied diatom growth under iron-light co-limitation. Given the large diversity within the group, including species adapted to different temperatures (Suzuki *et al.*, 1995) or different iron concentrations (Sunda *et al.*, 2005), we wish to base our model parameters on as many species as possible. As data from Sunda *et al.* (2005) refer to only two species (*Thalassiosira pseudonana* and *Phaeodactylum tricornutum*), we will carry out photosynthesis experiments on four species, including two from polar waters and two from temperate waters (Chapter 3).

We do not expect to find equal parameter values for every diatom species. One of the challenges faced by experimenters is to provide data averaged to fit most of the species. Furthermore, all data comes with a standard error, associated with the experimental procedure and the biological diversity. However, the PlankTOM5.3 sensitivity to diatom growth parameters has not been investigated yet. Therefore, one of the aims of the present study is to estimate the sensitivity of PlankTOM5.3 outputs associated with diatom growth parameters (Chapter 4).

The thesis will finish with a general discussion and conclusions (Chapter 5).

CHAPTER 2

REVISITING THE RELATIONSHIP BETWEEN DIATOM GROWTH RATE AND TEMPERATURE

2.1 INTRODUCTION

The temperature dependence of phytoplankton growth rate has been widely studied in the last 40 years, e.g. Eppley (1972), Thomas (1966), Suzuki *et al.* (1995), Montagnes *et al.* (2001). Temperature is recognised to be a major factor for growth rate variation. This relationship is used in aquatic ecosystem models, developed with the aim of estimating primary production amongst other parameters (e.g. Lancelot *et al.*, 2000; Moore *et al.*, 2002a).

In a pioneering attempt to generalise the relationship between temperature and growth rate, Eppley (1972) compiled data for different groups of marine and freshwater phytoplankton and drew an exponential curve through the highest values.

It is well established that the growth rate of any species increases with increasing temperature until a maximum is attained at an optimal temperature. However, an exponential relationship has not been unanimously chosen to represent the temperature dependence of species-specific growth rates. Indeed, some studies found more support for a linear relationship. Montagnes *et al.* (2003) reviewed several studies on dinoflagellates, diatoms and coccolithophores grown in culture at different temperatures. In a majority of cases, linear relationships represented the data better than exponential ones. Although Thompson *et al.* (1992) fitted the growth rate versus temperature to an exponential model, they suggest it could be as well represented by a linear function.

The linear and exponential relationships take into account the increase in growth rate up to the optimal temperature for growth. To model the decrease of growth rate above the optimal temperature, Schoemann *et al.* (2005) used another equation that we will refer to here as the "optimal function".

The temperature dependence of a phytoplankton community may differ from that of a single species. In fact, the variation of one species' growth rate is a matter of physiology,

whereas the growth of a community relies on the complementarities between the species and on their diversity. Here we attempt to define a growth rate versus temperature relationship within a phytoplankton community.

The Eppley relationship is based on a relatively small number of observations (n=162) including all phytoplankton taxa. Data range from 2°C (one data-point) to 45°C. Although this relation was not statistically demonstrated, the proposed equation and the Q_{10} value have since been widely used by modellers. In 2008, Bissinger *et al.* published a larger data-base (Liverpool phytoplankton database, LPD, n=1501) compiling phytoplankton growth rates from the many studies carried out since Eppley (1972). By applying a quantitative method (quantile regression) to Eppley's data, Bissinger *et al.* (2008) obtained an exponential relationship at the 99^{th} quantile and found general agreement with Eppley's equation. Although the slope of the 99^{th} quantile of the LPD was not different from Eppley's curve, it had a significantly greater intercept, leading to a higher curve over the whole temperature range. The various groups of phytoplankton are distinguishable by their size, morphology, physiology and growth strategy. As a consequence, temperature-dependent growth curves vary among phytoplankton groups. A number of recent marine ecosystem models are based on the differentiation of Planktonic Functional Types (PFTs) (Le Quere *et al.*, 2005*)* which differ by their growth parameters. Thus, a unique relationship is required for each PFT. For example, as has been pointed out by Eppley (1972), diatoms (*Bacillariophyceae*) cannot attain growth rates as high as those observed for some chlorophytes (*Chlorophyceae*). The relationships suggested by Eppley (1972) and Bissinger *et al.* (2008) might not be applicable for a specific PFT.

In this chapter, we focus on one type of phytoplankton: the marine diatoms. In order to estimate the maximum growth rate attainable by diatoms over a large range of temperature, we compiled laboratory-based data from the literature. Eppley (1972) made two implicit assumptions based on a visual examination of the data. The first one is that the growth rate of individual species as a function of temperature follows an optimum function (Fig. 2 in Eppley, 1972). The second one is that the growth rate of a phytoplankton community (here, all marine diatoms) can best be described by an exponential increase (Figs. 1 and 2 in Eppley, 1972). We statistically test these two assumptions. In order to test the first assumption we compare the fits of three different functions (exponential, linear and optimal) to the species-specific maximum growth rates as a function of temperature. We use two datasets to test the second assumption: we compare the fits of the three different functions to the optimal growth

rates as a function of the optimal temperature, and to the full database of maximum growth rates measured on different diatom species.

2.2 MATERIALS AND METHODS

2.2.1 Database

Growth rate data from laboratory experiments were taken from the literature, where they were presented in tables or in graphs. In the latter case, data were extracted using the programme GrabIt.

In order to compile only the maximum growth rates of diatoms, experimental conditions were carefully checked and only results obtained under replete conditions of nutrients and light were selected. Data with a growth rate equal to zero were not included (n=23). Although the nutrient concentrations and light intensity were optimal, other parameters can affect the growth rate: the day-length or light: dark (LD) cycle, the medium composition, the salinity and whether the cultures were axenic.

2.2.1.1 Nutrients

Cells were grown in most of the experiments in batch culture, or otherwise in turbidostats (Li and Morris, 1982). Cells were fully acclimated to the culture's conditions before sampling. This was considered to result in nutrient replete conditions.

2.2.1.2 Light

Light intensities varied from 2 to 740 μmol photon m^{-2} s^{-1}. The lowest light levels were used at low temperatures. At 0°C, the growth rate of some polar algae were not affected by the low irradiance (Karsten *et al.*, 2006), justifying that 2 and 5 μmol photon m^{-2} s^{-1} were considered, at this temperature and under continuous light, as saturating. When several light intensities were tested, only the optimal intensity (light-saturated growth) was taken into account. Irradiances lower than 10 μmol photon m^{-2} s^{-1} were only used when the temperature was under 10°C. Higher temperatures required higher irradiance: growth rates at 30°C were not measured under 80 μmol photon m^{-2} s^{-1}.

The LD cycle affects the growth rate of a species. Several papers presented diatom growth at different LD cycles, ranging from 4:20 LD to continuous light. The continuous light does

not always provide the optimal illumination: it seems some species grow better under a LD cycle. For instance, Brand and Guillard (1981) show that six diatoms species out of ten have a higher growth rate under 14:10 LD cycle than under continuous light. The optimal LD cycle varies not only with the species, but also with the temperature. At 10°C, *T. pseudonana* grew faster at 15:9 LD cycle, whereas at 15°C the optimal day-length was 9:15 LD (Durbin, 1974). Moreover, several studies revealed that at low temperature, generally between 0 and 5°C, the growth rate is not affected by the day-length (Durbin, 1974; Verity, 1982; Yoder, 1979). Therefore, selecting cultures grown at a particular day-length, for example only under continuous light, would not represent the maximum growth rate.

2.2.1.3 Medium composition

Most of the species have been studied by only one author and in the same experimental conditions. Moreover, different strains of the same species can have significantly different growth rates (Gallagher, 1982). This does not allow us to determine the effect of experimental conditions on the growth rate.

The composition of the medium differed among the different studies. Many added the f/2 enrichment (Guillard and Ryther, 1962: NO_3=883 µM; PO_4= 36.3 µM; SiO_3=54 to 107 µM; Fe= ca. 11.7 µM) to artificial sea water (Gallagher, 1982) or natural seawater (Brandt *et al.*, 1981; Rivkin & Putt, 1987) or used enriched artificial sea water (ESAW, Harrison *et al.*, 1980: NO_3=549 µM; PO_4=21.8 µM; SiO_3=105.6 µM) (Thompson *et al.*, 1992; Curl & McLeod, 1961; Fawley, 1984). Others used different media (nutrient replete AQUIL medium, El Sabaawi & Harrison, 2006; Goniaulax, Paasche, 1968; ground water medium, McGinnis *et al.*, 1997; MP1, Nishikawa and Tamaguchi, 2006). Some media contained ammonium rather than nitrate as the nitrogen source (Muggli *et al.*, 1996, Yoder, 1979) or higher iron concentration (Muggli *et al.*, 1996). Gallagher (1982) mentions a difference in growth between cultures grown in media based on natural seawater and cultures grown in artificial seawater. Both media were enriched with the same nutrient and trace metal concentration (f/2) and had the same salinity. Differences in growth rate varied among the strains, preventing us to draw any conclusion on medium effect on growth. No other paper in our database mentions the effect of medium composition on growth rate.

Among the most commonly studied species, *Thalassiosira pseudonana* is mentioned in five papers and grown in four different media. Although differences in temperature, light intensity, LD cycle and salinity do not allow us to test the effect of the medium on the growth

rate, a general plot of the data show points on a continuous curve (n=25). Rates at the same temperature are equal or close to each other.

Results from nine studies where the diatom *Skeletonema costatum* was grown in f/2 medium show a big range of growth rate for the same temperature. For instance, growth rates at 15ºC (n=12) range from 0.83 d^{-1} (Suzuki *et al.*, 1995; continuous light) to 2.06 d^{-1} (Burkhardt *et al.*, 1999; 15:9 LD cycle). Cultures with growth rate from 0.83 to 0.89 were grown in f/2 at 50 to 200 µmol photon m^{-2} s^{-1}, with LD cycle varying from 12:12 to continuous light. This observation indicates that differences in light conditions do not affect the growth rate. Variations could come from difference in strain or effect of the medium: among the three cultures with a growth rate of 2.1 to 2.2 d^{-1}, two are grown in constant dissolved inorganic carbon concentration. The data do not allow us to determine a single factor of variation.

2.2.1.4 Other effects

Salinity varied from 24 (Paasche and Ostergren, 1980) to 30 to 35. Growth rates of *Skeletonema costatum* and *Thalassiosira pseudonana* grown in salinity of 24 are similar to those obtained at higher salinity and at nearby temperatures of ± 2°C (Suzuki *et al.*, 1995; Thompson *et al.*, 1992).

All cultures were unialgal, while 7.4% of the cultures were axenic. Most of the papers do not mention axenicity (82.4% of the data); Maldonaldo and Price (1996) and Thomas (1966) mention cultures that are not axenic (2.9% of the data), while Brand *et al.* (1981) affirms cultures were not made axenic but bacteria were not apparent under the microscope (7.3% of the data). It has not been quantified whether the presence of bacteria has an effect on the maximum growth rate of phytoplankton.

2.2.2 Analysis

2.2.2.1 Minimum least squares regression

We tested 3 different equations for the growth rate (μ) as a function of temperature (T): an exponential:

$$\mu_{max} = \mu_{max,\,0°C} \times Q_{10}^{(T/10)} \quad (1)$$

a linear:

$$\mu_{max} = \mu_{max,\ 0°C} + \text{slope x } T \quad (2)$$

and an optimal function (Schoemann *et al.*, 2005):

$$\mu_{max} = \mu_{opt} \text{ x } \exp[-(T-T_{opt})^2 / dT^2] \quad (3)$$

where $\mu_{max,\ 0°C}$ is the maximum specific growth rate at 0ºC, μ_{opt} is the optimal growth rate at the optimal temperature (T_{opt}) and dT is the width of the optimum growth curve.

Parameters were determined using the software SYSTAT, by minimizing the residual sum of squares cost-function = $\Sigma (\mu_{obs} - \mu_{model})^2$ where μ_{obs} is the observed growth rate and μ_{model} is the modelled one. SYSTAT also calculates the asymptotic standard error (A.S.E.) for each parameter. The fitting of each function to the measured growth rates was compared using the Akaike's Information Criterion (AIC, Burnham and Anderson, 1998):

$$AIC = n_{obs} \log (\sigma^2) + 2n_{param}$$

in which n_{obs} is the number of growth rates, n_{param} is the number of parameters in each function, and

$$\sigma^2 = 1/(n_{obs} - n_{param}) \Sigma(\mu_{obs} - \mu_{model})^2$$

The AIC takes into account the likelihood of the model based on the number of parameters and the relative goodness of the fit. Since the optimal function contains three parameters and the other two functions, two parameters, the σ^2 is not sufficient to compare the three models. This explains that in cases where the three models are very close to each other, the better fit is given to the linear and/ or the exponential functions. If the difference in AIC is less than 2, there is substantial evidence for both functions, while if the difference is greater there is considerably more support for the function with the lowest AIC (Burnham and Anderson 1998).

This method was applied to individual cases (one study on one specific strain, figure 2.2), to the relationship of the optimal growth rate (μ_{opt}) as a function of the optimal temperature (T_{opt}) (figure 2.3), as well as to the whole database (figures 2.4 and 2.5).

Parameters were compared using their A.S.E. as a confidence interval.

2.2.2.2 Quantile regression

The quantile regression (Koenker and Bassett, 1978) is used to define the upper edge of the data. The 99th quantile is the line below which 99% of the data-points are found. Unlike ordinary least squares regression that uses the mean, quantile regression is based on the

median. Quantiles were calculated using the package “quantreg” in the software R (http://www.r-project.org). Exponential curves were obtained by applying a linear quantile regression to the logarithmic-transformed data. The linear quantile regression provides estimates of standard errors and confidence intervals (CI). Intercepts and slopes of the log-transformed exponential curves were compared by *t*-test. Optimal curves were obtained by applying a non-linear quantile regression.

2.3 RESULTS

2.3.1 Database

The database comprises published values for 70 diatom species and a total of 95 diatom strains. It consists of 689 growth rates measured over temperatures ranging from -2°C to 37°C. Amongst the 65 papers reviewed, 22 publications examine the growth of one or more species at a minimum of four different temperatures, while the rest describe experiments at three or fewer different temperatures. More than 70% of the data-points are at temperatures between 10 and 25°C. Polar species have been studied frequently (Gilstad & Sakshaug, 1990; Yoder, 1979; Rivkin & Putt, 1987; Sakshaug *et al.*, 1991; Suzuki *et al.*, 1995; Karsten *et al.*, 2006), giving data down to -2°C (Rivkin & Putt, 1987; Suzuki *et al.*, 1995). On the contrary, few data are reported at high temperature: 4% of the data-points were collected above 25°C (Thomas, 1966; Hulburt & Guillard, 1968; Suzuki *et al.*, 1995).

Growth rates range from 0.08 d^{-1} (*Chaetoceros pseudocurvesitus* at 0°C, Suzuki *et al.*, 1995) to 4.35 d^{-1} (*Chaetoceros sp.* at 30°C, Thomas, 1966) (Fig. 2.1). Up to 7°C, growth rates do not exceed 0.91 d^{-1}, whereas at 20°C the range extends from 0.36 to 3.47 d^{-1}.

2.3.2 Analysis of species-specific growth-rate vs. temperature

First we investigate the species-specific relationship between growth rate and temperature. If the experimental temperature range is wide enough, this relationship generally shows an increase of the growth rate up to an optimal temperature, followed by a decrease in the growth rate. We fit three functions to growth rate datasets of different species in order to identify the best model for the species-specific growth rate as a function of the temperature.

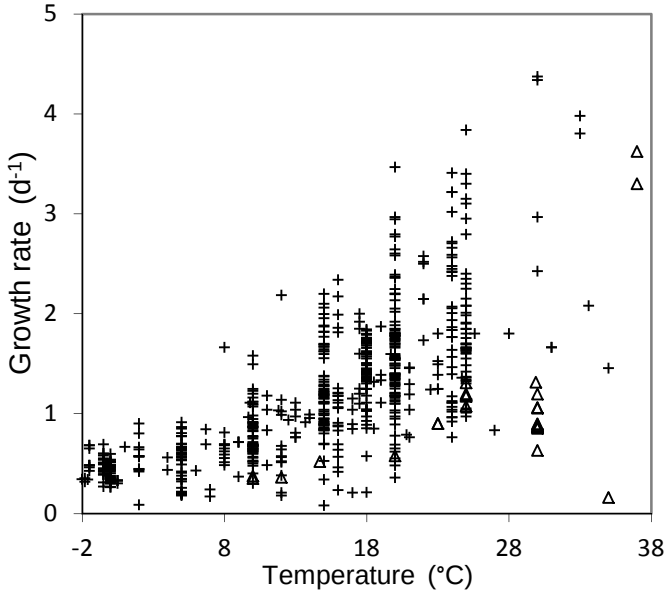

Fig. 2.1: Diatom growth rates as a function of temperature (n=689). Triangles are growth rates measured above the species optimal temperature.

We selected studies where diatoms were grown under at least 4 different temperatures. This gives a total number of 38 cases (38 strains of diatoms), extracted from 22 papers, grown under 4 to 7 different temperatures. The temperature ranges extend from 8 to 29°C. Unlike previously published work, which compared the exponential and linear functions, we include an optimal function, which takes into account the eventual decrease in growth rate above the optimal temperature. We fitted the 3 functions: exponential, linear and optimal, to these species-specific datasets, as presented in table 2.1. The different fits are compared by their AIC value, the lowest value indicating the best fit. The difference is significant if the difference in AIC is greater than 2. In 18 out of 38 cases, one function is significantly better than the other two; in the 20 other cases, at least two AIC values are not significantly different. In 17 out of 18 strains for which one function was significantly better than the other two, the data better fitted to the optimal function. We thus statistically confirm Eppley's first assumption.

Table 2.1: Parameters for the exponential, linear and optimal functions fitted to the species-specific growth rates measured at different temperatures and to different selections of the database. n, number of data-points; AIC, Akaike Information Criterion (if there is significantly more support for the best AIC this value is in bold); numbers in brackets, asymptotic standard error (A.S.E.); When A.S.E. is missing the standard error was not computable; * indicates dataset including growth rates above the species optimum temperature.

Table 2.1

Species	Source	n	exponential		linear		optimal			AIC		
			$\mu_{max,\ 0°C}$ (d^{-1})	Q_{10}	$\mu_{max,\ 0°C}$ (d^{-1})	Slope (d^{-1} .°C^{-1})	μ_{opt} (d^{-1})	T_{opt} (°C)	dT (°C)	Exp	Lin	Opt
Asterionella formosa	a *	12	0.55 (0.07)	1.41 (0.08)	0.45 (0.09)	0.034 (0.005)	1.24 (0.06)	24.7 (4.0)	22 (5)	-16.2	-17.0	-15.8
Chaetoceros affinis	b *	4	0.80 (0.33)	1.14 (0.27)	0.75 (0.40)	0.015 (0.024)	1.25 (0.02)	16.7 (0.2)	11 (0.4)	-0.5	-0.5	**-7.2**
Chaetoceros calcitrans	c	15	0.32 (0.07)	2.50 (0.23)	-0.92 (0.28)	0.155 (0.015)	124 (759)	111 (135)	45 (33)	-12.0	-10.4	-9.5
Chaetoceros gracilis	c	16	0.59 (0,17)	1.48 (0.20)	0.22 (0.31)	0.055 (0.016)	1.62 (0.11)	21.1 (0.9)	11 (2)	-9.9	-10.7	-12.3
Chaetoceros muelleri	d	5	0.37 (0.10)	1.89 (0.21)	-0.85 (0.24)	0.112 (0.011)	2.43 (0.07)	29.4 (1.1)	13 (1)	-2.4	-4.8	-5.3
Chaetoceros pseudocurvisetus	a *	10	1.13 (0.74)	0.99 (0.25)	1.14 (0.89)	-0.002 (0.034)	1.73 (0.07)	24.8 (0.3)	7 (0.4)	-0.3	-0.3	**-11.7**
Chaetoceros simplex	c	13	0.31 (0.09)	2.24 (0.28)	-0.77 (0.28)	0.123 (0.014)	2.31 (0.26)	26.8 (3.9)	13 (4)	-9.3	-10.7	-8.5
Chaetoceros sp.	a *	9	0.60 (0,08)	0.59 (0,14)	0.61 (0.07)	-0.028 (0.009)	0.58 (0.03)	4.6 (0.6)	8 (1)	-11.5	-12.4	**-15.3**
Chaetoceros sp.	e *	12	1.24 (0.61)	1.40 (0.09)	-0.21 (0.88)	0.124 (0.030)	4.30 (0.14)	30.4 (0.6)	13 (1)	3.0	1.9	-4.1
Dactyliosolen fragilissima	b	6	0.38 (0.08)	1.74 (0.18)	0.08 (0.11)	0.054 (0.007)	1.26 (0.10)	24.6 (3.1)	17 (3)	-7.7	-9.5	-8.1
Detonula confervacea	a	19	0.54 (0,02)	1.69 (0.09)	0.52 (0.02)	0.039 (0.003)	0.88 (0.02)	9.4 (0.8)	13 (1)	-41.0	-43.7	**-47.1**
Detonula confervacea	g *	4	1.23 (0.60)	0.70 (0.32)	1.22 (0.45)	-0.035 (0.040)	1.04 (0.14)	9.8 (0.7)	6 (2)	-0.9	-0.9	-1.1
Ditylum brightwelli	h *	4	0.86 (0.45)	1.23 (0.26)	0.66 (0.68)	0.032 (0.029)	1.72 (0.14)	24.0 (1.0)	12 (2)	0.5	0.4	-0.3
Eucampia zodiacus	i	11	0.40 (0.06)	2.03 (0.15)	-0.15 (0.10)	0.096 (0.008)	2.15 (0.11)	25.0 (2.0)	15 (2)	-11.6	-14.5	-14.5
Fragilaria barbaranum (ROS D125)	j	14	0.43 (0.05)	2.07 (0.20)	0.36 (0.05)	0.061 (0.006)	1.21 (0.05)	14.0 (1.2)	12 (1)	-18.4	-21.3	-22.5
Fragilaria striatula (ROS D99)	j	12	0.38 (0.03)	1.95 (0.12)	0.34 (0.02)	0.045 (0.002)	0.98 (0.04)	16.4 (1.4)	16 (1)	-22.7	-28.7	-27.9
Leptocylindrus danicus	k *	20	0.29 (0.08)	2.63 (0.28)	-0.38 (0.14)	0.118 (0.001)	2.05 (0.05)	17.4 (0.2)	7 (1)	-13.6	-18.8	**-32.6**

Table 2.1

Species	Source	n	exponential		linear		optimal			AIC		
			$\mu_{max,\ 0°C}$ (d^{-1})	Q_{10}	$\mu_{max,\ 0°C}$ (d^{-1})	Slope (d^{-1} .°C^{-1})	μ_{opt} (d^{-1})	T_{opt} (°C)	dT (°C)	Exp	Lin	Opt
Nitzschia seriata	l *	7	0.37 (0.04)	1.22 (0.19)	0.37 (0.04)	0.009 (0.007)	0.48 (0.05)	7.5 (1.8)	13 (5)	-11.2	-11.2	-9.8
Phaeodactylum tricornutum	c	13	0.47 (0.08)	1.66 (0.14)	0.06 (0.16)	0.064 (0.009)	1.64 (0.20)	27.9 (5.3)	19 (5)	-16.7	-17.9	-15.8
Phaeodactylum tricornutum	m *	6	0.80 (0.18)	1.28 (0.14)	0.63 (0.28)	0.034 (0.014)	1.46 (0.03)	21.6 (0.5)	12 (1)	-6.4	-6.6	**-9.2**
Phaeodactylum tricornutum	f	5	0.45 (0.12)	1.62 (0.22)	0.13 (0.18)	0.055 (0.010)	1.40 (0.04)	23.3 (1.1)	15 (2)	-3.4	-4.7	-6.3
Phaeodactylum tricornutum	n *	7	0.32 (0.09	1.73 (0.24)	0.05 (0.13)	0.048 (0.009)	1.19 (0.04)	21.2 (0.6)	12 (1)	-6.1	-7.8	**-12.4**
Pseudo-nitzschia granii	o *	5	1.03 (0.26)	0.85 (0.15)	1.03 (0.22)	-0.015 (0.015)	0.99 (0.04)	12.9 (0.4)	10 (1)	-4.2	-4.3	**-6.6**
Skeletonema costatum	a *	20	0.47 (0.09)	1.35 (0.11)	0.29 (0.13)	0.030 (0.007)	1.32 (0.05)	22.2 (0.40)	13 (1)	-16.9	-18.5	**-32.4**
Skeletonema costatum	p	4	0.59 (0.12)	1.68 (0.21)	0.36 (0.16)	0.064 (0.011)	1.60 (0.24)	21.7 (7.5)	17 (8)	-2.8	-3.6	-0.8
Skeletonema costatum	b *	5	0.67 (0.29)	1.28 (0.30)	0.53 (0.41)	0.029 (0.024)	1.25 (0.01)	17.2 (0.1)	10 (0.1)	-1.5	-1.6	**-13.6**
Skeletonema costatum (Sk6c)	q *	6	0.55 (0.22)	1.29 (0.23)	0.38 (0.28)	0.029 (0.015)	1.25 (0.08)	20.7 (0.9)	14 (1)	-1.2	-1.7	**-5.2**
Skeletonema costatum (Sk6c)	r	11	0.70 (0.07)	1.77 (0.09)	0.10 (0.12)	0.107 (0.007)	3.11 (0.48)	32.5 (5.7)	22 (4)	-13.7	**-16.6**	-14.3
Skeletonema costatum (Sk6c)	s	18	0.47 (0,06)	2.22 (0.15)	0.25 (0.05)	0.107 (0.004)	2.55 (0.06)	22.5 (0.8)	15 (1)	-17.2	**-25.8**	**-32.2**
Skeletonema tropicum (21-L)	t	5	0.13 (0.13)	2.26 (0.79)	-1.01 (0.74)	0.082 (0.030)	2.56 (11.80)	47.5 (116.3)	23 (61)	-0.7	-0.9	2.2
Skeletonema tropicum (S.trop)	t	7	0.77 (0.22)	1.34 (0.14)	0.38 (0.42)	0.050 (0.016)	1.94 (0.18)	32.4 (7.4)	21 (11)	-4.1	-4.3	-2.1
Stephanodiscus hantzschii	a *	9	0.58 (0,16)	1.31 (0.16)	0.37 (0.25)	0.032 (0.012)	1.33 (0.04)	23.0 (0.4)	12 (1)	-7.2	-7.7	**-14.8**
Thalassiosira nordenskioeldii	a	14	0.52 (0,02)	1.51 (0.07)	0.50 (0.02)	0.031 (0.002)	0.92 (0.02)	15.3 (1.6)	19 (2)	-28.8	-31.8	-33.3
Thalassiosira nordenskioldii	u	19	0.56 (0.07)	1.69 (0.15)	0.50 (0.07)	0.048 (0.007)	1.15 (0.02)	12.37 (0.3)	13 (1)	-26.3	-29.4	**-34.2**

Table 2.1

Species	Source	n	exponential		linear		optimal			AIC		
			$\mu_{max,\ 0°C}$ (d^{-1})	Q_{10}	$\mu_{max,\ 0°C}$ (d^{-1})	Slope (d^{-1} .°C^{-1})	μ_{opt} (d^{-1})	T_{opt} (°C)	dT (°C)	Exp	Lin	Opt
Thalassiosira pseudonana	b	4	0.39 (0.09)	1.92 (0.21)	0.07 (0.27)	0.069 (0.016)	180 (861)	174 (152)	70 (37)	-3.2	-1.9	0.1
Thalassiosira pseudonana	c	14	0.44 (0.12)	1.81 (0.24)	-0.18 (0.31)	0.084 (0.016)	1.87 (0.24)	26.2 (5.1)	15 (6)	-10.1	-10.8	-8.6
Thalassiosira rotula A8	v	15	0.35 (0.05)	1.94 (0.15)	0.05 (0.04)	0.069 (0.003)	1.69 (0.03)	23.2 (0.44)	14 (1)	-15.8	-26.3	**-34.1**
Thalassiosira rotula C8	v *	18	0.74 (0,16)	1.30 (0.13)	0.53 (0.22)	0.038 (0.012)	1.72 (0.11)	21.5 (0.9)	14 (2)	-8.4	-9.3	**-14.4**
selection μ_{opt} *vs*. T_{opt}		29	0.34 (0.16)	2.06 (0.27)	-0.06 (0.32)	0.081 (0.024)	39.47 (-)	138 (-)	65 (-)	**-15.6**	-11.9	-12.6
all database (up to 37°C)		689	0.56 (0.03)	1.59 (0.04)	0.33 (0.04)	0.058 (0.002)	2.15 (0.21)	35.8 (6.4)	27 (4)	-392.9	-405.2	**-407.9**
all database (up to 33°C)		684	0.53 (0.03)	1.64 (0.04)	0.32 (0.04)	0.058 (0.002)	2.07 (0.12)	34.3 (10.6)	26 (4)	-405.0	-413.4	**-416.8**
database without data above T_{opt} (up to 31°C)		658	0.47 (0.03)	1.80 (0.04)	0.28 (0.04)	0.063 (0.002)	4.71 (0.18)	60.9 (10.8)	39 (6)	**-447.9**	-430.7	**-446.1**
database (up to 25°C) without data above T_{opt}		649	0.46 (0.04)	1.81 (0.05)	0.30 (0.18)	0.062 (0.002)	3.35 (0.18)	49.7 (10.1)	34 (11)	**-461.3**	-453.9	**-461.9**

a Suzuki & Takahashi, 1995
b Paasche & Ostergen, 1980
c Thompson *et al.*,1992
d McGinnis *et al.*, 1997
e Thomas, 1966
f Montagnes & Franklin, 2001
g Guillard & Ryther, 1962
h Paasche, 1968
i Nishikawa & Yamagushi, 2006
j Karsten *et al.*, 2006
k Verity, 1982
l Smith *et al.*, 1994
m Fawley, 1984
n Li & Morris, 1982
o El Sabaawi & Harrison, 2006
p Jorgensen, 1968
q Falkowski, 1977
r Langdon, 1988
s Yoder, 1979
t Hulburt & Guillard, 1968
u Durbin, 1974
v Krawiec, 1982

Figure 2.2 presents the observed growth rates of those 18 diatom strains, as well as the modelled growth rates with the best-fitting functions, i.e. the optimal function in 17 cases and the linear function in 1 case.

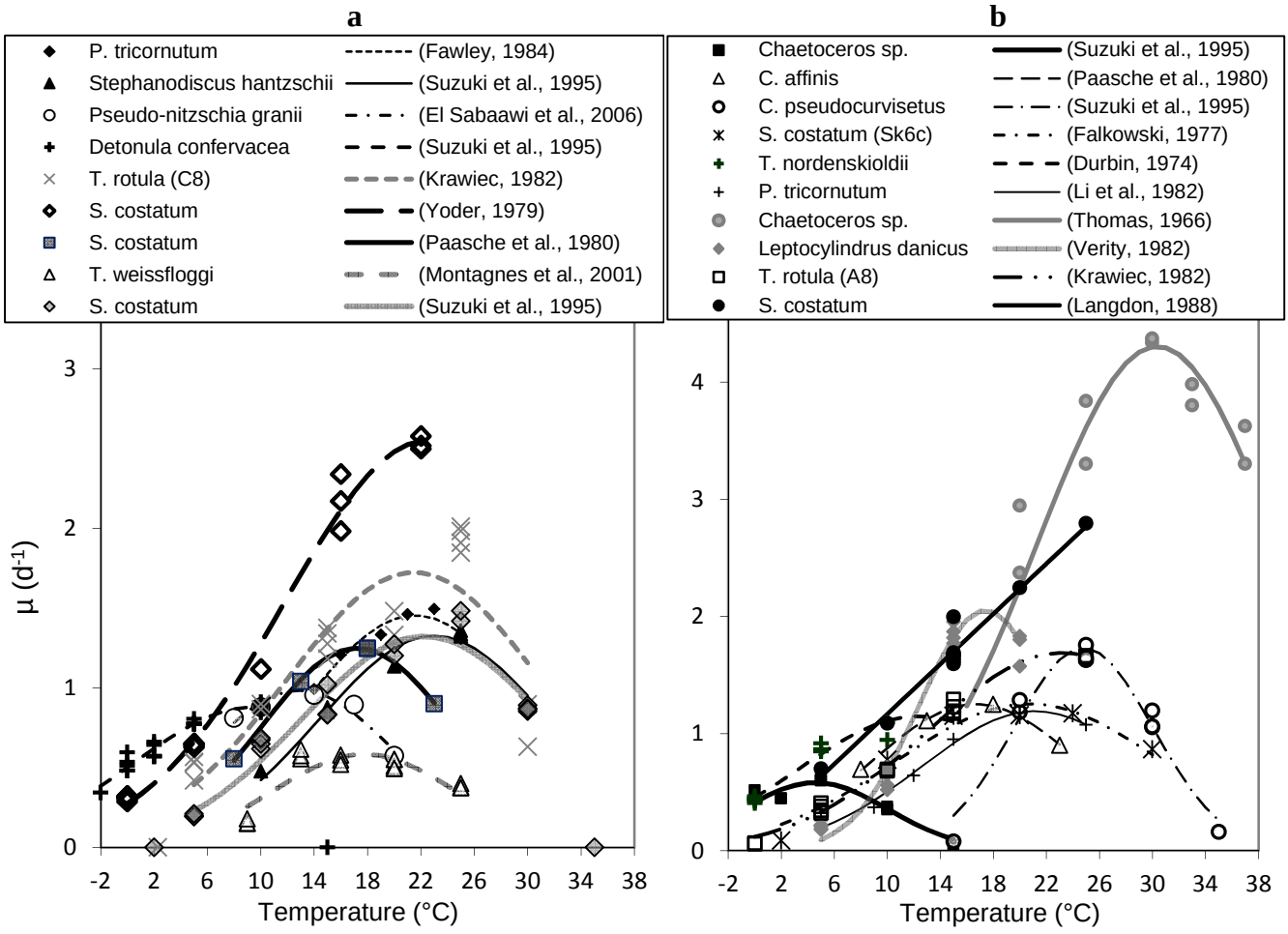

Fig. 2.2. a and b) Measured (symbols) and modelled (lines) growth rates at different temperatures for the 18 diatom strains for which one function was significantly better than the others. In (a) the scale is increased for better clarity.

We can separate the data in two groups: 20 cases where the published data do not exceed the optimal temperature of the species, and 18 cases that reported a positive growth rate at 1 or 2 temperatures above the optimal temperature (indicated by * in table 2.1). In the first group, the optimal function was significantly the best fit out of the three functions in 4 cases (Fig.2.2 a: *Detonula confervacea* (Suzuki *et al.*, 1995), and *Skeletonema costatum* Sk6c (Yoder, 1979), Fig.2.2 b: *Thalassiosira rotula* A8 (Krawiec, 1982), *T. nordenskioldii* (Durbin, 1974)) while the linear function was significantly the best fit in 1 case (Fig.2.2 b: *Skeletonema costatum* Sk6c (Langdon, 1988)). In 12 cases, the optimal and/ or the linear functions were

better than the exponential function, whereas in the 8 other cases the exponential and/ or the linear functions were better than the optimal one.

In the second group, where the published data include measurements above the optimal temperature, the linear and exponential fits do not represent the decrease of the growth rate at supra-optimal temperatures. As a consequence, the optimal function is the best fit in most of the cases (14) of this group. In the other 4 cases, no function fits better than another.

2.3.3 Analysis of diatom optimum growth rates vs. optimum temperature

Eppley (1972) assumed an exponential increase of the optimum growth rate with temperature. To illustrate this assumption was reasonable he plotted the growth rates of four species in his figure 2 (Eppley, 1972). To test Eppley's second assumption, we looked for the maximum growth rate for each strain. Although we could extract from an exponential or linear curve the growth rate at the highest temperature, this rate may not be the absolute maximum growth rate, as the experiment may have omitted the optimal temperature. The datasets presenting a growth rate above the optimal temperature allow us to extract the maximum growth rate. The optimal function is advantageous for modelling the growth rate through its absolute temperature optimum, and for having as parameters the maximum growth rate and the optimal temperature. Therefore, we selected the 29 strains where the AIC for the optimal function is one of the lowest. The optimal function parameters give us directly a set of optimal growth rate and optimal temperature values, ranging from 0.48 to 4.30 d^{-1} and from 4.6 to 30.4°C. These data represent one way to constrain the temperature dependence of marine diatoms as a group.

To find the best equation to fit these data, we applied our method to the new set of μ_{opt} as a function of T_{opt} (n=29). The results are detailed in figure 2.3 and table 2.1. The exponential function presents the lower AIC, so is the best fit to this dataset. The maximal growth rate as a function of the temperature can be written as:

$$\mu_{max} = 0.34 \times 2.06^{(T/10)} \quad (4)$$

This equation is applicable between 4.6 and 30.4°C.

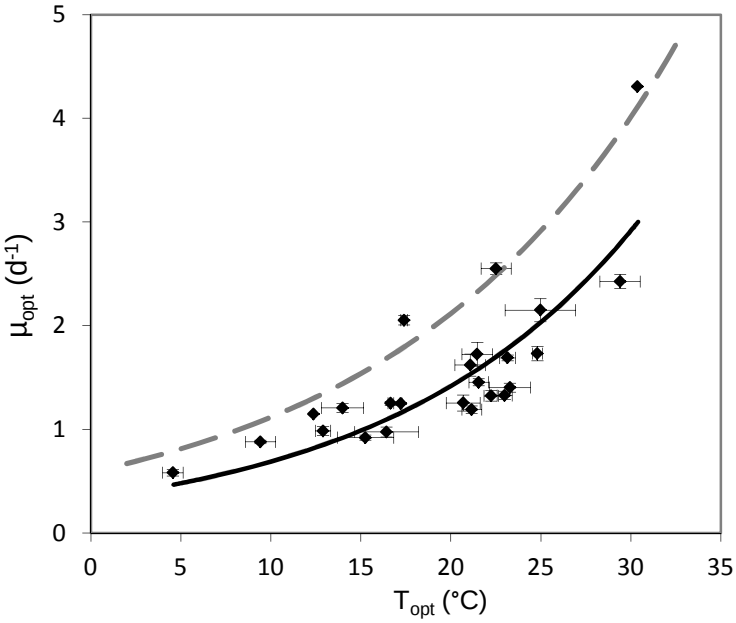

Fig.2.3: Optimal growth rate (μ_{opt}) as a function of optimal growth temperature (T_{opt}) (n=29). Error bars represent the A.S.E for each parameter; black line, exponential fit; dashed line, Eppley's curve.

2.3.4 Analysis of the diatom's community average growth rate

Another way to establish the temperature dependence of growth rate for diatoms as a community is to use the whole database of growth rates measured at different temperatures. These data do not represent the absolute maximum growth of each species, but rather give a range of growth rates attainable at each temperature. The database contains the data for the 45 cases analysed previously, as well as growth rates measured at only 1, 2 or 3 temperatures, increasing significantly the range of growth rates and the number of data. The advantage compared to the previous set (optimum growth rate vs. optimum temperature) is that growth rates measured at very low or very high temperatures are included, even though they may not be the optimal growth rates of the species considered.

The three functions are fitted to the whole database (-2 to 37°C, n=689), and the parameters presented in table 2.1. The optimal function gives the best fit to the dataset, which is justified by the decrease of growth rates above 30°C:

$$\mu_{max} = 2.15 \times \exp\left[-(T-35.8)^2 / 27^2\right] \quad (5)$$

However, given the small number of data at high temperatures and given the maximal temperature of the ocean, we took only into account data from -2°C up to 33°C (n=684). The three functions are fitted to these data and the parameters are presented in table 2.1. Once again, the optimal function was the best fit to the data.

The database contains 25 data-points corresponding to growth rates measured above the optimal temperature, distributed between 10 and 37°C (Fig. 2.1, triangle). The temperature ranges of species play an important role in algal competition and phytoplankton community composition (Goldman & Carpenter, 1974). However, the optimal temperature for a species can differ substantially from the temperature at which it dominates the community (Smayda, 1969; Durbin, 1974; Eppley, 1977). The temperature where a species dominates depends not only on the *in situ* temperature, but also on the temperature history and on the temperature range of other species. By comparing the temperature dependence of the growth rate of eight diatom species with the annual temperature range of their habitat, Suzuki and Takahashi (1995) show each species predominated the ecosystem at a temperature below their optimal temperature. More precisely, three temperate species predominated at a temperature around the centre of their growth temperature range (15 to 25°C), while one temperate and four polar species predominated at the lowest part of their growth range (8 and -1.8°C). Although cold water species can have an optimal temperature between 2 to 15°C (Durbin, 1974; Suzuki and Takahashi, 1995), they predominate the community at sub-zero temperatures where no other species can grow. Among the eight species, only the temperate species *Chaetoceros pseudocurvisetus* appears to predominate at its optimal temperature, 25°C (Suzuki and Takahashi, 1995).

Therefore, as it is unlikely that a species would predominate at a temperature above its optimum, we excluded the growth rates measured above the specific optimum temperature. The three functions are fitted to this dataset (-2 to 31°C, n=658), and the parameters presented in table 2.1. The exponential and optimal functions give the significantly best fits (AIC=-447.4 and -447.5, respectively):

$$\mu_{max} = 0.47 \times 1.80^{(T/10)} \quad (6)$$

$$\mu_{max} = 4.71 \times \exp\left[-(T-60.9)^2 / 39^2\right] \quad (7)$$

Although the parameters of the optimal function are significantly different from those of (5), the curves obtained are very close to each other. Equ.7 gives a higher growth rate from 22°C upward. However, if we take into account the parameter's errors (A.S.E.), the curves (5) and (7) are not significantly different: they are contained between the upper and lower deviation curves (Fig. 2.4). Compared to the optimal function (7), the exponential function (6) results in a higher intercept and higher growth rates from 26°C upward. However, considering the A.S.E., there is no significant difference between the curves.

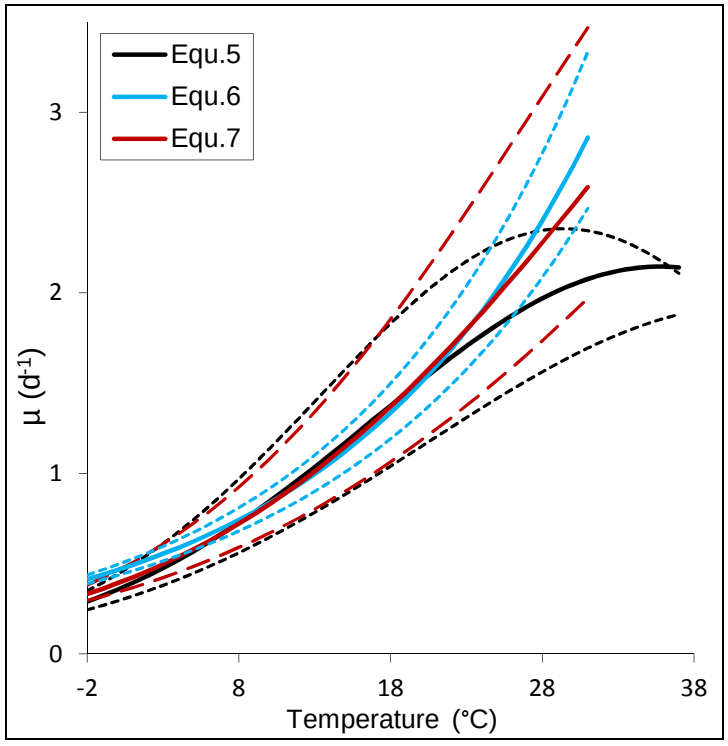

Fig. 2.4: Diatom growth rates as a function of temperature, as defined by Equ.5 (black), Equ.6 (blue) and Equ.7 (red) and respective lower and upper edges defined by the A.S.E. (dots and dashes).

The importance of data at high temperature:

The vast majority of the data (97%) are below 25°C. Although data-points above 25°C are rare, they may play an important role in the fit of the curves. Namely, as growth rates tend to decrease at high temperature, we tested the influence of high temperature data by fitting the three curves to a dataset containing data up to 25°C (n=649). The best fits are the exponential and the optimal functions (Table 2.1). Parameters of the exponential function do not vary from those of Equ.6. Although the optimal function presents different parameters, the resulting curve is similar to the previous one (Equ.7).

99th quantile regression:

The exponential and optimal functions are fitted to the 99th quantile regression of the whole database (n=689) and to that of the dataset including growth rates up to 31°C and excluding data measured above T_{opt} (n=658). Parameters are presented in table 2.2.

Table 2.2: Parameters for the exponential and optimal 99th quantile regression functions fitted to different dataset of growth rates vs. temperature. Standard errors of each parameter are in brackets.

		exponential		optimal		
	n	$\mu_{max,\ 0°C}$ (d^{-1})	Q_{10}	μ_{opt} (d^{-1})	T_{opt} (°C)	dT (°C)
All database up to 37°C	689	0.99 (0.14)	1.71 (0.12)	5.66 (1.83)	46.9 (12.0)	33 (6)
Data up to 31°C, without data above T_{opt}	658	0.96 (0.12)	1.74 (0.12)	4.50 (-)	35.8 (2.1)	27 (2)
Eppley's curve	153	0.59	1.88			
Bissinger *et al.*, 2008	1501	0.81	1.88			

The parameters of the exponential curve are compared to those of Eppley's and Bissinger's curves. The intercepts of our curves (0.99 and 0.96) are significantly higher than those in Eppley (1972) and Bissinger *et al.* (2008) (0.59 and 0.81, respectively). The Q_{10} value of the 99th quantiles (1.71 and 1.74) are significantly lower than those of Eppley (1972) and Bissinger *et al.* (2008) (both equal to 1.88).

The exponential and optimal functions fitted to the whole database are included in Fig. 2.5:

$$\mu_{max} = 0.99 \times 1.71^{(T/10)} \quad (8)$$

$$\mu_{max} = 5.66 \times \exp\left[-(T-46.9)^2 / 33^2\right] \quad (9)$$

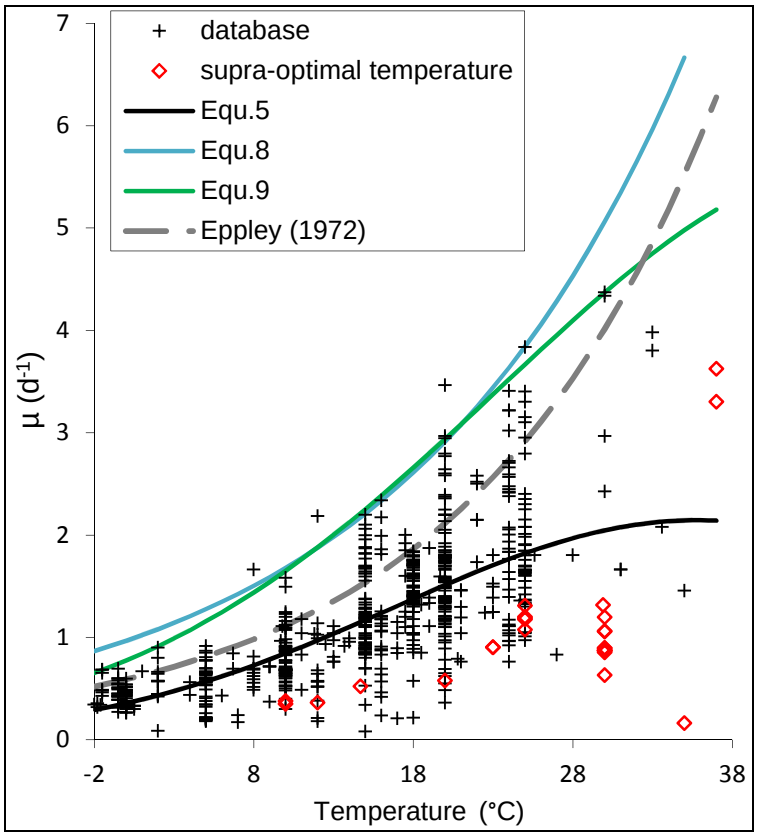

Fig. 2.5: Diatom growth rates as a function of temperature. The average optimal function (Equ.7) and 99th quantiles (exponential function (8), blue line; optimal function (9), green line) are fitted to the database, from -2 to 37°C (n=689); dashed line, Eppley curve; red diamonds, growth rates measured above the species' optimal temperature.

2.4 DISCUSSION

Eppley (1972) suggested (1) that the maximum growth rates of individual species increases up to an optimal temperature and decreases above that temperature and (2) that the maximum growth rate of a phytoplankton community follows an exponential curve.

2.4.1 Species-specific growth rate

In 17 out of 38 strains the optimal function gave the best fit, and in an additional 13 strains there is substantial support for the optimal function. The optimal function represents better than the exponential and linear ones the gradual decrease of growth rate both below and above the optimal temperature.

It should be emphasised that the output of our analysis depends on the number and range of the data-points. If the growth rate was measured up to the optimal temperature, thus always increasing, the exponential and/ or the linear function may fit as well as (12 out of 20 cases),

or better than (4 out of 20 cases) the optimal function. On the contrary, in all the 18 cases where the growth rate was also measured above the optimal temperature, the optimal function fitted better (13 out of 18 cases), or as well as (5 out of 18 cases) the exponential and/ or linear function.

Some authors recommended the use of the linear (Montagnes and Franklin, 2001) or the exponential function (Goldman and Carpenter, 1974; Yoder, 1979) to model the increase of the growth rate of one species up to its optimal temperature. This study shows that in only 5 cases out of 20 the exponential function is better than the optimal function. In the other cases, the sub-optimal growth rate is better modelled by the optimal and/ or the linear function. Montagnes *et al.* (2003) fitted the response of algae to temperature to a linear function. For this they considered data-points below the optimal temperature, excluding the optimal growth rate (Fig. 1 in Montagnes *et al.*, 2003). In 24 out of 30 diatom studies the linear function appeared to represent better the growth rate increase with temperature. Our results support Montagnes' *et al.* (2003) findings: if we considered only the growth rates measured below the optimal temperature, in 10 out of 20 cases, the linear function fitted significantly better than the exponential one, while in the remaining 10 cases the growth rate can be represented equally with a linear or an exponential function.

The linear function can be used to represent the increase of the growth rate of one species up to its optimal temperature. The approach of the growth rate to the optimal temperature is better illustrated by the optimal function, though the latter requires three parameters instead of two for the linear function. While Eppley (1972) assumed this to be the case, it has not been statistically verified until now. The exponential function is not recommended to model the species-specific relationship between growth rate and temperature.

2.4.2 Optimal growth rate *vs.* optimal temperature

As Eppley (1972) pointed out, and as we have demonstrated here, the temperature dependency of the growth rate of one species can be distinguished from the growth rate of the whole diatom population. The temperature dependency of an individual's growth rate depends on the physiology of that species; the temperature dependency of a diatom community growth rate relies on the variety of species and on their genotypic differences (e.g., some are adapted to cold water, other to temperate waters).

Eppley's second statement was also verified within the range of data available. We found that a fit to the optimum growth rate as a function of the optimum growth temperature of these 34 strains does indeed follow an exponential increase, ranging from 4.6 to 30.3°C. Nevertheless our equation gives much lower rates than those Eppley (1972) found (Fig.2.3). The difference is explained by the methodology: we fitted the curve at the average optimum growth rate by minimising the residual sum of squares, whereas Eppley (1972) estimated graphically the maximum growth rate. Our curve does not take into account some higher rates present in the whole database, and is applicable between 4.6°C to 30°C.

2.4.3 Diatom community growth rate

Our database is built on the same criteria as that used by Eppley (1972): we compiled maximum growth rates obtained in saturated conditions of light and nutrients.

The 99th quantile regression is a statistical approach to Eppley's graphical fit. Bissinger *et al.* (2008) reviewed Eppley's curve by calculating the 99th quantile of Eppley's growth rates dataset (99_{EPP}, n=153). This statistical method gave a similar curve to Eppley's, although the dataset is not large enough to statistically test the difference.

Compiling a larger database of phytoplankton growth rates from the research undertaken since 1972, Bisssinger *et al.* (2008) applied the 99th quantile regression to their new dataset (99_{BIS}; -2 to 38°C, n=1501). This resulted in equal slope and Q_{10} (1.88) but a significantly higher intercept than that of the curve 99_{EPP} (0.81 and 0.59 d^{-1}, respectively), making the whole curve higher.

The same method is applied in the present study. The 99th quantile calculated between -2 and 31°C (n=658) is also higher than Eppley's curve. The slope is not significantly different (t-test, df=658, p=0.0238), whereas the intercept is significantly higher. The Q_{10} value of our 99th quantile is lower than that of the Eppley curve (1.75 and 1.88, respectively). The log-transformed parameters of our curve are not significantly different from those of Bissinger *et al.* (2008).

About 9 % of our data-points were cited by Eppley (1972). Most of the datapoints above Eppley's curve were published after 1972. There is no doubt that growth rate data published since 1972 have affected the fit of the curve. Our study confirms results from Bissinger *et al.* (2008), which showed the maximal growth rate of phytoplankton in cold water was under-

estimated by Eppley (1972). At 9°C and beyond Eppley's curve falls under the 95% CI of our 99th quantile.

Since diatoms are known for their high growth rates (Furnas, 1990), their proportions within the database of Bissinger *et al.* (2008) could eventually affect the fit of the curve. The maximum growth rate curve would be affected not only by the number and range of data, but also by the taxa or phytoplankton types. Bissinger *et al.* (2008) tested this hypothesis by using a dataset containing only 43% of diatoms, the same proportion than that in Eppley's (1972). The slope and intercept of the 99th quantiles fitted to both Bissinger's dataset were not significantly different, showing that a difference in diatom proportion does not necessarily create a difference in the curve fitting. Moreover, the parameters of our curve (100% of diatoms) and those of Bissinger *et al.* (68% of diatoms) are not significantly different. By consequence, the dissimilarities between Eppley's curve and ours cannot be totally attributable to a difference in PFT proportions.

The exponential function is valid to represent the diatom maximum growth rate up to 31°C. Above that the observed maximum diatom growth rates decrease, therefore we do not recommend the use of an exponential function at high temperature. Exponential functions can over-estimate growth rates at high temperature. The issue was raised by Bissinger *et al.* (2008), who recommended not using the 99th quantile above 29°C. Applying the 99th quantile regression to different datasets containing diatom growth rates up to 25°C, 31°C or 37°C give similar curves. Although growth rate data above 25°C are not numerous enough to affect the fit of the exponential 99th quantile, they clearly indicate that the diatom growth rate reaches its maximum around 30°C. Therefore the exponential quantile would over-estimate diatom growth rate from 30°C upwards. In consequence, the alternative is to use an optimal function, which models the growth rate decrease above the optimal temperature.

The optimal 99th quantile regression applied to our whole database (up to 37°C, n=689) and to the dataset up to 31°C (n=658) give similar curves (data not shown). As we want to include growth rates at high temperatures, the former one will be considered. At 30°C the modelled growth rate is 4.37 d^{-1}, which is much more realistic than the rate of 5.06 d^{-1} given by the exponential quantile, or of 6. . At 37°C the optimal quantile gives a growth rate of 5.18 d^{-1}, which is still higher than the observed rates. At low temperatures, the optimal function gives lower rates than does the exponential one, for instance, 25% lower at -2°C,

down to 11% lower at 4°C. The maximum observed rate up to 0.5°C is 0.69 d^{-1}. The optimal model gives a growth rate of 0.77 d^{-1} at 0°C, which is more realistic than the growth rate of 0.97 d^{-1} given by the exponential model.

The optimal curve is a good alternative to the exponential function. Therefore, if the 99th quantile is to be chosen to model the diatom's growth rate, the use of the optimal function instead of Eppley's (1972) or other exponential curve is recommended.

It should be noted that it is possible to force parameters for the calculation of the optimal quantile, for instance to choose the optimal temperature or the optimal growth rate. By imposing T_{opt}=33°C the curve obtained gives realistic rates at high temperature. However, rates between 8 and 23°C are increased by about 10%. By imposing μ_{opt}= 4.5 d^{-1} different curves are obtained, whose parameters are not significantly different from each other.

2.4.4 Application to PlankTOM5

The purpose of this study was to statistically define the temperature-dependency of diatom assemblages for modelling purposes. Up to now, many modellers relied on Eppley's function, statistically verified by Bissinger *et al.* (2008), based on growth rates of any phytoplankton type.

When seeking to incorporate a growth rate vs. temperature relationship into a model, two criteria should be taken into account. First either the maximum growth rate, represented by the 99th quantile, or the average growth rate of the community should be chosen. Then the range of temperatures involved in the simulation will determine if an exponential function is suitable or if the optimal one should be considered.

One may incorporate into a model the maximum growth rate, represented by the 99th quantile, and apply the limitations of the environmental conditions, such as light and nutrients that would therefore decrease the growth rate. We refer to the above discussion for the choice of the function. One should note that our exponential and optimal curves fitted to the upper edge of the data are approximately 40% higher than Eppley's curve. This may have an impact on modelling global primary production.

Although this method seems theoretically correct, there is a risk of over-estimating the diatom growth rate. In fact, the maximum growth of various diatom species will vary, for the

same temperature, depending on their size, the smaller cells dividing faster (Sarthou *et al.*, 2005). Hence, the upper edge of the diatom's growth rate, or 99th quantile, represents the maximum rate of the fastest species, which might not be the one present in the ecosystem. Moreover, given that several diatom species are likely to live in the same ecosystem, either at the same time or successively, an average growth rate would be more appropriate. Thus, we will incorporate in our model the average growth rate of the diatom community.

Let us first consider the dataset up to 31°C (n=658). According to the AIC, the exponential function fits as well as the optimal one (table 2.1). The number of parameters involved influences the AIC. As a consequence, an optimal curve that fits the dataset as well as the exponential one would have a higher AIC, i.e. a worse fit, than the exponential function. It is interesting to look at the correlation coefficient of our functions: for our dataset (n=658), the correlation coefficient is 0.9713 for the exponential curve and 0.9864 for the optimal curve. Therefore, the optimal curve fits better to our data but has the disadvantage of requiring a third parameter. The exponential and optimal curves are very close to each other (Fig. 2.4, lines red and blue). Differences are mostly located at low and high temperatures. From -2 to 2°C, the optimal function gives a growth rate 20% to 10% lower, respectively, than the exponential one. At high temperature, the growth rate for the optimal function is lower as well, for instance by 10% at 31°C. The exponential function should not be extrapolated at higher temperatures, as it would over-estimate the growth rate, up to 4.07 d^{-1} at 37°C. The optimal function extrapolated at 37°C would give a growth rate of 3.21 d^{-1}, which is coherent with our observations.

Although seawater temperatures barely reach more than 33°C, our model requires a correct estimation of the growth rate at high temperatures. Let us consider the dataset up to 37°C (n=689). The optimal function fits the best to our database. The growth rate is 0.36 d^{-1} at 0°C and 2.14 d^{-1} at 34-37°C.

For the modelling of growth in temperate and warm water, the use of an optimal function is recommended, applicable up to 37°C (Equ. 5).

2.5. CONCLUSION

This study shows:

- the optimal function fits best to the growth rates of individual species in 17 cases out of 18,

- the exponential function fits best to the optimum growth rates as a function of the optimum temperatures,

- the optimal function fits best to the complete dataset of diatom growth rates, from -2 to 37°C,

- the exponential 99th quantile of our diatom growth rate database differs from Eppley's curve: the intercept at 0°C is higher.

The optimal function is an alternative to the exponential function to represent the maximum or average diatom growth rate at high temperatures. The parameters of the optimal function can be adjusted to represent better the growth rate decrease at high temperature. It is possible to force a parameter for the calculation of the optimal quantile, for instance to choose the optimal temperature or the optimal growth rate. By imposing T_{opt}=33°C the curve obtained gives realistic rates at high temperature. However, rates between 8 and 23°C are increased by about 10%, which could over-estimate global primary production. By imposing μ_{opt}= 4-5 d^{-1}, different curves are obtained whose parameters are not significantly different from each other. They model a similar growth rate from -2 to 25°C but differ above that, showing an maximal growth rate from 4 d^{-1} at 34°C to 4.9 d^{-1} at 37°C. A deeper comparison of those quantiles may able us to find a function fitting the observed growth rates in cold water as well as in warm water.

For modelling purposes, we will use the optimal function applicable up to 37°C (Equ. 5).

CHAPTER 3

PHOTOSYNTHESIS OF 4 DIATOM SPECIES ACCLIMATED TO DIFFERENT LIGHT INTENSITIES

3.1 INTRODUCTION

Photosynthesis has been a major field of research since the beginning of phytoplankton study. As autotrophs, phytoplankton growth is determined by photosynthesis, depending on light intensity, temperature, nutrient concentrations and changes occurring in those parameters. Amongst these, light intensity is particularly variable by latitude, season, time of the day, cloud cover and water properties, such as turbidity. Light can be limited in some areas, such as at high latitudes, in turbid waters or beneath the euphotic zone; it can also attain a lethal level, when cells cannot process the energy input.

Studies of the light-dependence of diatom growth rate involve studies of photosynthesis processes, described by many parameters such as fluorescence, pigment content, and maximum absorbance capacity. Photosynthesis metabolism is very complex, as it involves assimilation of nitrate and carbon, biosynthesis of chlorophyll and the photosynthetic conversion of photons into chemical energy and reducing power.

Phytoplankton responds to variations in irradiance by physiological processes of acclimation, expressed in changes in pigment content or elemental composition. Collectively, these processes are called photoacclimation. There are two types of response of phytoplankton to light variations: a long-term and a short-term one. The long-term response (time-scale of hours to days) involves changes of synthesis of chlorophyll or pigments and changes of elemental composition and growth rate (Geider, 1993). The photosynthesis vs. irradiance (PI) curve reflects the ability of the algae to respond to short-term light fluctuations (time-scale of seconds to minutes). Characteristics of PI curves are dependent on the photoacclimation status of the algae, i.e. on the light exposition history.

Modelling the algal productivity as a function of the irradiance is necessary to estimate the primary production. Marine photosynthesis has been modeled as a function of irradiance using PI curves (Ryther 1956, Jasby and Platt 1976, Falkowski 1981). Some described light-dependent

growth rate (Bannister and Laws 1980; Kiefer and Mitchell 1983; Geider *et al.* 1986; Sakshaug 1989), while Sakshaug *et al.* (1989) described a steady-state nutrient-deficient growth of the diatom *Skeletonema costatum* at different irradiances and day-lengths, using the parameter chlorophyll :carbon (θ_m). A later version of this model was built from the study of nutrient-saturated growth of the diatoms *Thalassiosira nordenskioeldii* and *Chaetocros furcellatus* (Sakhaug *et al.*, 1991). Parameters measured are usually cellular elemental composition (carbon, nitrogen, chlorophyll), growth rate, dark respiration and light absorption. Nevertheless, those models are valid for a stable environment, with no short-term variations.

A dynamic photosynthesis model (Buitenhuis and Geider, 2010) takes into account the variability (time-scale of hours to days) of the environmental conditions, where the phytoplankton is in non-steady-state growth. It also takes into account the iron-light co-limitation. The model describes the cellular ratios Fe:C and Chl:C (θ) and growth rate as a function of light intensity and free iron seawater concentration. Values of nine parameters are required to run the model (Table 3.1). The maximum carbon-specific photosynthetic rate (P_m) is also one of the parameters in some equations. It is calculated from the maximum growth rate (μ_m) and Fe:C minimum and optimum ratios. The chlorophyll-specific light-limited photosynthetic rate (α^{Chl}) is calculated as a function of its maximum value, θ and the dependence factor of α^{Chl} on θ.

There are two ways of calibrating the model parameters. Buitenhuis and Geider (2010) fitted the parameters to the experimental results of Sunda and Huntsman (1995, 1997), which were, according to the authors, the only dataset available that provided those parameters. They optimized the model parameters using experimental data on growth rate, θ and Fe:C ratio obtained for iron-limited cultures grown at different light intensities. The nine model parameter values were optimised by minimising a cost function.

In Buitenhuis and Geider (2010), the model results after a parameter optimisation fitted well with experimental data. However, for some species parameter values were not physiologically realistic. One of the reasons may be the small light intensity range tested (175 and 500 µmol photon m^{-2} s^{-1}) for those species. As a consequence, the light intensity was not low enough to generate the maximum chlorophyll: carbon ratio. Moreover, no other experimental data were available for validation.

We aim to improve the model by producing more experimental data. We suggest optimising the model parameters by calculating directly the photosynthetic parameters P_m and α^{Chl}. Instead of calibrating the parameters from experimental data on cellular ratios Fe:C and Chl:C and growth rate, as in Buitenhuis and Geider (2010), we intend to measure directly P_m and α^{Chl} from PI curve experiments. Effectively, as α^{Chl} and P_m are easily measurable from the PI curve, it would be relevant to get those parameter values from experiments, rather than to estimate them from μ_m and θ. This method requires knowing not only the photosynthetic parameter values, but also cellular contents (Chl:C ratio) and growth rate.

In the present study we focused on light-limited diatoms grown in iron-replete conditions. Therefore the five iron-related parameters of the model were not changed (Table 3.1).

PI curves were performed on diatoms grown at three to five irradiances, ranging from low light intensity to light-saturation. We obtained data on α^{Chl}, P_m, μ_m, θ_m, and cellular content in carbon, nitrogen and chlorophyll.

Table 3.1: list of parameters of the photosynthesis model, Buitenhuis and Geider (2010). p: parameter; m: model predicted; i: independent variable.

Function	Symbol	Description	Units	Original paper
p	ρ	iron-limited: iron-saturated maximum uptake rate ratio	-	29
p	K	dependence of α^{Chl} on θ	-	-
p	$K_{1/2}$	half-saturation constant	nmol L^{-1}	5.2
p	Q_{min}	minimum Fe_P:C ratio	µmol mol^{-1}	2.5
p	Q_{max}	maximum Fe_P:C ratio	µmol mol^{-1}	47
p	Q_{oPt}	optimum Fe_P:C ratio	µmol mol^{-1}	3.2
p	$\alpha^{Chl}{}_m$	maximum initial slope of PI curve	g C g Chl^{-1} m^2 mol $photon^{-1}$	29
p	θ_m	maximum Chl:C ratio	g g^{-1}	0.049
p	μ_m	maximum growth rate	d^{-1}	1.68
m	P_m	maximum photosynthetic rate	d^{-1}	
m	θ	Chl:C ratio	g Chl^{-1} g C	
m	μ	growth rate	d^{-1}	
i	I	light intensity	mol $photon^{-1}$ m^2 s^{-1}	
i	Fe’	dissolved iron	pmol L^{-1}	

Given the inter-specific variability of photosynthetic parameters as well as their intra-specific variability under different treatments, we considered several species, including *Thalassiosira pseudonana*, used in Buitenhuis and Geider (2010) to calibrate the model. Among

the four species, two are from polar waters whereas two others are from temperate waters, in order to take into account an eventual effect of the water temperature.

3.2 MATERIALS AND METHODS

3.2.1 Cultures

Unialgal, non-axenic diatom cultures from temperate waters (*Thalassiosira pseudonana* CCMP 1335, Coscinodiscophyceae and *Phaeodactylum tricornutum* CCMP 632, Bacillariophyceae) and from polar waters (*Chaetoceros brevis* and *Thalassiosira antarctica*, Coscinodiscophyceae) were grown at 17 and 4°C, respectively, as previously determined in a temperature experiment (see annexe I).

Culture medium was made from natural seawater collected in the North Atlantic (salinity 34.5) filtered through a 0.22 µm filter and autoclaved (30 min at 120°C). Nutrients were added according to the f/2 recipe (Guillard and Ryther, 1962), ensuring replete conditions of nutrients.

Choice of the day-length

The day-length can affect phytoplankton physiology. Previous studies show different responses of phytoplankton to variation of day-length. Some species grow faster under continuous light while others, on the contrary, prefer light: dark cycles. *P. tricornutum* do not show changes of growth rate when grown at continuous light, under a 12:12 LD cycle or under alternation of 2 hrs light:2 hrs dark (Mortain-Bertrand, 1987). However, the C:N ratio is smaller under continuous light. *T. pseudonana* grows faster at continuous light (Brand and Guilard, 1981). Nevertheless, according to this author its optimal irradiance is 0.1 ly/min under continuous light, instead of 0.25 ly/min when grown under 14:10 LD cycle. Experimental data on *C. brevis* were not found. For *T. antarctica*, the growth rate increases with the light period (Gilstad, 1990).

We did not aim to use the optimal cycle for each strain. In order to model phytoplankton growth *in situ*, it is more relevant to use light: dark cycles, as plankton rarely experience continuous light in the field. Thus we would tend to choose a cycle closed to 12:12 LD. As we are interested in photosynthetic processes, it is easier to work with a longer light period, which allows us more time for day sampling. For this reason we used, as a convenient compromise, a 14:10 LD cycle.

Light was provided by white fluorescent tubes, situated laterally in the 17°C incubator and vertically in the 4°C room. A different number of layers of neutral-density light filters were wrapped around the culture flasks in order to expose the cells to different light intensities. Irradiance was measured with a light-meter (model QSL-2101, Biospherical Instr. Inc., US) inside flasks filled with water to the same level as the cultures. Light intensity ranged from 30 to 700 µmol photon m^{-2} s^{-1} in the 17°C incubator, whereas it reached only 147 µmol photon m^{-2} s^{-1} in the 4°C room. For technical reasons related to the electrical wiring, we were not able to add extra fluorescent tubes in the cold room. The highest intensity was reached by positioning the flasks higher on the bench, closer to the light tubes.

Diatoms were grown in 2-L flasks and acclimated to the experimental light intensity during at least five generations prior to experimentation. Cells were maintained in exponential growth by dilution every two to six days in fresh medium. Daily swirling assured a regular remix of the nutrients. Growth rates were measured by daily counting with a Coulter counter Multisizer. Each count is an average of three measurements, and growth rates were determined from three to six daily counts. The average error on cell counting was 1.7%.

Cells were sampled for experimentation in the middle of the exponential growth phase, at a concentration of approximately 1,000,000 cells ml^{-1} for *P. tricornutum*, 800,000 cells ml^{-1} for *T. pseudonana* and 400,000 cells ml^{-1} for *C. brevis* and *T. antarctica*. All culture manipulations were done under aseptic conditions.

3.2.2 Chlorophyll

Sampling and preservation:

The culture was sampled for chlorophyll analysis less than one hour before each PI curve experiment, which took place one to three times per day. Cells were also harvested for counting with the Coulter counter.

Duplicate or triplicate samplings of 6 to 10 ml of culture were filtrated through 25-mm GF/F glass fibre filters. The filter was wrapped in aluminium foil and immediately deep-frozen in liquid nitrogen, before being stored at -80°C.

Calibration:

Purified extract of chlorophyll *a* from *Anacystis nidulans* (Sigma) was dissolved in 90% acetone in magnesium carbonate-saturated solution. The concentration was checked on a spectrophotometer (Vernon, 1960). Dilutions of this standard solution were used to calibrate the fluorometer. Glassware was soaked in distilled water for 24 hours before use, in order to remove any trace of acid.

Sample preparation and analysis:

After extraction in 90% acetone in magnesium carbonate-saturated solution for 24 hours, fluorescence was read on a fluorometer (Turner, model 10-AU, kit 10-037R) at 685 nm, with excitation at 340-500 nm. The magnesium carbonate diluent was used to decrease the risk of destruction of the sample by acidification. The optical density was read before and after acidification of the sample with 0.15 ml of 0.1 N hydrochloric acid, in order to subtract any signal due to the presence of chlorophyll degradation products (Pheophytin). The chlorophyll concentration of the samples was calculated with the equations of Lorenzen (1966).

The average error on chlorophyll measurements was 4%. Results are given per cellular volume, which was determined by a Multisizer counter.

3.2.3 Carbon and nitrogen

Sampling and preservation:

A culture was first sampled for carbon and nitrogen analysis at the end of the dark period preceding the day of experiment. Like for chlorophyll analysis, the culture was sampled on the day of experiment less than one hour before each PI curve.

Duplicate or triplicate samples of 6 to 10 ml of culture were filtrated through pre-combusted (450°C, 4 hrs) 13-mm GF/F glass fibre filters. Filters were dried at 30°C during at least 24 hours and stored in a dried incubator until analysis.

Carbon and nitrogen contents were measured with a CHN analyser (Exeter Elemental analyser CE440).

Calibration:

The instrument is calibrated with acetanilide (Acros Organic), which contains 71.09% of carbon and 10.36% of nitrogen. The acetanilide is stored in a desiccator and weighed into pre-combusted nickel capsules. The calibration standards are analysed in the same run as the

samples, as detailed below. After the run, a two-point calibration curve is obtained by regression between the standard, corrected for the blank value, and the origin. The calibration curve is used to correct the carbon and nitrogen contents of the samples.

Sample preparation and analysis:

The whole 13-mm filters were transferred into pre-combusted nickel capsules. All nickel capsules are sealed, placed into pre-cleaned tin-capsules and then transferred to the auto-sampler tray of the analyser. Each run started with two "bypass" runs, consisting of a non-specific amount of acetanilide weighed into a nickel capsule, performed to verify the combustion and to determine the retention times of the combustion products. The three blanks following consist of empty nickel capsules and provide a mean for correcting standard runs for background contributions of carbon and nitrogen. Then, two calibration standards, of nominal weight of approximately 2 mg of acetanilide, are performed. The next three runs are blank-filters, consisting of pre-burnt GF/F filters. The mean is used to correct samples for carbon and nitrogen contributions of the filter. A known amount of acetanilide is analysed every ten samples to check the instrument consistency.

The average error on carbon and nitrogen contents was 3.6 and 9.0%, respectively. Cellular content results are expressed per cellular volume.

3.2.4 Measurement of photosynthesis

The evolution of oxygen concentration within a concentrated suspension of diatoms was measured with an Oxygraph (Hansatech, UK). A cylindrical chamber filled with culture was mounted on an oxygen electrode. The platinum cathode was covered with a plastic membrane selectively permeable to oxygen. The culture was kept at the growth temperature by a water jacket connected to a cooler bath.

Sampling:

The same culture was sampled one to three times during the day of experimentation, approximately three, five and seven hours after the light period started. Each sample was divided and measured simultaneously in two Oxygraph chambers, resulting in two to six PI curves.

Calibration:

A two-point calibration was done at the beginning of each day of experimentation. The 100% oxygen concentration was measured in f/2 medium previously bubbled with air over night and at 4°C to favour gas dissolution; the 0% oxygen concentration was measured in f/2 medium previously bubbled with N_2 over night. The Oxygraph chamber was closed during the calibration to prevent any gas exchange with the atmosphere.

Sample preparation and analysis:

Prior to each PI curve, cells were concentrated by centrifugation (5000 rpm, 15 min) and resuspended in 10 ml of f/2 medium partially deoxygenated by bubbling with N_2. Measuring chambers of the Oxygraph were filled with 3 ml of a 4 to 20-fold concentrated suspension and immediately closed. First, oxygen concentration was measured after 10 to 15 min in the dark (until a stable rate was achieved). Then cells were exposed to increasing light intensities, in seven to ten steps ranging from 12 to 1800 µmol photon m^{-2} s^{-1}. Each step lasted 6 to 10 min while the total experiment was no longer than 90 min.

An estimate of the oxygen evolution in medium contaminated by bacteria is obtained from experiments by Beate Stawiarski (personal comm.). Cultures of Prochlorococcus were filtered through 1 µm to remove phytoplankton cells while leaving any bacteria. The oxygen evolution was measured in the medium obtained. This background, that we call “blank-medium”, is subtracted from our measurements.

Before PI curve measurements were performed, cells from the growing culture flask were harvested for analysis of cellular chlorophyll, carbon and nitrogen as well as for cell counting. Cell density of the concentrated suspension was also measured with the Multisizer counter. pH was checked.

3.2.5 PI curve

Cellular chlorophyll and carbon contents measured prior to each PI curve are used to convert oxygen production per ml into oxygen production per chlorophyll or per carbon, which is then plotted against the light intensity.

α^{Chl}

Oxygen evolution relative to chlorophyll content is used to calculate, at very low light intensity, the initial slope of the PI curve (α^{Chl}). The extent of the linear phase is determined graphically.

P_m

The maximal photosynthetic rate is determined from the average photosynthetic rate at saturating light. Since our cultures were grown under a 14:10 L:D cycle, the net photosynthetic rate (P_m) is calculated from the maximal photosynthetic rate per 14 hours from which we subtract the respiration rate (R_d) per 24 hours.

R_d

The PI curve intercept on the ordinate axes, expressed by carbon content, gives us the respiration rate in darkness (R_d), in mol O_2 mol C^{-1} 24 h^{-1}, or d^{-1}.

Because nitrate was the main source of nitrogen in our medium, the oxygen evolution is converted into carbon production using a photosynthetic quotient (PQ) of 1.4 moles O_2 produced per mole CO_2 assimilated (Laws, 1991). This leads to α^{Chl} expressed in g C g Chl^{-1} m^2 mol $photon^{-1}$ and P_m expressed in mol C mol C^{-1} d^{-1}, or d^{-1}. The oxygen consumption in darkness is converted into carbon production using a respiratory quotient RQ = 1/PQ = 0.7 mole CO_2 produced per mole O_2 consumed. Rd is finally expressed in mol C mol C^{-1} d^{-1}, or d^{-1}.

Errors coming from the different parameters involved, such as cell count, carbon content analysis and linear regression of the oxygen production rate, were calculated and combined to calculate the total error on the oxygen production, which was 1.6% on average.

3.2.6 Statistical analyses

We compared cellular contents and photosynthesis parameters of the different cultures to detect any effect of growth irradiance, temperature, time of day or growth rate. Homogeneity of the variances of the different groups was checked by the test of Hartley (1950). Difference is considered significant at 0.05.

For homogenous samples, a significant effect of a treatment on one of the variables was detected by ANOVA (R).

Because several cultures show heterogeneous variances, we compared their median instead of their mean. This method prevents influence of outsider values. The function `t.test` (R) was used to compare two treatments. In fact, this function does not use the T-test, but the Welch's

test, particularly recommended when variances are not equal. The Welch's test is equivalent to the t-test but compares the median, while the t-test compares the mean. To allow same treatment for homogenous and heterogeneous samplings, the Welch's test was used for any treatment comparison. Unless stated, results show statistics from Welch tests.

3.2.7 Optimisation

The model parameters α^{Chl}, θ_m and μ_m were optimised as in Buitenhuis and Geider (2010). The method and results are described in Annexe II.

3.3 RESULTS

3.3.1 Cell composition

Carbon and nitrogen content

Average contents are 223±57 fg C μm^{-3} and 49±17 fg N μm^{-3} (Table 3.2). Carbon and nitrogen contents of *T.antarctica* (165 fg C μm^{-3} and 42 fg N μm^{-3}, respectively) are significantly lower than those of the three other species (237 fg C μm^{-3} and 47 fg N μm^{-3}, respectively) (carbon: n=103, p=8.18 x 10^{-13}; nitrogen: n=95, p=0.034).

There is no trend of variation with the light intensity common to the four species. In temperate species, cellular content increases at the lowest light intensity. Some cultures show a low standard deviation between samplings, whereas others have a large deviation. Contents are compared by Welch test.

In *P.tricornutum*, both carbon and nitrogen contents do not differ significantly among cells grown at 335 and 700 µmol photon m^{-2} s^{-1}. However, despite large variations within some treatments, contents are significantly larger in cells grown at 30 µmol photon m^{-2} s^{-1} than in those grown at 120, 335 and 700 µmol photon m^{-2} s^{-1} (for carbon: n=17, p=4.95 x 10^{-4}, n=15, p=1.68 x 10^{-5} and n=13, p=3.94 x 10^{-5}, respectively; for nitrogen: n=13, p=0.0318, n=11, p=1.35 x 10^{-5}; n=9, p=2.20 x 10^{-4}, respectively). Low-light acclimated cells contain about 67% more carbon and 44% more nitrogen than high-light acclimated cells.

The trend is similar for the carbon content of *T. pseudonana*: low-light acclimated cells contain 32% more carbon than cells grown at the highest irradiance (n=21, p=1.82 x 10^{-6}). On

the contrary, nitrogen content does not differ between cells grown at 30 and 700 µmol photon m^{-2} s^{-1} (n=19, p=0.572). Nevertheless, cells grown at 120 µmol photon m^{-2} s^{-1} contain less nitrogen than cells grown at 700 µmol photon m^{-2} s^{-1} (43 and 49 fg N μm^{-3}, respectively; n=14, p=0.0023).

In polar species, cellular content of carbon and nitrogen, are not correlated with the light acclimation. However, the carbon content in *C. brevis* grown at 64 µmol photon m^{-2} s^{-1} is significantly higher than that at other light intensities (n=14-18, p<0.0006). Nitrogen content is significantly higher in cells grown at 25 µmol photon m^{-2} s^{-1} (n=31, p=6.00 x 10^{-5}).

There is no variation of cellular content in *T. antarctica* (ANOVA, carbon: n=20, p=0.111; nitrogen: n=20 , p=0.111).

Table 3.2: Average values of chemical content for *Phaeodactylum tricornutum*, *Thalassiosira pseudonana*, *Chaetoceros brevis* and *Thalassiosira antarctica* acclimated to different light intensities. Numbers in brackets are the standard deviations.

	I	C (fg C. μm^{-3})	Chl:C (mg. g^{-1})	C:N (g. g^{-1})
P. tricornutum	700	193 (4)	5.4 (0.3)	4.7 (0.3)
	335	184 (6)	7.7 (0.7)	5.2 (0.5)
	120	221 (14)	11.3 (1.1)	4.4 (0.8)
	30	314 (48)	13.8 (1.7)	5.5 (2.1)
T. pseudonana	700	197 (11)	6.3 (0.2)	4.0 (0.5)
	120	227 (14)	16.1 (2.1)	5.3 (1.0)
	30	258 (28)	15.9 (1.5)	6.2 (1.9)
C. brevis	147	212 (11)	6.2 (0.6)	6.4 (1.2)
	64	299 (33)	12.7 (1.1)	6.7 (2.6)
	25	166 (30)	18.3 (2.1)	2.2 (0.5)
	32	252 (11)	21.4 (2.1)	4.7 (1.8)
	6	197 (21)	19.3 (1.7)	6.7 (2.2)
T. antarctica	147	156 (14)	9.5 (0.7)	3.9 (0.8)
	50	171 (20)	12.1 (1.0)	4.1 (1.3)
	6	175 (30)	28.1 (3.0)	4.0 (1.7)

Carbon: nitrogen ratio

The average C:N ratio of the four diatoms is 5.0±1.1 g C g N^{-1} (n=94). It does not show any correlation with the light intensity.

In *P. tricornutum*, the C:N ratio is significantly lower at 120 µmol photon m^{-2} s^{-1} (4.4 g C g N^{-1}) than at 30 or 335 µmol photon m^{-2} s^{-1} (5.5 and 5.2 g C g N^{-1}, respectively; n=13, p=0.0264 and n=10, p=0.0026, respectively). However, the C:N ratio *in T. pseudonana* is significantly lower at 700 µmol photon m^{-2} s^{-1} (4.0 g C g N^{-1}) than at 50 or 120 µmol photon m^{-2} s^{-1} (5.3 and 5.1 g C g N^{-1}, respectively; n=18, p=0.0028 and n=14, p=0.0058, respectively).

C:N ratio in *C. brevis* grown at 25 µmol photon. m^{-2} s^{-1} is significantly lower than those in cells grown at other light intensities (2.2 g C g N^{-1}, n=13-17, p<0.0042). The C:N ratio in *T. antarctica* does not vary with the growth irradiance. However it is significantly lower than in the three other species (n=94, p<0.0048).

There is no effect of the water temperature on C:N ratio (ANOVA, p=0.830).

Chlorophyll content

Chlorophyll content decreases significantly with increasing growth irradiance (ANOVA: p=2.64 x 10^{-13}). It drops by 26 and 34% from 30 to 120 µmol photon m^{-2} s^{-1} in the temperate species *P. tricornutum* and *T. pseudonana*, respectively. At 700 µmol photon m^{-2} s^{-1}, it has dropped on average for those species by 63%. In cold-water species, the chlorophyll content decreases by 60% in between 6 and 147 µmol photon m^{-2} s^{-1}.

Chlorophyll: Carbon ratio

Although carbon content shows only small variations with the growth irradiance, there is a significant effect on the Chl:C ratio (ANOVA, n=30, p=0.0014) (Fig.3.1, Table 3.2). In the four species, the Chl:C ratio decreases in cells acclimated to increasing light. There is a twofold decrease in the Chl:C ratio of *P. tricornutum*, from 13.8±1.7 mg Chl g C^{-1} at 30 µmol photon m^{-2} s^{-1} to 5.4±0.3 mg Chl g C^{-1} at 700 µmol photon m^{-2} s^{-1}. *T. pseudonana* shows a similar trend and slightly higher values, with a Chl:C ratio decreasing by 70% from 16.1±2.1 mg Chl g C^{-1} at 120 µmol photon m^{-2} s^{-1} to 6.3±0.2 mg Chl g C^{-1} at 700 µmol photon m^{-2} s^{-1}.

The decrease of the Chl:C ratio is about threefold in the cold-water species *C. brevis*, from 19.3±1.7 mg Chl g C^{-1} at 6 µmol photon m^{-2} s^{-1} to 6.2±0.6 mg Chl g C^{-1} at 147 µmol photon m^{-2}

s^{-1}. *T. antarctica* grown under 6 µmol photon m^{-2} s^{-1} presents the highest value of 28.1±3.0 mg Chl g C^{-1}, decreasing twofold to 9.5±0.7 mg Chl g C^{-1} at 147 µmol photon m^{-2} s^{-1}.

Maximal Chl:C ratio (θ_m) varies from 13.8 to 28.1 mg Chl g C^{-1}. θ_m was significantly lower in temperate-water species than in polar species, with 13.8±1.7 mg Chl g C^{-1} for *P. tricornutum* and 16.1±2.1 mg Chl. g C^{-1} for *T. pseudonana*, 21.4±2.1 mg Chl g C^{-1} for *C. brevis* and 28.1±3.0 mg Chl g C^{-1} for *T. Antarctica* (Welsh test, n=5, p=0.1072).

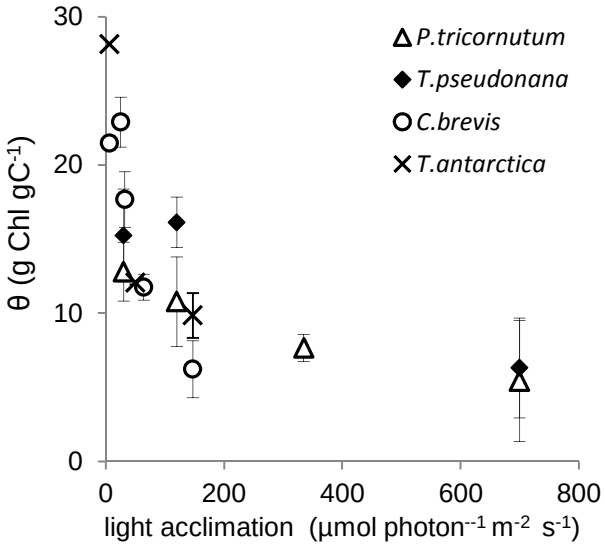

Fig.3.1. Chlorophyll: carbon ratio in four diatoms species, as a function of the acclimation light intensity. Error bars represent the standard deviation between replicates (n= 2 or 3).

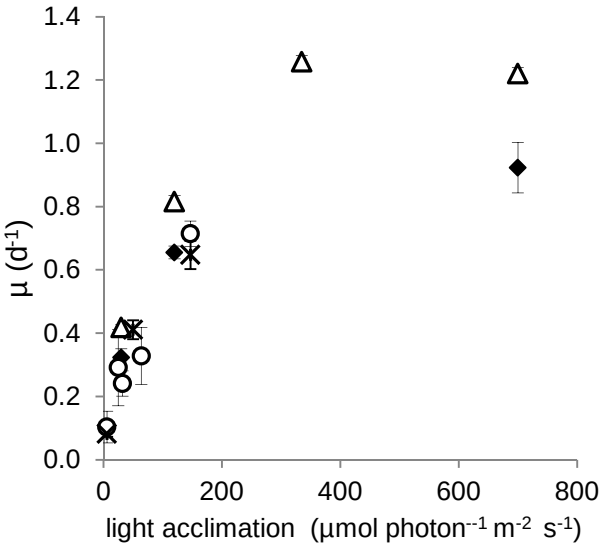

Fig.3.2. Growth rates as a function of the acclimation light intensity.

Growth rate

Diatom growth rates increase with the light intensity (Table 3.3 and Fig.3.2). *P. tricornutum* reaches a maximum of 1.26 d^{-1} at 335 µmol photon m^{-2} s^{-1}, above which the growth rate is saturated, while *T. pseudonana* has a maximum growth rate of 0.92 d^{-1}. The lack of data for *T. pseudonana* between 120 and 700 µmol photon m^{-2} s^{-1} does not allow us to identify the light-saturating irradiance.

The cold-water species show a similar increase in growth rate with a maximum of 0.71 d^{-1} for *C. brevis* and 0.65 d^{-1} for *T. antarctica* at 147 µmol photon m^{-2} s^{-1}. Growth rate data above 147 µmol photon m^{-2} s^{-1} would be necessary to determine their optimum growth irradiance.

3.3.2 Light-limited photosynthesis

Average values are 28±5 g C g Chl^{-1} m^2 mol photon^{-1} for *P. tricornutum*, 27±7 g C g Chl^{-1} m^2 mol photon^{-1} for *T. pseudonana*, 16±6 g C g Chl^{-1} m^2 mol photon^{-1} for *C. brevis* and 21±2 g C g Chl^{-1} m^2 mol photon^{-1} for *T. antarctica* (Table 3.3). There is a significant difference between polar and temperate species (n=55, p=1.21 x 10^{-10}). Morevoer, the average α^{Chl} for *C. brevis* is significantly lower than those for the three other species (n=55, p=1.49 x 10^{-7}).

Table 3.3: Average values of growth rate and photosynthetic parameters for *Phaeodactylum tricornutum*, *Thalassiosira pseudonana*, *Chaetoceros brevis* and *Thalassiosira antarctica* acclimated to different light intensities I (µmol photon m^{-2} s^{-1}): µ (d^{-1}), P_m and R_d (d^{-1}), α (g C g Chl^{-1} m^2 mol photon^{-1}); in brackets, standard deviations between PI curves.

	I	µ	Net P_m	R_d	α^{Chl}
P. tricornutum	700	1.21 (0.02)	4.17 (0.33)	0.60 (0.05)	34 (6)
	335	1.26 (0.02)	3.14 (0.23)	0.66 (0.06)	22 (1)
	120	0.81 (0.02)	2.29 (0.22)	0.62 (0.07)	26 (3)
	30	0.42 (0.01)	1.54 (0.16)	0.51 (0.03)	29 (4)
T. pseudonana	700	0.92 (0.08)	2.28 (0.17)	0.43 (0.04)	32 (3)
	120	0.66 (0.02)	1.95 (0.14)	0.13 (0.01)	18 (3)
	30	0.32 (0.03)	1.84 (0.16)	0.05 (0.01)	36 (4)
C. brevis	147	0.71 (0.04)	0.67 (0.07)	0.16 (0.02)	16 (4)
	64	0.33 (0.09)	1.29 (0.12)	0.24 (0.01)	24 (3)
	32	0.24 (0.12)	1.98 (0.05)	0.85 (0.07)	11 (2)
	25	0.29 (0.04)	0.52 (0.05)	0.16 (0.02)	20 (2)
	6	0.10 (0.05)	0.24 (0.06)	0.65 (0.04)	20 (2)
T. antarctica	147	0.60 (0.05)	1.36 (0.08)	0.50 (0.04)	21 (2)
	50	0.41 (0.03)	0.93 (0.04)	0.30 (0.02)	20 (1)
	6	0.08 (0.01)	1.04 (0.03)	0.52 (0.02)	25 (2)
average				**0.41 (0.27)**	**23 (6)**

The chlorophyll-specific light-limited photosynthetic rate shows small variation with the acclimation light intensity in the temperate species (Fig.3.3). In *P. tricornutum*, a Welch test reveals a significant difference of α^{Chl} between cultures grown at 700 and 335 µmol photon m^{-2} s^{-1} (n=8, p=0.0306). In *T. pseudonana*, α^{Chl} is significantly lower at 120 µmol photon m^{-2} s^{-1} that at 30 and 700 µmol photon m^{-2} s^{-1} (n=7, p=0.0014 and p=0.0013, respectively).

3.3.3 Light-saturated photosynthesis

The net light-saturated photosynthesis rate varies, after removal of the blank medium (see results below), from 1.09 to 4.76 d^{-1} in temperate species and from 0.41 to 2.43 d^{-1} in cold-water species (Fig. 3.4 and Table 3.3). P_m is significantly higher in temperate than in cold-water species (2.41±0.90 and 1.02±0.49 d^{-1}, respectively; ANOVA, n=58, p=2.30 x 10^{-9}).

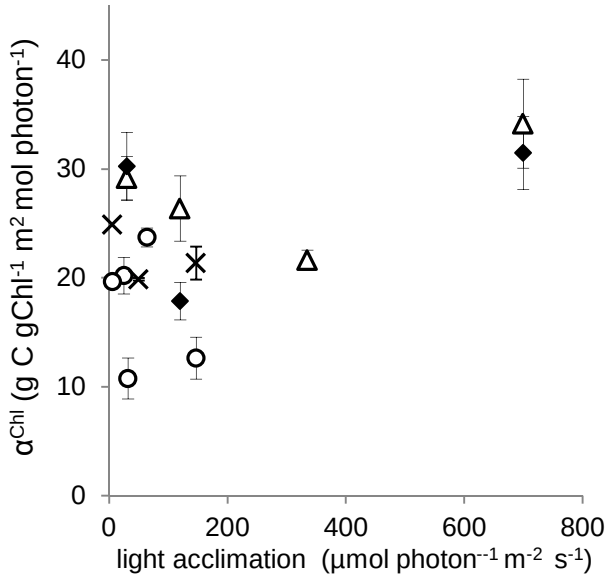

Fig. 3.3. Average values of the initial slope of the PI curve as a function of the acclimation light intensity. Error bars represent the standard deviation between PI curves.

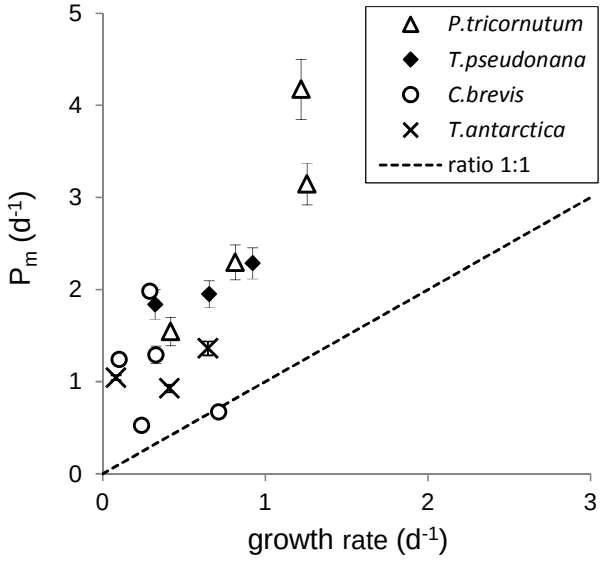

Fig. 3.4. Average of the gross maximal photosynthetic rate as a function of the growth rate. Error bars represent the standard deviation between PI curves.

There is a significant correlation between P_m and the acclimation light in *P. tricornutum* and *T. pseudonana*. Correlation coefficients are 0.9090 (ANOVA, n=20, p=2.92 x 10^{-8}) and 0.7316 (ANOVA, n=11, p=0.0105), respectively. P_m increases also significantly with the growth rate in *P. tricornutum* (ANOVA, r=0.8517, n=20, p=2.26 x 10^{-6}) and in *T. pseudonana* (ANOVA, r=7054, n=11, p=0.0248). In *T. Antarctica*, P_m at 147 µmol photon m^{-2} s^{-1} is significantly higher than P_m at 50 µmol photon m^{-2} s^{-1} (n=5, p=0.0085).

There is no significant difference in P_m for *C. brevis* with the light intensity (ANOVA, n=21, p=0.111) or the growth rate (p=0.199).

3.3.4 Respiration

A series of 14 PI curve experiments on Prochlorococcus shows an average oxygen consumption in darkness of 0.20 ± 0.10 nmol O_2 ml^{-1} min^{-1}. This result is used as the blank-medium. Assuming the same concentration of contaminant in concentrated samples of diatom cultures, we subtracted the blank-medium from our measurements.

The blank medium respiration is equal to 16 to 149% of our measured rates in darkness, with an average of 49%. In five PI curves, the oxygen evolution rate in darkness is lower than the rate of the blank medium, leading to negative respiration rates, i.e. oxygen production.

The final oxygen evolution rate in darkness ranges, in our experiments, from -0.06 to 1.32 d^{-1}. Rd is negative when the measured oxygen production rate is lower than the estimated blank-medium value. The average R_d for the four species is 0.41 ± 0.27 d^{-1} (Fig. 3.5).

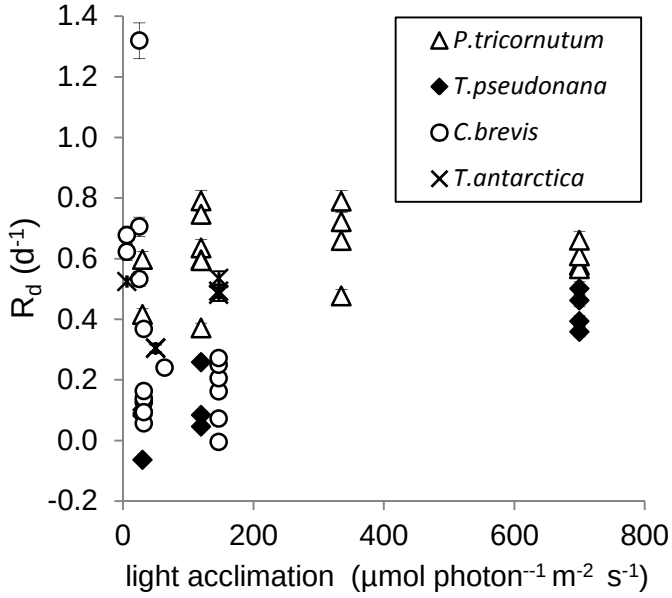

Fig. 3.5. Respiration rates per 24 hours for the four species as a function of the acclimation light intensity. Error bars represent the standard deviation between duplicates.

The experiments do not show any variation of R_d correlated with the temperature or the sampling time. However there is a significant difference between species (ANOVA, n=51, p=0.0003). In some species, R_d varied significantly among the cultures, as we detail below.

In *P. tricornutum*, R_d do not differ among the four cultures (p=0.2941 to 0.7821). In *T. pseudonana*, R_d in cells grown at the highest light irradiance is significantly higher than R_d in the two other cultures (n=7, p=0.0264 and n=8, p=0.0003). In this last species, we also observe a

significant linear correlation between R_d and the light intensity or the growth rate (ANOVA, n=11; r=0.9184, p=6.58 x 10^{-5} and r=0.8687, p=0.0022, respectively): R_d increases with the light intensity or the growth rate.

There is no relation between R_d and the light intensity or growth rate in *C. brevis* and *T. antarctica*. R_d varies from -0.005±0.000 d^{-1} to 1.32±0.06 d^{-1} in *C. brevis* (n=18), while it is more stable in *T. antarctica* since it varies among cultures from 0.30±0.01 d^{-1} to 0.53±0.02 d^{-1} (n=6). Nevertheless, some cultures differ to each other: in *C. brevis*, R_d is significantly higher at 6 µmol photon m^{-2} s^{-1} than at 32 and 147 µmol photon m^{-2} s^{-1} (n=8, p=1.36 x 10^{-4} and n=8, p=1.37 x 10^{-4}, respectively). In *T. Antarctica*, there is a significantly difference of R_d between cells grown at 147 and those grown at 50 µmol photon m^{-2} s^{-1} (n=5, p=0.0062).

3.4 DISCUSSION

3.4.1 Carbon, nitrogen and chlorophyll content

Carbon and nitrogen content

The carbon and nitrogen cellular contents, expressed per cellular volume, do not present any trend of variation common to the four species. The increase of carbon in the temperate species grown at low light intensity (30 µmol photon m^{-2} s^{-1}) is similar to observations by Langdon (1988) on *Skeletonema costatum*: although carbon and nitrogen contents did not vary between 110 and 450 µmol photon m^{-2} s^{-1}, the cellular content increased by 50% at 5 µmol photon m^{-2} s^{-1}. Bucciarelli et al. (2010) showed as well 25% increase of carbon content per volume in the diatom *Thalassiosira oceanica* grown at low light intensity (7.5 µmol photon m^{-2} s^{-1}), compared to cells grown at high light intensity (75 µmol photon m^{-2} s^{-1}). The increase of carbon content per cell at low light intensity is also visible in *Dytilum brightwelli*. There is not a common trend for the nitrogen content. Nitrogen content per cell and per volume in *Dytilum brightwelli* is twice higher at low-light intensity than at high-light intensity. On the contrary, nitrogen content in *Thalassiosira oceanica* does not differ with light intensity (Bucciarelli *et al.*, 2010).

Carbon: nitrogen ratio

Although three species showed a different C:N ratio at one irradiance, there is no evidence of a correlation between C:N ratio and the light intensity (Verity, 1981). C:N ratio values are similar to previously published data, where 85% of the C:N ratios vary from 4.3 to 8.3 g C g N^{-1}

(Sarthou *et al.*, 2005). In our experiments on *C. brevis*, the C:N ratio ranges from 2.48 to 8.14 g C g N^{-1}.

Chlorophyll content and chlorophyll: carbon ratio

The observed decrease of chlorophyll content with the light intensity has been widely reported (Beardall and Morris, 1976; Falkowski, 1985; Langdon, 1988), as well as the decrease of the Chl:C ratio. θ varies from 5.41 to 23.66 mg Chl g C^{-1}, which falls in the range of published data, though θ for temperate species are slightly lower in our experiments, with 13.75±1.65 mg Chl g C^{-1} for *P. tricornutum* and 16.14±2.10 mg Chl g C^{-1} for *T. pseudonana*. Literature data for *P. tricornutum* grown at continuous light range from 19.4 mg Chl g C^{-1} at 250 µmol photon $m^{-2}s^{-1}$ (Greene *et al.*, 1991) to 21.4 mg Chl g C^{-1} at 90 µmol photon m^{-2} s^{-1} (Kudo *et al.*, 2000) to 78.0 mg Chl g C^{-1} (Geider, 1985). For *T. pseudonana* grown in continuous light at 14 to 515 µmol photon m^{-2} s^{-1}, Geider (1984) reported 59 mg Chl g C^{-1}, which is about three times the present values.

Cold-water species present the highest θ_m, whose values are close to previous results (*T .antarctica* (grown in continuous light at 110-160 µmol photon m^{-2} s^{-1}): 21.41 mg Chl g C^{-1} (Hegseth, 1989); *C. calcitrans* (grown under 12:12 LD at 150 µmol photon m^{-2} s^{-1}): from 15 to 50 mg Chl g C^{-1} at 6 to 25°C, respectively (Anning *et al.*, 2001)). Ratios up to 36.0 mg Chl g C^{-1} (*Chaetoceros sp.* grown under 180 µmol photon. $m^{-2}.s^{-1}$: Lomas, 1998) or 31.25 mg Chl g C^{-1} (*C. debilis* grown under 250 µmol photon m^{-2} s^{-1}, Harrison *et al.*, 1977) have been observed.

Despite differences of θ values with literature data, diatom cells show a similar decrease of θ with the light intensity: in temperate species, the ratio still equals about 70% of its maximum in diatoms exposed to 50% of its saturation light for growth. The cold species reach about 40% of θ_m when grown at 30-50% of the saturation light for growth. Cellular contents for carbon, nitrogen and chlorophyll are variable among species and may vary under different growing conditions. However, the Chl:C ratio, by normalising the pigment content over the carbon content, represents the current photosynthetic state of the cell. The Chl:C ratio is clearly related to the acclimation light intensity of the cultures, which makes it one of the key parameters of the phytoplankton cell light-acclimation.

3.4.2 Light-limited photosynthesis rate

All species and acclimation conditions considered, the average light-limited photosynthesis rate is 22.46 g C g Chl^{-1} m^2 mol photon^{-1}, which is much higher than that found in previous studies. We develop below possible causes of this difference, as well as sources of variation of α^{Chl} within a species and within a sample.

In our experiments, the average initial slope of the PI curve for *P. tricornutum* and *T. pseudonana* are 27.66±5.11 and 27.30±6.65 g C g Chl^{-1} m^2 mol photon^{-1}, respectively. Data reported in the literature are much lower, as α^{Chl} values for *P. tricornutum* varies from 3.61 (Terry *et al.*, 1983) and 5.37 g C g Chl^{-1} m^2 mol photon^{-1} (Greene *et al.*, 1991) to 7.9 (Geider *et al.*, 1985) and 9.17 g C g Chl^{-1} m^2 mol photon^{-1} (McKay *et al.*, 1997). Published data for *T. pseudonana* are in the same range (6.39 g C g Chl^{-1} m^2 mol photon^{-1} in Geider, 1984). Our experiments on cold-water species show larger variability of α^{Chl} within species, with 16.11±5.52 g C g Chl^{-1} m^2 mol photon^{-1} for *C. brevis* and 21.44±2.08 g C g Chl^{-1} m^2 mol photon^{-1} for *T. antarctica.* As a comparison, rates for *C. calcitrans* range from 3.61 to 5.56 g C g Chl^{-1} m^2 mol photon^{-1} when grown at 6 to 25°C (Anning *et al.*, 2001).

As cellular content analysis shows, phytoplankton cells acclimate to different light intensities by modifying their chlorophyll content. Expressing the light-limited photosynthesis per chlorophyll instead of, for instance, per cell or per carbon, allows us to compare α values in cells grown at different irradiances. Therefore we would expect α^{Chl} not to vary with the acclimation intensity. The independence of α^{Chl} from the growth irradiance was shown in early experiments (Myers, 1970). Although there is no correlation between growth irradiance and α^{Chl} in our experiments, significant differences between some groups exist. This variability could come from the way the initial slope is graphically calculated from the curve, as is discussed below.

Variations in the light-limited photosynthesis rate can have several origins, such as the apparatus calibration, the chlorophyll content analysis, the light intensity measurement, the photosynthetic quotient used or the method used to calculate the initial slope, as we discuss later. While each of these parameters may have affected our results, it seems a major part of the difference with other data comes from the cellular chlorophyll content. When looking at the light-limited photosynthesis rate relative to the cell (α^{Cell}), our results for *P. tricornutum* (4.27 pg C cell^{-1} m^2 mol photon^{-1}) are similar to that of Greene (1991) (1.88 pg C cell^{-1} m^2 mol photon^{-1}). But chlorophyll contents widely differ: while we measured 45 to 123 fg Chl

cell^{-1}, Greene (1991) reported 250 fg Chl cell^{-1} in Fe-replete medium (and 57 in Fe-deficient medium). As a consequence, the initial slope expressed by cellular chlorophyll is much higher in our experiments: 28.6 g C cell^{-1} m^2 mol photon^{-1} (in diatoms grown under 335 µmol photon m^{-2} s^{-1}), whereas Greene found 5.28 g C cell^{-1} m^2 mol photon^{-1}. The same observation is made for *T. antarctica*, in which we measured up to 160 fg Chl cell^{-1}, while Hegseth (1989) reported 20,000 fg Chl cell^{-1} in the same species. Light-limited photosynthesis rate for *C. brevis* in our experiments was 16.14 g C g Chl^{-1} m^2 mol photon^{-1} while Anning (2001) reported 3.61 g C g Chl^{-1} m^2 mol photon^{-1} in *C. calcitrans*. This difference by four-threshold is likely to come from our chlorophyll content analysis, since we detected 71.6 fg Chl cell^{-1} in *C. brevis* when Anning reported 180.0 fg Chl cell^{-1} in *C. calcitrans*.

Comparison of α^{Chl} values from different publications is not straight forward, as the estimate of the initial slope of a PI curve is subject to variations depending on the method used. When determined with a model, the choice of the model affects the value of α^{Chl} (Henley, 1993; Frenette *et al.*, 1993). The convexity of the curve influences the length of the linear part, and this can vary depending on the model used (Jassby and Platt, 1976). Models from Webbs (1981) and from Jassby and Platt (1976) are commonly used within the literature. Although they both describe the photosynthetic rate as an exponential function of the light, the one from Jassby and Platt (1976) is more complex, requiring one more variable. As a consequence, the minimal cost function is smaller, the regression coefficient between model and observations is bigger and parameters such as P_m and α^{Chl} differ.

When using a graphic method, as we did in this experiment, consistency within a group is not obvious and determination of α^{Chl} can be easily subject to deviation. The initial part of the PI curve is calculated from the lowest light intensity. Therefore, the accuracy of the respiration rate and the number of points at light-limitation play a big role in the deviation of α^{Chl} within samples. The more points there are, the more accurate the slope will be. It is important to have not only data in the linear part but also close to the saturation point, when the slope approaches zero. For this reason, intervals between the light intensities chosen for the PI curve depended on the light acclimation of the cells: since high-light acclimated cells achieved saturation later than low light acclimated cells, the interval between each light intensity was larger for the latter than for the former ones. For example, we exposed *P. tricornutum* high-light acclimated cells to five different irradiances from 0 to 626 µmol photon m^{-2} s^{-1}, whereas for low-light acclimated cells, the five first irradiances ranged from 0 to 72 µmol photon m^{-2} s^{-1}, in order to be able to draw a

line before light-saturation. With *C. brevis*, five irradiances were used, from 0 to 224 µmol photon m^{-2} s^{-1}, for high-light acclimated cells, whereas five from 0 to 45 µmol photon m^{-2} s^{-1} were used for the low-light acclimated cells. Initial slopes were easily identified for *P. tricornutum*, whereas PI curves for *C. brevis* did not show a clear initial slope, because of a too small number of points, a very low dark respiration rates or a deviation between samples. With cells grown at 6 µmol photon m^{-2} s^{-1}, the photosynthesis rate is saturated at the third measurement (31 µmol photon m^{-2} s^{-1}), meaning that only three points are used to calculate the slope: the dark respiration rate and the two first photosynthetic rates (22 and 31 µmol photon m^{-2} s^{-1}).

Determination of α^{Chl} is subject to the difficulty of determining graphically the extent of the linear part of the curve, as no rule applies. In this study, we used two to five measurements (as in example above) to calculate α^{Chl}. The slope would be up to 50% higher if the linear part was considered shorter. As an example, in *C. brevis* grown at 6 µmol photon m^{-2} s^{-1}, α^{Chl} measured in duplicate between 0 and 18 µmol photon m^{-2} s^{-1} equals 28.4 and 32.5 gC $gChl^{-1}$ m^2 mol $photon^{-1}$. These rates fall to 19.3 and 20.0 gC $gChl^{-1}$ m^2 mol $photon^{-1}$, respectively, if the initial slope is prolonged until 36 µmol photon m^{-2} s^{-1} (Fig. 3.6).

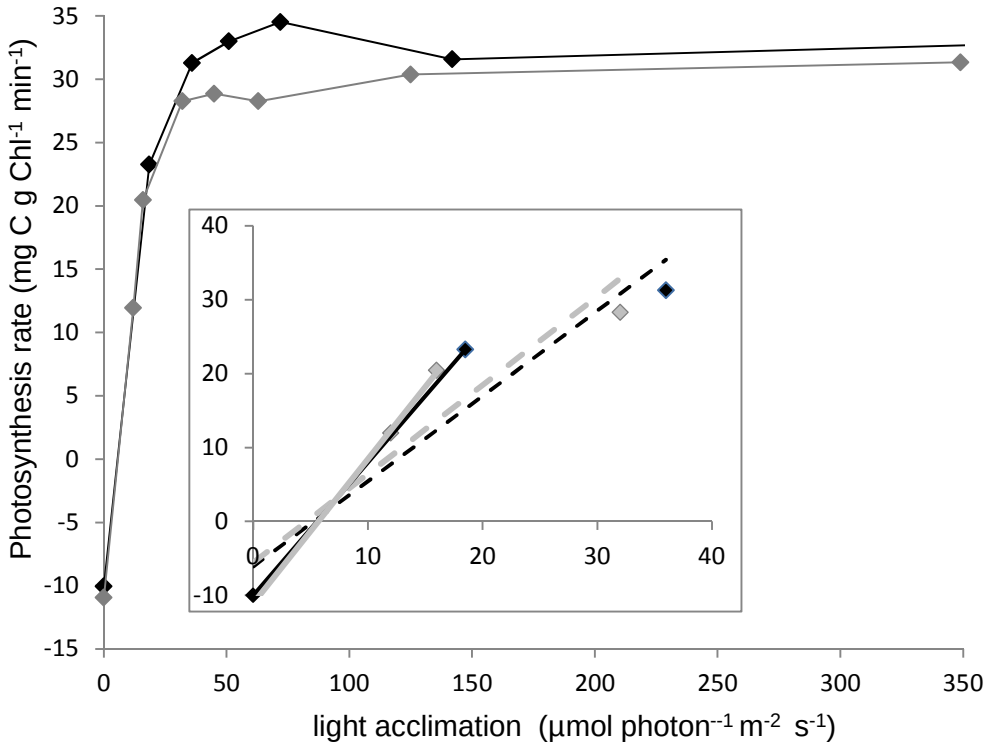

Fig.3.6. PI curves for *C. brevis* grown at 6 µmol photon m^{-2} s^{-1} (duplicates). Inset: initial slopes for each duplicate: solid lines, slopes from 0 to 18 µmol photon m^{-2} s^{-1}; dashed lines: slopes from 0 to 36 µmol photon m^{-2} s^{-1}.

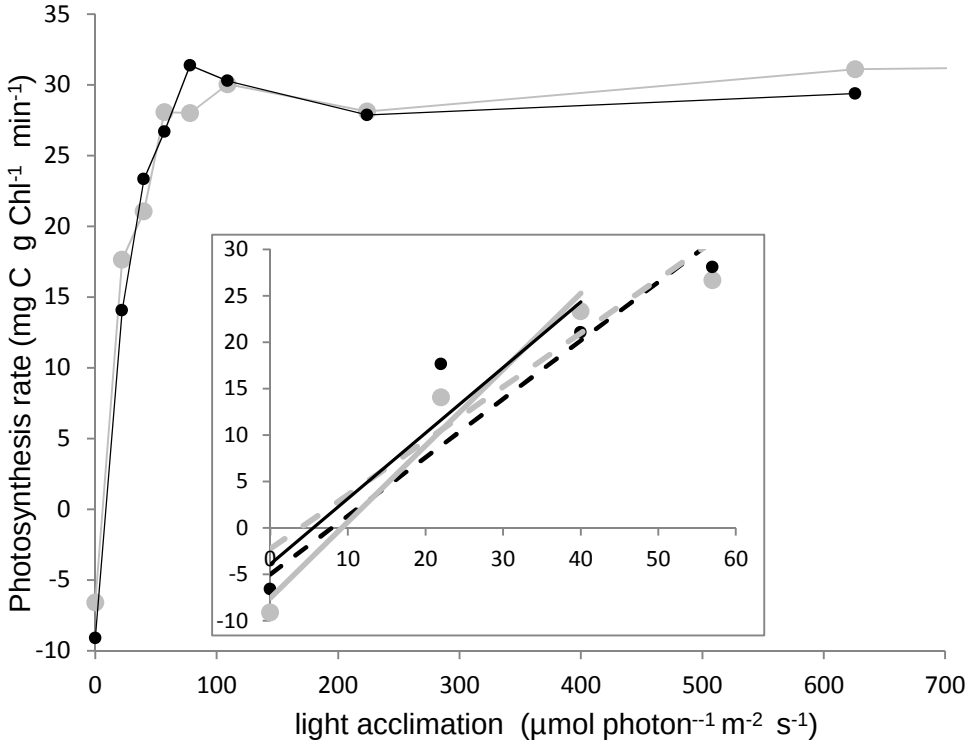

Fig.3.7. PI curves for *C. brevis* grown at 32 µmol photon m^{-2} s^{-1} (duplicates). Inset: initial slopes for each duplicate: solid lines, slopes from 0 to 40 µmol photon m^{-2} s^{-1}; dashed lines: slopes from 0 to 56 µmol photon m^{-2} s^{-1}.

3.4.3 Maximum photosynthetic rate

The maximum photosynthetic rate (P_m), expressed by carbon content, represents the cell growth. As the growth rate increases with the light intensity, we would expect an increase of P_m with the growth irradiance. This is the case for *P. tricornutum* (r=0.9090) and *T. pseudonana* (r=0.7316). However, there is no correlation between P_m and the light intensity in *C. brevis* and *T. antarctica*, though P_m in high-light acclimated cultures of *T. antarctica* is significantly higher than in the two other groups (p=0.0077).

Since cells adapt their physiology as a function of the environmental conditions, exposing cells to increasing light intensities can in theory affect their physiology. Henley (1993) recommends PI curve experiments should not last more than one hour and that light exposure should not last more than five minutes, to avoid acclimation of the cells to the new light intensity (Steemann Nielsen, 1949). We used this recommendation during our experiments on *P. tricornutum* and *C. brevis*. It was not always respected in our earlier experiments on

T. pseudonana. However, we did not find any correlations between experiment duration and any sign of photo-inhibition.

The maximum oxygen production per cell in *P. tricornutum* ranges from 0.80 to 2.40 pg C $cell^{-1}$ hr^{-1}, which is similar to the production reported by Greene (1991) (1.45 pg C $cell^{-1}$ hr^{-1} under 250 µmol photon m^{-2} s^{-1}). This shows our results of oxygen production per cell are close to the literature. A difference in oxygen production per chlorophyll content would be due to a low content in chlorophyll in our cultures.

Our lowest results for *T. pseudonana* maximum oxygen production per chlorophyll content show good agreement with the literature. It is equivalent to 8.0 to 20.7 g C g Chl^{-1} hr^{-1}, while previous results for the same species gave 8.6 and 9.4 g C g Chl^{-1} hr^{-1} (Dunstan, 1973 and Kolber *et al.*, 1988, respectively).

Our findings for *C. brevis* are closer to the literature data. The maximum oxygen production per cell, converted in carbon production, ranges from 0.29 to 0.84 pg C $cell^{-1}$ hr^{-1}, except for cells grown under 64 µmol photon m^{-2} s^{-1} where rates range from 1.06 to 1.15 pg C $cell^{-1}$ hr^{-1}. Anning (2001) reported 0.39 pg C $cell^{-1}$ hr^{-1}, for *C. calcitrans* grown under 150 µmol photon m^{-2} s^{-1}.

3.4.4 Respiration rate in darkness

One of the issues of our experiments is the variability in R_d. The standard deviation of R_d for the four species is equal to 67% of the average value itself.

A part of this variation comes from experimental procedures. The average standard deviation between replicates experiments (carried out at the same time of the day and the from same sample on two different Oxygraph) is 0.10, 0.06, 0.09 and 0.005 mol C mol C^{-1} 24 hr^{-1} for *P. tricornutum, T. pseudonana, C. brevis* and *T. antarctica*, respectively. This difference takes into account the variability between the two Oxygraph and the variation in oxygen concentration due to different calibration or mixing of the medium with a left-over of rinsing water in the chamber. The standard deviation of R_d within each species is 0.12, 0.19, 0.33 and 0.11 mol C mol C^{-1} 24 hr^{-1}, for *P. tricornutum, T. pseudonana, C. brevis* and *T. antarctica*, respectively.

Respiration rates found in the literature vary within and among species. Values from *P. tricornutum* range from <0.1 to 0.23 d^{-1} (Geider *et al.*, 1985; Laws and Bannister, 1980). Our results for this species are higher (average: 0.61 d^{-1}).

According to a review by Geider and Osborne (1989) of 15 publications, diatoms see their ratio of dark respiration to net maximal photosynthetic rate (R_d: P_m) ranging from 0.05 to 0.50. This ratio ranges, in our experiments, from 0.01 to 0.54, with an average of 0.24. The lowest ratio, below 0.06 in seven cases, were caused by a low R_d (between -0.005 and 0.1 d^{-1}). Although our respiration rates were sometimes very low, we obtain in a majority of cases a similar ratio R_d: P_m than reported in the literature.

3.4.5 Variations of P_m and R_d within a same sample or a same culture

As in any experiment, the measurement of P_m and R_d are subject to error, causing a variation of the parameters among several measurements. The error can have several origins.

As explained in Materials and Methods, a culture was sampled several times during the day of experiment. Each sample was used for two PI curve experiments, carried out with different Oxygraphs, resulting in duplicates. Oxygen measurements for both duplicates were processed using identical data on cell counting and carbon analysis. Therefore, the error between duplicates, i.e. the variations of parameter values between the two Oxygraphs, was due to variability in the oxygen measurement itself.

Although the same culture was sampled through the day, the parameter values obtained for the different samples can vary. If this variation is not due to biological effects, such as the time of day, it is considered to be due to measurement error. The error within the same culture is the combination of errors in sampling, cell counting, carbon and chlorophyll analysis as well as the oxygen evolution rates.

The relative error of R_d between duplicates ranges from 0.8% for *T. antarctica* grown at 147 µmol photon m^{-2} s^{-1} and sampled during the morning, to 923% for *T. pseudonana* grown at 30 µmol photon m^{-2} s^{-1} and sampled during the morning. The average error for all species is 75%.

Deviations of R_d values within the same culture range from 0.59% for *T. antarctica* grown at 50 µmol photon m^{-2} s^{-1} (n=2) to 150% for *P. tricornutum* grown at 30 µmol photon m^{-2} s^{-1} (n=4).

The relative error of P_m between duplicates ranges from 0.1% for *C. brevis* grown at 32 µmol photon m^{-2} s^{-1} and sampled during the afternoon, to 27% for *C. brevis* grown at 32 µmol photon m^{-2} s^{-1} and sampled during the evening. In 89% of the experiments, the relative deviation of P_m between duplicates is lower than 20%.

Deviations of P_m values within the same culture range from 1.2% for *C. brevis* grown at 6 µmol photon m^{-2} s^{-1} (n=2) to 35% for *P. tricornutum* grown at 30 µmol photon m^{-2} s^{-1} (n=6).

Variations of P_m measurements may result from an error in cell counting (0.08%), in carbon content analysis (0.1%) and in oxygen reading (0.16%), which, combined, create an error of 6.9% (in average for the four species). Therefore, we can expect a difference of at least 6.9% between duplicates. Some variations of P_m between duplicates are larger than 6.9%, meaning either our estimation of errors in P_m measurements was underestimated, or there is a factor, during the experiment, we did not take into account. This factor could be the measurement of R_d itself. Effectively, relative errors of R_d are greater than errors for P_m, showing the sensitivity of R_d measurements. Moreover, the large errors of P_m between replicates coincide with large errors in R_d, enhancing the consequence of an error of R_d measurement on the P_m value.

On the eventual presence of bacteria in our cultures.

Although precautions were taken during experiments to handle the cultures in axenic conditions, medium and glassware, we cannot assure the cultures were axenic. The Coulter counter, used during our experiment for cell counting, detects particles down to 2 µm. Bacteria would therefore not be detected, as their size ranges from around 0.1 to 1 µm. Bacteria can be autotroph, as cyanobacteria, or heterotroph, free-organism or attached to microalgae or particulate matter. Presence of bacteria in a culture can causes bias for photosynthesis measurements: heterotrophic organisms can consume dissolved nutrients and oxygen, while autotrophic organisms' oxygen production may interfere with the plankton photosynthesis to study.

Numerous studies report estimates of respiration in natural phytoplankton communities. An average respiration rate of bacteria and microheterotroph up to 3µm ranges from 1.25 to

2.81 mmol O_2 ml^{-1} d^{-1} (Hoppe *et al.*, 2008). A natural population filtered at 0.8 µm presents a respiration rate of 1.4 mmol O_2 $cell^{-1}$ d^{-1} (Reinthaler and Herndl, 2005).

However, it is obviously very difficult to estimate the eventual bacterial concentration in our culture. As an example, Soto et al (2005) studied the culture of *P. tricornutum* in the presence of bacteria. When the diatoms reach their maximum yield at 10^6 cells ml^{-1}, the bacteria population yields 10^7 cells ml^{-1}.

As batch cultures are inoculated in sterile medium every few days, it is unlikely that bacterial population would build up to high levels. Moreover, the centrifugation may have concentrated bacteria with the diatoms, or on the contrary may have separated them from bigger cells. The average oxygen evolution rate in darkness in our cultures was 820 nmol O_2 ml^{-1} d^{-1}, which is three-fold the rate in natural population reported by Hoppe *et al.* (2008). One could suppose that effect of bacterial respiration on our measurement would be negligible.

Although blank oxygen measurements were not carried out during our experiments, measurements in other culture media can give us some insight on the influence of bacteria. Values for blank were taken from experiments on a small strain of Prochlorococcus.

The oxygen evolution in the culture medium, filtered through 0.22 µm, can be used as the blank value for an axenic medium. The oxygen consumption rate in darkness varies from 0.051 to 0.201 nmol O_2 ml^{-1} min^{-1}, with an average of 0.099 ± 0.054 nmol O_2 ml^{-1} min^{-1} (Beate Stawiarski, personal communication). This indicates a loss of oxygen, probably through the electrode. The same culture filtered through 1 µm would contain contaminating bacteria. Oxygen consumption rate in darkness in this sample ranges from 0.052 to 0.361 nmol O_2 ml^{-1} min^{-1}, with an average of 0.202 ± 0.102 nmol O_2 ml^{-1} min^{-1}.

Considering the filtration through 0.22 µm eliminates bacteria, the difference in oxygen evolution between the two treatments gives an indication of the potential effect of bacteria respiration on oxygen level. This would reach in average 0.103 nmol O_2 ml^{-1} min^{-1}.

The standard error of oxygen evolution measurement in our duplicates approximates 0.156 to 0.649 nmol O_2 ml^{-1} min^{-1}. Therefore, the influence of bacteria respiration and oxygen depletion due to the medium does not affect our results.

3.5 CONCLUSION

Despite the many studies on photosynthesis in the last 70 years, very few of them report sets of photosynthesis parameters for different growth irradiances, coupled with cellular content. Our experiments on two temperate and two polar diatom species were an attempt to acquire α^{Chl} and P_m data as well as growth rate and cellular content, for several diatom strain cultures acclimated to different irradiances.

In general, our experiments confirm trends of photosynthesis parameters reported in previous studies, as for instance the independence of α^{Chl} with the growth irradiance, as well as the increase of P_m or growth rates with light, as for *P. tricornutum*. However, variability arising within our samples and between our samples and the literature deserves deeper examination. As previously described (Geider *et al.*, 1997), the Chl:C ratio decreases with the light intensity. However, values for this study are lower than those previously reported, mainly because of lower chlorophyll content values. This affect as well α^{Chl}: the chlorophyll-dependent initial slope ends up very much higher than that in the literature.

Moreover, the measurement itself of the initial slope can be improved. For instance, initial slope of PI curve measured over only two or three light intensities, as for *T. antarctica* grown at 6 µmol photon m^{-2} s^{-1} proved to be not reliable. Then, R_d affects the initial slope. In our experiments, R_d is often low, therefore increasing the slope of the initial part of the PI curve. For *T. antarctica* grown at 147 and 50 µmol photon m^{-2} s^{-1}, α^{Chl} would decreases from 21.3 and 19.9 g C g Chl^{-1} m^2 mol $photon^{-1}$, respectively, to 16.3 and 16.0 g C g Chl^{-1} m^2 mol $photon^{-1}$, respectively, if the slope was calculated without taking into account the dark respiration rate.

In order to decrease error in α^{Chl} and to identify the origins of variation, variability coming from light measurement, chlorophyll and carbon content analysis or oxygen measurements should be minimized throughout all the experiment. This involves a closer monitoring of the algal growth, more replicate sampling and a more consistent determination of the respiration rate in darkness. Although the technique of oxygen measurements with the Oxygraph is reliable, supplementary experiments would help identifying the origin of the variations. Experiments at different stages of the exponential growth phase would reveal any variation of α^{Chl} and P_m over the day or the growing phase. Tests on the Oxygraph with blank medium and filtered medium (free from algae but containing any eventual bacteria) would give useful insight on the impact of bacteria on oxygen production. Light intensity measurements can simply be improved by using

a sensor fitting inside the Oxygraph chamber. Experiments on species growing in warm water would give us information on the dependence of cellular content and photosynthesis parameters on temperature.

Data on growth rates and cellular content of the four species can be used to optimise the photosynthesis model. Observational data of growth rate, Chl:C ratio and growth irradiance are used to calibrate the photosynthesis model (Buitenhuis and Geider, 2010), as explained in Appendix II. The optimisation of α^{Chl}, θ_m and μ_m (Annexe II) gives θ_m values similar to those we measured on our cultures. However, α^{Chl} and P_m are lower in the optimisation. The PI curve parameters were calculated directly from oxygen production measurements, cell count and chlorophyll content. On the contrary, the optimisation program uses the growth rate, and Chl:C ratioto constrain the parameters. The optimised values for θ_m figure at the lower edge of the dataset of compiled data (Fig. B.2 in annexe II). A difference between measured and optimised parameters would mean either an error in our analysis or calculation, e.g. chlorophyll analysis, growth or respiration rate, or poorly constrained parameters in the model. Points from measured parameters α^{Chl} and θ_m are situated along a line (r=0.8699), suggested a constant ratio α^{Chl}: θ_m in our experiments. However, this should not be considered to be always the case.

CHAPTER 4

DIATOMS IN THE GLOBAL OCEAN BIOGEOCHEMICAL MODEL PLANKTOM5

4.1 INTRODUCTION

Ocean modelling is of great interest, and so is plankton modelling: understanding ecosystem processes and quantifying them could help predicting the response of the oceans to future climate.

Building a model involves three stages: establishing the complexity and structure of the ecosystem, finding the best representative equations and finally their parameters. Choosing the right parameter value for the model is of key importance to modelling. In the PlankTOM5.3 model, plankton species realizing the same specific biochemical reactions are grouped into five Plankton Functional Types (PFTs). This study focuses on one of them, the diatoms, characterised by their silicate envelope and their high growth rate in nutrient replete conditions.

Diatom growth is calculated as a function of temperature, irradiance, nutrient concentration and mortality. Data presented in chapter 2 and 3 showed the wide range of physiological parameter values such as temperature dependence and photosynthetic rates. Apart from finding good representation of the average, modellers should also be able to estimate the error associated with each parameter and the consequent deviation of the model output. Effectively, until now, no sensitivity study has been done on plankton growth parameters of PlankTOM5.3. Parameter values are estimated from experimental work or field data.

This chapter examines the representation of diatom growth as a function of the temperature and of their photosynthesis. The objective of this study is twofold. First we aim to improve the representation of diatoms, i.e. to implement growth parameters that fit better to observations than the current ones. Secondly, our data analysis allows us to estimate the parameter variability within diatoms. Diatoms are diverse in size and by consequence in growth rate. Photosynthetic parameters can vary as well depending on the species. Therefore it is very difficult to provide modellers with average parameter values still representing the whole PFT. However, the deviation of those parameter values gives an indication of the diatom diversity. By running the model using extreme values we can estimate the extreme impact of the PFT on ocean ecosystems.

While temperature dependence is modelled in the current model PlankTOM5.3 by the Eppley curve (1972), we suggest another equation based on experimental data (Chapter 2) and present the associated changes in biological outputs. Simulations using an average function and a maximal function give us an estimate of the model deviation. Photosynthesis is represented by a light-iron co-limitation model (Buitenhuis and Geider, 2010). According to the results of photosynthesis-irradiance experiments (PI curves, chapter 3) we modified the photosynthesis parameters of PlankTOM5.3 and investigated the effects on biological production and carbon export. The range of parameter values among our results and between our results and literature data is considered as the plausible natural deviation among diatoms.

4.2 MATERIALS AND METHODS

4.2.1 PlankTOM5.3 model

The PlankTOM models are global dynamic green ocean models, composed of a biogeochemical model coupled to a physical model. The PlankTOM series of models are based on the ocean biogeochemistry model PISCES-T (Aumont *et al.*, 2003), in which ecosystem dynamics are represented by Plankton Functional Types (PFTs). PlankTOM5 describes the full cycles of N, Si, C, and O_2, a simplified cycle of Fe and biogeochemical processes such as nitrogen fixation and particle ballasting. The physical characteristics of the ocean are described in the general circulation model NEMO (Madec, 2008). The sea-ice dynamic is also included through the thermo-dynamic sea-ice model LIM (Timmermans *et al.*, 2005). PlankTOM5 has a horizontal resolution of 2° longitude and on average 1.1° latitude, and a vertical resolution of 10 m in the upper 100 m, increasing to 500 m at 5 km depth.

PlankTOM5 includes three phytoplankton PFTs (pPFTs: diatoms, coccolithophores and mixed-phytoplankton) and two zooplankton PFTs (zPFTs: proto- and meso-zooplankton). The lastest version, PlankTOM5.3 (Buitenhuis and Le Quéré, submitted) was developed from PlankTOM5.2 (Buitenhuis *et al.*, 2010) and includes the dynamical light-iron co-limitation photosynthesis model (Buitenhuis and Geider, 2010), the biophysical feedback through heat absorption by chlorophyll for each pPFT (Manizza *et al.*, 2006) and a new parameterisation of the ballasting effect.

4.2.2 Photosynthesis model

Phytoplankton growth is described in the six equations, as follows. The variation of phytoplankton concentration is calculated as:

$$\frac{\delta P_i^e}{\delta t} = (1\text{-}d)\ \mu_{Pi}^e\ P_i^C - w_{Pi}\ P_i^C\ P_i^e - \Sigma^j\ g_{Zj}^{Pi}\ Z_j\ P_i^e \qquad (1)$$

where P_i^e is the concentration of element e in phytoplankton i (diatoms, coccolithophores and mixed phytoplankton), in which the elements e are C, Fe or Chl, d is the fraction of primary production that is exuded as DOC, μ_{Pi}^e is the growth rate of phytoplankton (Eqs. 2, 4, 5), w_{Pi} is the generic loss rate (Eq. 6), and g_{Zj}^{Pi} is the grazing rate of zooplankton Z_j on phytoplankton P_i (Buitenhuis *et al.*, 2006; 2010). The loss rates are the same for all elements. The ratio O: C: N: P in phytoplankton is fixed to 172: 122: 16: 1. Content in O, N and P vary as a function of the carbon content, which is calculated as in (2). Fe:C, Chl:C and Si:C ratios are variable.

The growth rates are different for each element, based on the iron-light colimitation model of Buitenhuis and Geider (2010), as follows. The growth rate for carbon is:

$$\mu_{Pi}^C = P^C_m \times (1\text{-}\exp(\ \frac{-\alpha^{Chl}\,\theta\,I}{P^C_m}\ ))\ \qquad (2)$$

where P^C_m is the maximum photosynthesis rate (Eq. 3), α^{Chl} is the constant initial slope of the PI curve, θ is the variable Chl:C ratio, and I is the light intensity.

The maximum photosynthesis rate is:

$$P^C_m = \mu_{max,\,0°} \times Q_{10}^{(T/10)} \times \min(\ \frac{Q - Q_{min}}{Q_{opt} - Q_{min}},\ \frac{NO_3}{K_{½,\,NO3} + NO_3},\ \frac{SiO_3}{K_{½,\,SiO3} + SiO_3}, 1) \qquad (3)$$

where $\mu_{max,\,0°}$ is the maximum growth rate at 0°C, Q_{10} is the temperature dependence of growth, T is temperature in degrees Celsius, Q is the internal phytoplankton Fe:C quota, NO_3 and SiO_3 are the seawater nutrient concentrations, and $K_{½}$ are the half saturation concentrations for growth.

The growth rate for iron is:

$$\mu_{Pi}^{Fe} = (\rho^{hi}_{max} - (\rho^{hi}_{max} - \rho^{lo}_{max}) \times (\ \frac{Q - Q_{min}}{Q_{max} - Q_{min}})) \times Q_{10}^{(T/10)} \times (\frac{Fe'}{K_{½,\,Fe} + Fe'}\ ) \qquad (4)$$

where ρ^{hi}_{max} is the maximum iron uptake rate at iron limitation, and ρ^{lo}_{max} (= $\mu_{max}\, Q_{max}$) is the steady state iron uptake rate at saturating iron concentrations, Fe' is the dissolved iron concentration and $K_{½,\,Fe}$ is the half saturation concentration for iron uptake. The maximum rate of uptake is down-regulated with the accumulation of cellular iron (Q_{max}), while it is enhanced at low cellular iron content (Q_{min}). PFTs are allowed for excess iron uptake, or "luxury uptake".

The growth rate for chlorophyll is:

$$\mu_{Pi}^{Chl} = (P^{C}_{m} \times (1-\exp(\frac{-\alpha^{Chl}\,\theta\, I}{P^{C}_{m}})))2 \times \frac{\theta_m}{\alpha^{Chl}\,\theta\, I} \quad (5)$$

where θ_m is the maximum Chl:C ratio.

The loss term, which is increased in diatoms during nutrient limitation, is

$$w_{Pi} = (L + L_{dia} \times (1 - \min (\frac{Fe'}{K_{½,\,Fe}} , \frac{NO_3}{K_{½,\,NO3}} , \frac{SiO_3}{K_{½,\,SiO3}} ,1))) \quad (6)$$

where L is the loss rate and L_{dia} is the additional loss term for diatom aggregation. Here, the loss term is represented only by the respiration (R_d).

4.2.3 Parameterisation

As can be seen from the above equations, the physiology and ecosystem turnover rates of diatoms (and other phytoplankton) are controlled by 15 parameters. The nutrient limitation parameters ($\rho^{hi}_{max}/\rho^{lo}_{max}$, $K_{½,\,Fe}$, Q_{min}, Q_{opt}, Q_{max}, $K_{1/2,NO3}$, $K_{1/2,SiO3}$) and phytoplankton turnover rates (L, L_{dia}) were as in Buitenhuis and Geider (2010) (table 4.1). The grazing rates of zooplankton (g_{Zj}^{Pi}) are as in Buitenhuis *et al.* (2006, 2010). The diatom maximum growth rate parameters ($\mu_{max,\,0°}$, Q_{10}) for the original simulation are as in Eppley (1972). The new parameter values result from our temperature-dependence study described in chapter 2.

The values of the light-limitation parameters (α^{Chl}, θ_m) in the original simulation are the average values for three PFTs from Geider *et al.* (1997). The new parameters are from our light-acclimation experiments described in chapter 3. The loss rate in the original simulation was from Aumont *et al.* (2003). We used in the experimental simulations the respiration rate (R_d) from chapter 3.

4.2.4 Simulations

The PlankTOM5.3 model was run eight times. The initial run (EPP, as for Eppley curve) includes parameters as they were before any modifications related to this study were done (Buitenhuis and Le Quere (*submitted*). Most of the parameters were taken from the literature. By comparing two simulations where only one parameter was different, we are able to study the effect of each parameter on the plankton distribution.

Table 4.1: Phytoplankton parameters in PlankTOM5.3

description	parameter	value	n	reference
fraction of PP as DOC	d	0.05	46	Nagata 2000
increase in Fe-limited uptake rate	$\rho^{hi}_{max}/\rho^{lo}_{max}$	29	1	Buitenhuis and Geider 2010
half saturation Fe uptake (diatoms)	$K_{½,Fe}$	5.2	1	Buitenhuis and Geider 2010
minimum Fe:C ratio (diatoms)	Q_{min}	2.5	1	Buitenhuis and Geider 2010
optimum Fe:C ratio diatoms	Q_{opt}	3.2	1	Buitenhuis and Geider 2010
maximum Fe:C ratio (diatoms)	Q_{max}	47	1	Buitenhuis and Geider 2010
half saturation growth N (diatoms)	$K_{½,\ NO3}$	6.6		Buitenhuis *et al.* 2010
half saturation growth Si (diatoms)	$K_{½,\ SiO3}$	4		Aumont *et al.* 2003
additional nutrient limited loss rate (diatoms)	L_{dia}	0.1		Aumont *et al.* 2003

In the first series of experiments, we tested the model sensitivity to the maximum growth rate parameters (Fig.4.1). In the original model PlankTOM5.3 (simulation EPP), the relationship between diatom growth rate and temperature is represented by the exponential function from Eppley (1972)

$$\mu_{max} = 0.59 * 1.066^{T} \quad (7)$$

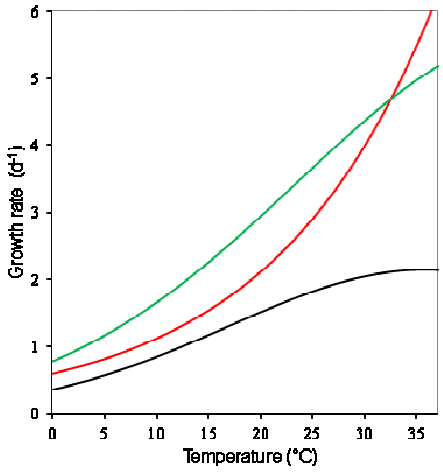

Fig.4.1: Temperature dependence of the diatom growth rate, as defined by Eppley curve (red, simulation EPP), Equ.(5) (black, simulation OPT) and Equ.(9) (green, simulation OPTm).

According to results from chapter 2, the function fitting the best to the average diatom growth rate is an optimal function. While some modellers may use the function fitted to the upper-edge of the plot (Equ. 9), we have chosen, as explained in chapter 2, to use the average function. Therefore, the simulation OPT uses the average growth rate defined by Equ. (5).

Table 4.2: Parameter values used for the different simulations of PlankTOM5.3: A) change in temperature-dependence function, B) change in photosynthetic parameters, C) change in loss rate (respiration rate); grey shading indicates same value than in the original model (EPP); simulations in bold are used as control for each experiment.

A	run	**μ_{max}**	**Temperature function**	α^{Chl}	θ_m	loss rate (R_d)
	EPP	0.59	1.066^{T}	9.48	0.056	0.10
	OPT	2.15	$\exp[-(T-35.8)^2/27^2]$	9.48	0.056	0.10
	OPTm	5.66	$\exp[-(T-46.8)^2/33^2]$	9.48	0.056	0.10

B	run	μ_{max}	Temperature function	**α^{Chl}**	**θ_m**	loss rate (R_d)
	OPT	2.15	$\exp[-(T-35.8)^2/27^2]$	9.48	0.056	0.10
	Alp	2.15	$\exp[-(T-35.8)^2/27^2]$	18.36	0.056	0.10
	Tht	2.15	$\exp[-(T-35.8)^2/27^2]$	9.48	0.030	0.10
	AT1	2.15	$\exp[-(T-35.8)^2/27^2]$	18.36	0.030	0.10
	AT2	2.15	$\exp[-(T-35.8)^2/27^2]$	27.48	0.015	0.10

C	run	μ_{max}	Temperature function	α^{Chl}	θ_m	**loss rate (R_d)**
	AT1	2.15	$\exp[-(T-35.8)^2/27^2]$	18.36	0.030	0.10
	RD	2.15	$\exp[-(T-35.8)^2/27^2]$	18.36	0.030	0.18

Moreover, we want to estimate the sensitivity of the model to the diatom growth rate, i.e. to test the extreme values. In order to estimate the maximum diatom production, we apply in the simulation OPTm the optimal function fitted to the upper edge of the database (Equ. 9). Testing the model with OPTm will provide us with an estimate of the sensitivity of the model to high diatom growth rates.

Outputs of simulation OPT and OPTm are compared to those of the simulation EPP.

In the second series of experiments, we incorporate photosynthetic parameters described in chapter 3 and in Annexe I. The temperature-dependence function used as in OPT.

First we experiment an increase of α^{Chl} (simulation Alp), then a decrease of θ_m (simulation Tht) and, in the simulation AT1 we change both parameters. Finally, in the simulation AT2, α^{Chl} and θ_m are both changed again, increasing the difference with the original parameter.

All simulations are compared to the run OPT.

For the third experiment, the temperature-dependence function is as in OPT and photosynthetic parameters are as in AT1. The diatom respiration rate in darkness (R_d) was increased in simulation RD. Outputs are compared to those of the simulation AT1.

PlankTOM5.3 was run for six years, from 1990 to 1996, minimum time necessary to obtain balanced outputs. Results presented are the output for the last year simulation.

The simulation OPT was also run during six more years, from 1997 to 2002, in order to calculate the inter-annual variability of each parameter (Table 4.3). This period was chosen because it covers a period of El Nino event, known to cause changes in plankton production.

4.2.5 Interpretation

The effects of changes in parameters were studied through phytoplankton and zooplankton abundance and distribution. Global primary production and carbon export at 100m were compared, as well as grazing rates and PFT biomass. Global distribution, concentration over latitude and over time are presented for each PFT. Concentrations are integrated vertically, i.e. summed over the first 200m, resulting in a concentration in µg C m^{-2}. Zonal average

concentrations per depth, presented as a function of latitude, are expressed in µg C L^{-1}. Hoffmüller plots are used to present vertically-integrated PFT concentration per latitude and per month, expressed in µg C m^{-2}. Nutrients and iron concentrations over the year, averaged over the first 200m, are expressed in µmol L^{-1} or pmol L^{-1}.

Our analysis focuses on two specific areas presenting a high diatom production: the North Atlantic (NAt) and the South East Pacific (SEP). We will describe the outputs of our simulations as increasing (decreasing) or higher (lower) when the output is higher (lower) than that in the simulation of reference.

The simulations were evaluated comparing PFT biomass and abundance field data compiled in the Marine Ecosystem Biomass Data (MAREDAT) database. Observations were gridded into the model grid. For each PFT we calculated the average residual sum of squares:

$RSS = \Sigma (\text{model - observation})^2$

We calculated 95% confidence intervals of phytoplankton biomass from the ratio of two RSS values, using the formula [*Abramowitz and Stegun*, 1972]:

$$\frac{RSS}{RSS_{min}} = 1.645 \times \frac{n}{n-2} \times \sqrt{\left(\frac{2(2n-2)}{n(n-4)}\right)} + \frac{n}{n-2} \qquad (8)$$

where RSS_{min} is the value for the simulation that best fit the observations, RSS are the values for the model simulations that are inside or just outside the confidence interval, 1.645 is the F distribution value for p = 0.05, and n is the degree of freedom. We approximated n with the number of observations.

4.3 Results and Analyses

4.3.1 Global primary production

Primary production ranges from 47.99 to 50.22 Pg C yr^{-1} (simulations EPP and AT1, respectively). Global production of diatoms ranges from 0.202 to 0.250 Pg C yr^{-1}, that of mixed-phytoplankton from 0.799 to 1.044 Pg C yr^{-1}, that of coccolithophores from 0.282 to 0.414 Pg C yr^{-1}, that of meso-zooplankton from 0.068 to 0.079 Pg C yr^{-1} and that of proto-zooplankton from 0.157 to 0.246 Pg C yr^{-1} (Table 4.3).

We observe a large variation in PFTs abundance other than diatoms. Small changes in diatom biomass lead to large variations in other PFT production (e.g. after change in growth parameters), and reciprocally (e.g. after change of α^{Chl}). Increase of diatom biomass causes increases or decreases of other PFTs biomass. The biggest variation of primary production occurs with the simulation AT1 (change of α^{Chl} and θ_m), where it increases by 3.7%, from 48.64 Pg C yr^{-1} in OPT to 50.44 Pg C yr^{-1} in AT1.

Table 4.3. Primary production, export at 100 m (Pg C yr^{-1}), and PFTs biomass (Pg C) for each simulation. Inter-annual var.: inter-annual variability calculated over a run of 6 years; Mean and standard deviation (St.Dev.) and error do not take into account simulations Alp and Tht. PP: primary production, DIA: diatoms, COC: coccolithophores, MIX: mixed-phytoplankton, PRO: protozooplankton, MES: mesozooplankton; DIA %: proportion of diatoms among total phytoplankton.

	PP	Export	DIA	COC	MIX	PRO	MES	DIA %
EPP	48.0	9.42	0.219	0.335	1.012	0.211	0.077	14.0
OPT	47.3	10.05	0.235	0.297	1.044	0.193	0.079	15.7
OPT_m	48.6	9.05	0.213	0.336	0.809	0.190	0.068	14.9
Alp	49.2	9.13	0.250	0.282	0.847	0.157	0.078	18.1
Tht	50.0	8.38	0.122	0.467	0.750	0.211	0.065	9.1
AT1	50.4	8.50	0.202	0.414	0.962	0.246	0.074	12.8
AT2	49.2	8.93	0.205	0.343	0.810	0.203	0.067	15.0
RD	49.0	9.00	0.210	0.414	0.962	0.192	0.068	15.4
Inter-annual variation	(0.2)	(0.14)	(0.006)	(0.011)	(0.007)	(0.002)	(0.001)	(0.3)
MEAN	**48.8**	**9.16**	**0.214**	**0.348**	**0.906**	**0.206**	**0.072**	**14.6**
St. Dev.	**1.08**	**0.53**	**0.012**	**0.039**	**0.113**	**0.021**	**0.005**	**1.1**
St. error (%)	**2.2**	**5.7**	**5.6**	**12.4**	**11.2**	**10.3**	**7.2**	**7.3**

4.3.2 Plankton distribution in the original simulation (EPP)

In the following sections we describe the distributions of each functional type for the simulation EPP. Global distributions are displayed in Fig. 4.2.

4.3.2.1 Diatoms

The largest abundance of diatoms is situated in the Equatorial Pacific and the Southern Ocean (Fig. 4.2 A and B). They are also well represented in the North-East Pacific, North Atlantic and equatorial Atlantic. They are absent from tropical gyres of the Pacific. The highest

concentration reaches 2.1 µg C m^{-2} in the Equatorial Pacific and 1.8 µg C m^{-2} in Southern Ocean waters. Production in the North Atlantic just reaches 1.3 µg C m^{-2}.

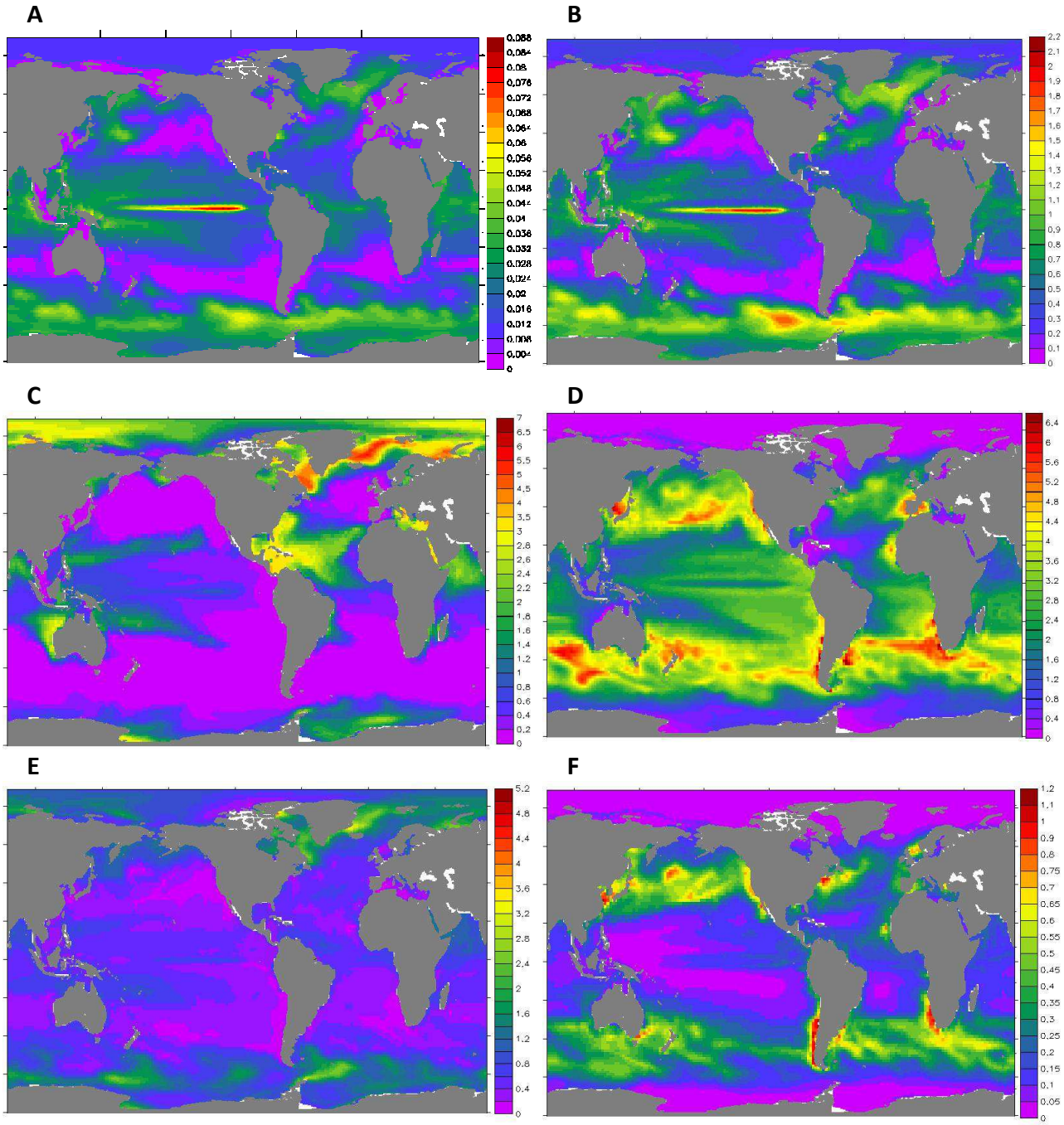

Fig. 4.2: Global PFTs distribution for simulation EPP: vertically integrated concentrations. A) diatom chlorophyll [µg Chl m^{-2}], B to F [µg C m^{-2}] B) diatoms, C) coccolithophores, D) mixed-phytoplankton, E) proto-zooplankton, F) meso-zooplankton.

Primary production at low latitudes and in polar areas differs by two main criteria:

- The production in polar areas is subjected to high seasonality, whereas the equatorial production is quasi-constant over the year (Fig. 4.3 A).

- The polar biomass is concentrated in the surface layer (0-100m), whereas the maximum at low latitudes is situated at 50-100m (Fig. 4.3 B).

Moreover, in the Southern Ocean, the bloom starts in September at 50°S and extends both northward and southward up to 40-80°S, with a peak in November and December of 2.5 µg C m^{-2} (Fig. 4.3 B). In the North Atlantic, maximal concentrations occur in April-May at 60°N, with a peak of up to 2.2 µg C m^{-2}.

This distribution pattern is close to observations, which have shown the predominance of diatoms in nutrient-rich waters of up-welling, as the Equatorial Pacific, and in polar waters (Uitz *et al.*, 2006, based on satellite data).

In the Southern Ocean, concentrations are maximal at the surface, from 0 to 50 m, up to 9.2 µg C l^{-1} (Fig. 4.3 A). The annual and zonal average concentration is up to 2.5 µg C m^{-2} at 55°S (Fig. 4.3 B). The diatom distribution in the Southern Ocean reflects the physical dynamic and chemical properties of this area. The upwelling of deep waters south of the Antarctic Polar Front at 45-50°S brings nutrient-rich water to the surface and enables the bloom. Moreover, diatoms could not grow without the required iron. Recent observations have shown the presence of available dissolved iron in surface waters of the Southern Ocean (Sarthou *et al.*, 2011; Klunder *et al.*, 2011).

The distribution of the diatom chlorophyll biomass differs slightly from that of the carbon. The depth-integrated annual average chlorophyll concentration reaches its maximum not in the Southern Ocean, but in the Pacific equatorial gyre (up to 0.088 µg Chl m^{-2}) (Fig. 4.2 A). The annual average concentration in the Southern Ocean is up to 0.060 µg Chl m^{-2}. The distribution over depth differs as well: the maximum concentrations in Chlorophyll are slightly deeper, likely because the Chl:C ratio increases with a decrease in light intensity. The peak in the equatorial zone is situated at 80/100 m, with a zonal average of 0.32 µg Chl l^{-1} (Fig. 4.3 C). At 60°S, the maximum chlorophyll concentration extends until 80 m (0.24 µg Chl l^{-1}). In the northern hemisphere, the chlorophyll concentration is maximal at 100 m (0.14 µg Chl l^{-1}). The distribution over time shows higher chlorophyll concentration at the beginning of the blooms, when the carbon biomass is still at low level (Fig. 4.3.D).

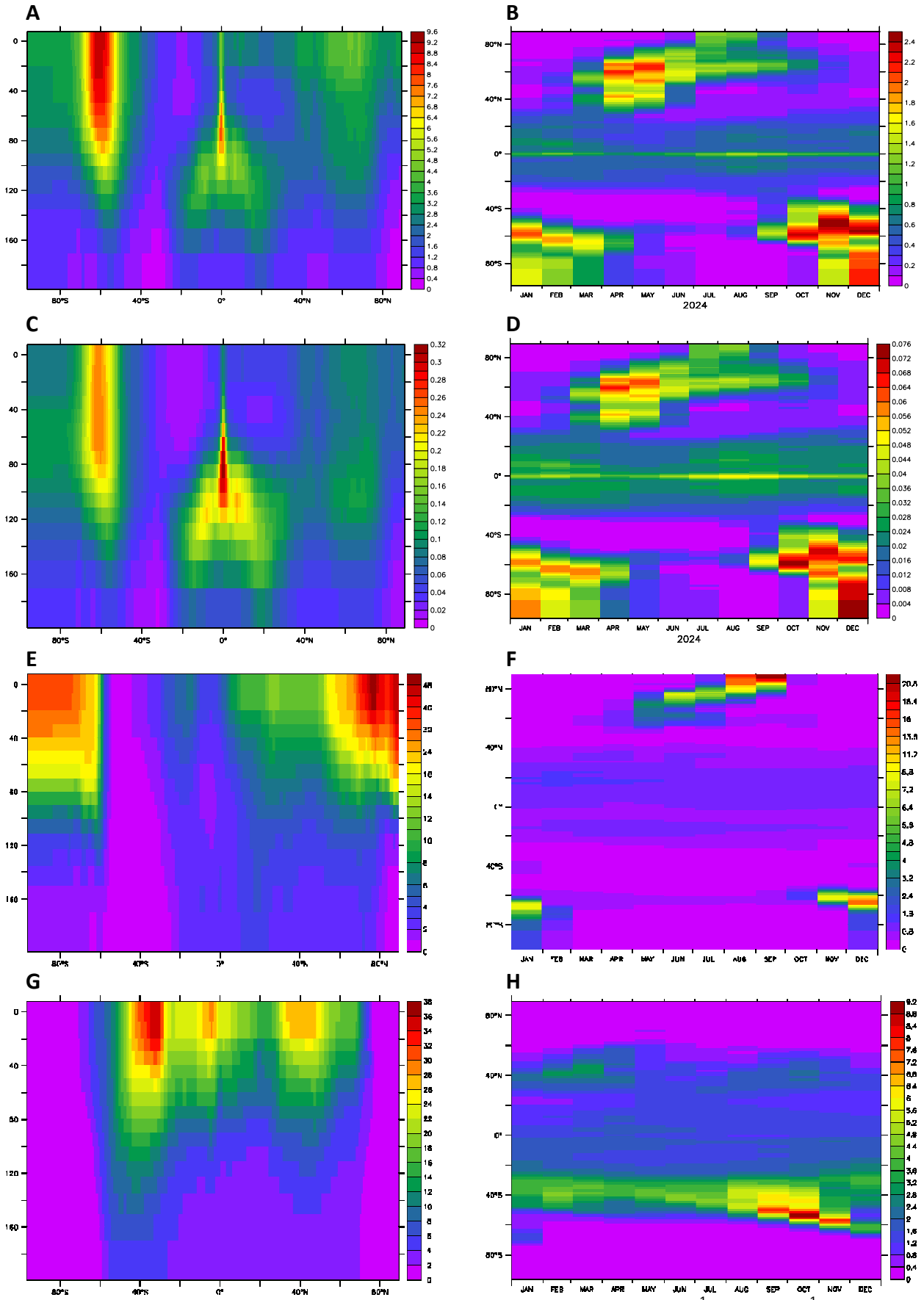

Fig. 4.3: Results of simulation EPP. A, C, E, G) zonal average per depth [µg C l^{-1} or µg Chl l^{-1}], and B, D, F, H) Hoffmüller plots [µg C m^{-2} or µg Chl m^{-2}]. A, B) diatoms; C, D) diatom chlorophyll; E-H: E and F) coccolithophores, G and H) mixed-phytoplankton.

4.3.2.2 Other PFTs

Coccolithophores are present in the Arctic Ocean down to the Labrador Sea and at sub-tropical latitudes. They appear in coastal upwelling of West Africa and east of South-America, as well as along the Antarctic coast. The highest integrated concentration (averaged over the year) is 6 µg C m^{-2} in the North Atlantic (Fig. 4.2 C).

Mixed-phytoplankton is largely spread over mid-latitudes and in coastal upwellings. It is absent from polar waters (Fig. 4.2 D). They grow throughout the year, with a peak at 50°N in March and 50-55°S in October (Fig. 4.3H), where they reach 100 m and 120 m, respectively (Fig. 4.3 G).

The protozooplankton grows essentially in polar waters, although low concentrations are predicted in tropical latitudes (Fig. 4.2.E). However it does not grow in oligotrophic gyres of the Pacific. The proto-zooplankton grows in the whole surface layer in the Southern Ocean: the maximum concentration layer extends from the surface to 60 m with 13 µg C l^{-1} (Fig. 4.4 A). At low latitudes, the biomass is concentrated in the top 50 m.

The mesozooplankton grows in well-delimited latitudinal bands, from around 65°S to the southern tropics and between 70°N to the Northern tropics (Fig. 4.2 F). The biomass is the most concentrated between 0-50 m, though it reaches 120 m (Fig. 4.4 C).

4.3.3 Effect of the temperature dependence function

When the average optimal function replaces Eppley curve (1972) (simulation OPT), the global diatom biomass is lower than in simulation EPP by 3%, which is not significantly different. This does not mean changes at local scale are not significant, which we are going to examine below. Changes are located in sub-polar latitudes, between 30-50°S and 30-60°N, with decreases up to 50% in high productive areas. Global production of mixed-phytoplankton, proto- and meso-zooplankton in OPT are significantly lower than in EPP (Table 4.3). Changes in pPFT concentrations lead to an increase of the diatom proportion over the total phytoplankton.

On the contrary, the use of the maximal optimal function (OPTm) causes a 7% increase of the global diatom biomass, stronger in the North Hemisphere (Fig. 4.5.A). Diatom production around the Antarctic increases by about 5%. We also note changes in other PFTs biomass, in particular the decrease of coccolithophores production by 11% (Table 4.3).

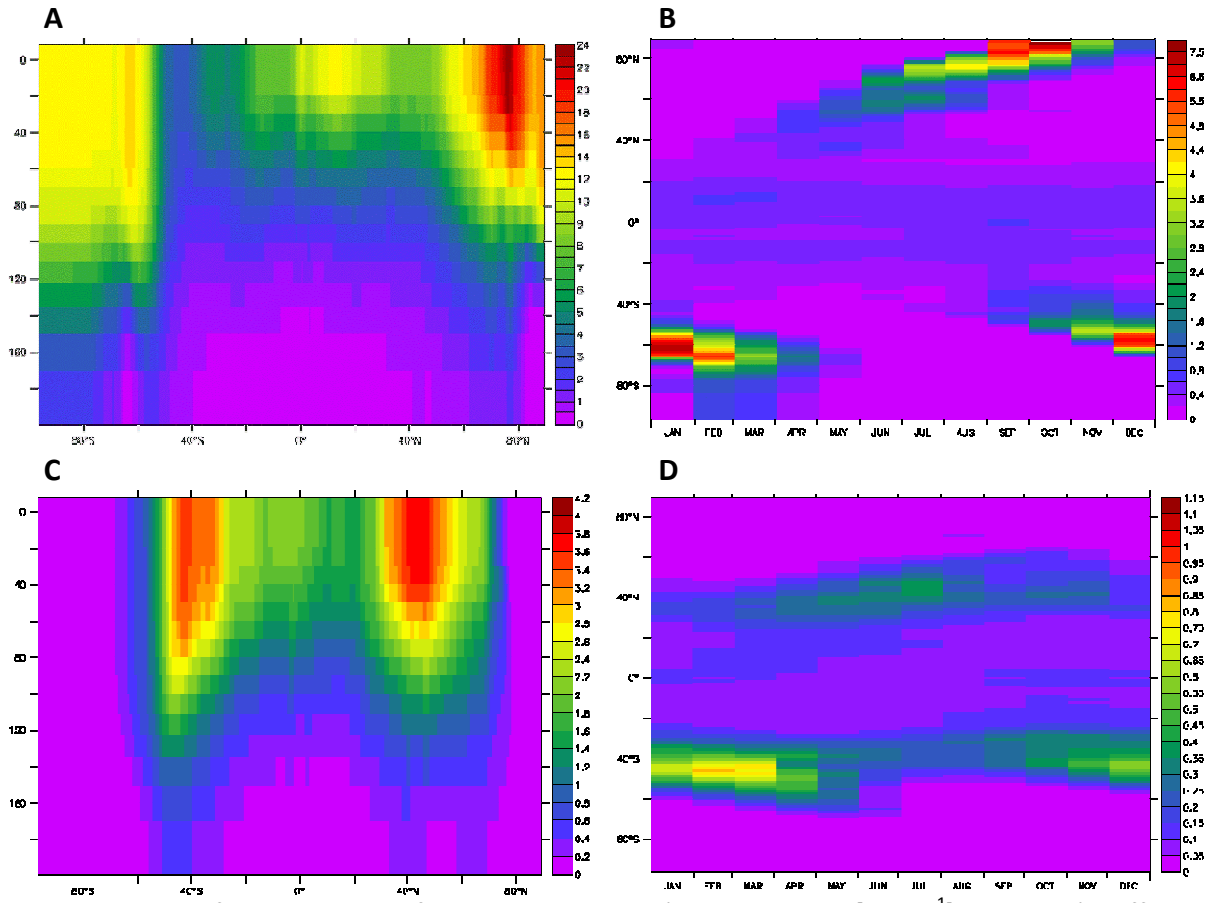

Fig. 4.4: Results of simulation EPP for zooplankton. A, C) zonal average [µg C l^{-1}], and B, D,) Hoffmüller plots [µg C m^{-2}]. A, B) protozooplankton; C, D) mesozooplankton.

A change of diatom production can affect other PFTs through nutrient availability, light intensity and/ or changes in grazing. A lower biomass leaves more nutrients available for other phytoplankton. It might also affect the zooplankton grazing. A closer look at PFTs distribution over depth and time in the South-East Pacific (SEP) and in the North Atlantic (NAt) will enable us to better understand their relationships.

4.3.3.1. Use of the average optimal function instead of Eppley curve (EPP to OPT)

In South East Pacific (SEP):

A small (less than 10%) but significant decrease of diatom biomass during the spring leads to larger changes for other PFTs. (Fig. 4.6.A) Mixed-phytoplankton and meso-zooplankton concentrations are lowered in the simulation OPT throughout the year, whereas coccolithophore bloom biomass increases massively (Fig. 4.6).

Decreases of diatoms and mixed-phytoplankton biomass in spring allow coccolithophores to take advantage: their peak biomass increases by three-fold, at the surface and northward, precisely where diatom and mixed-phytoplankton biomass decrease.

At the same time, the zooplankton is affected by the lower mixed-phytoplankton and diatom concentrations: proto- and meso-zooplankton biomass decrease in OPT, relative to EPP, by 20 and 30%, respectively (Fig. 4.6 D and E). The feedback effect is a decrease in zooplankton grazing on diatoms during the months following the bloom, which would explain the slightly higher diatom concentration, in OPT, from December to February.

The mixed-phytoplankton produces a bloom in spring (March to May) when the nutrient concentration starts increasing (Fig.4.8). It is likely to be the main food for the meso-zooplankton at this time of the year. Indeed, this bloom is 50% lower in OPT than in EPP and the consequence is a decrease of both proto- and meso-zooplankton biomasses.

In North Atlantic (NAt):

The geographical distribution of PFTs in the North Atlantic shows distinct area of growth: proto-zooplankton and coccolithophores are found in the North, in Labrador Sea and Greenland Sea whereas mixed-phytoplankton and meso-zooplankton are close to European coasts and from the South of New-Foundland toward the South of Iceland. Diatoms grow in open waters.

Diatom concentration decreases when the optimal function (OPT) is applied. More exactly, the density is reduced, relative to EPP, during the spring bloom (Fig. 4.7.A) and over all latitudes (Fig. 4.5.A). This decrease in diatom growth does affect other PFTs to a larger extent than the change in diatom biomass itself. While mixed-phytoplankton and meso-zooplankton biomass are about 7% lower, coccolithophore and proto-zooplankton see their biomass peak reduced by about 25% (Fig 4.7.C and D).

Unlike observations in SEP, the decline of diatoms does not lead to other pPFTs development, but to a decrease of biomass for pPFTs and their grazers.

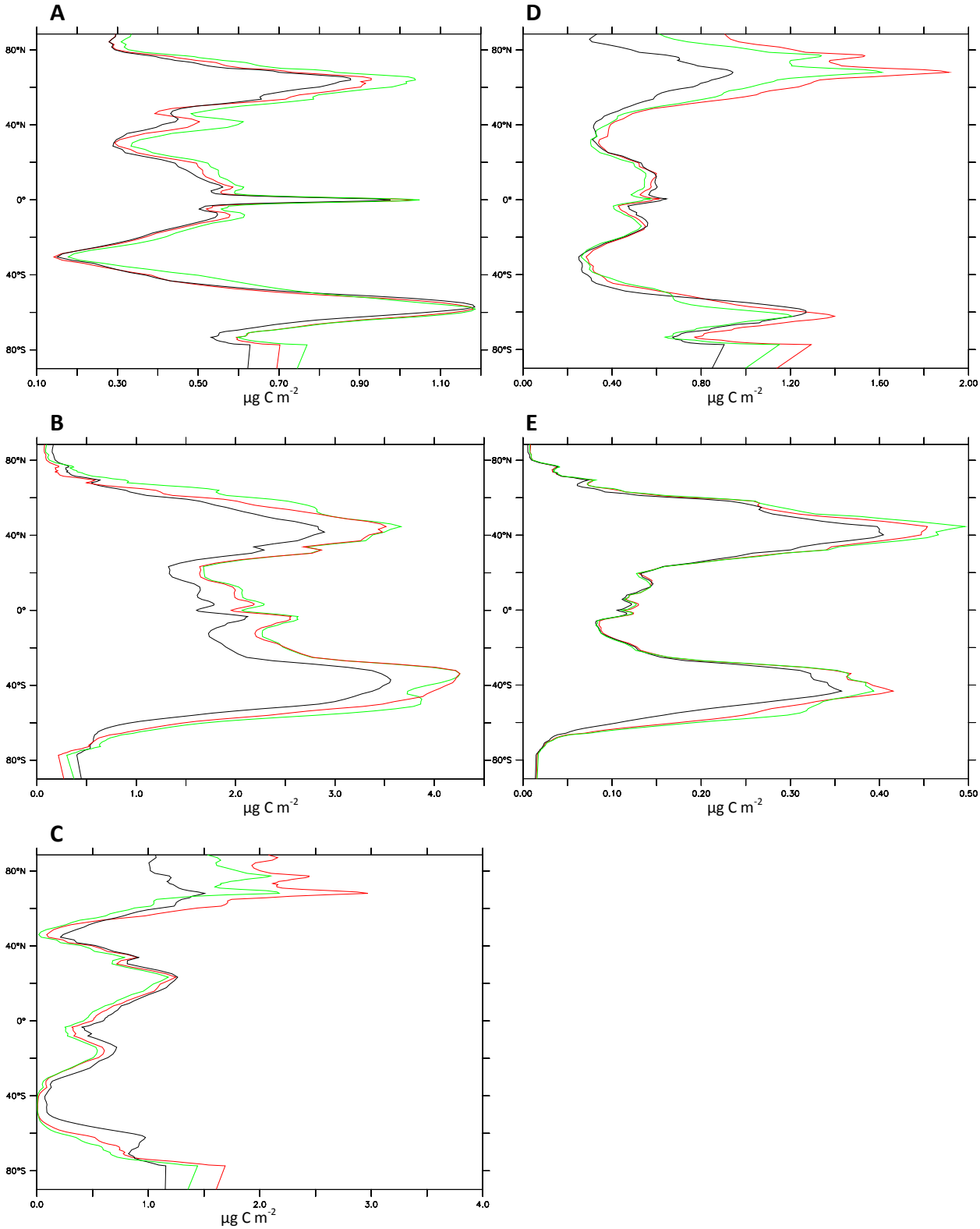

Fig. 4.5. Change in temperature dependence parameters: integrated annual concentrations as a function of latitude; red= EPP, black=OPT, green=OPT_m ; A) Diatoms, B) mixed-phytoplankton, C) coccolithophores, D) proto-zooplankton, E) meso-zooplankton

The drop in phytoplankton biomass is likely to explain why the meso-zooplankton feeds more on proto-zooplankton than it did in EPP, while grazing on phytoplankton decreases (Table 4.4). Output data indicates as well that proto-zooplankton feeds more on particulate organic matter (POC) and less on phytoplankton. The level of nutrient is lower in OPT (Fig.4.8), which would explain why all phytoplankton biomasses are lower as well.

Plankton growth in the Southern Ocean is subjected to important physical constraint, such as iron concentration, polar front, surface mixing and nutrients upwelling. In the simulation OPT we observed slight changes of PFTs distribution along latitude and over depth.

Table 4.4. Total grazing, grazing by meso-zooplankton and by proto-zooplankton (Pg C yr^{-1}) for each simulation. Inter-annual var.: inter-annual variability calculated over a run of 6 years; Mean and standard deviation (St.Dev.) and error do not take into account simulations Alp and Tht. MESO: mesozooplankton; PROTO: protozooplankton; POC: particulate organic carbon.

	Total grazing	Grazing by MESO	On phyto only	On PROTO only	Grazing by PROTO	On phyto only	On POC only
EPP	48.2	18.01	11.86	6.15	30.23	29.03	1.20
OPT	44.09	16.52	10.42	6.10	27.57	26.25	1.32
OPT_m	46.44	18.08	12.42	5.94	28.36	27.18	1.18
Alp	43.99	17.50	11.31	6.19	26.49	25.21	1.28
Tht	46.80	16.49	10.08	6.41	30.31	29.05	1.26
AT1	51.7	17.61	11.32	6.29	34.06	32.79	1.27
AT2	44.8	16.37	10.23	6.14	28.38	27.02	1.36
RD	44.3	16.49	10.36	6.13	27.81	26.47	1.34
Inter-annual variation	(0.23)	(0.18)	(0.12)	(0.10)	(0.27)	(0.24)	(0.05)
MEAN	**46.6**	**17.2**	**11.06**	**6.13**	**29.40**	**28.12**	**1.28**
St. Dev.	**2.95**	**2.9**	**0.83**	**0.11**	**2.47**	**2.49**	**1.64**
St. error (%)	**6.3**	**0.18**	**7.50**	**1.80**	**8.40**	**8.8**	**5.9**

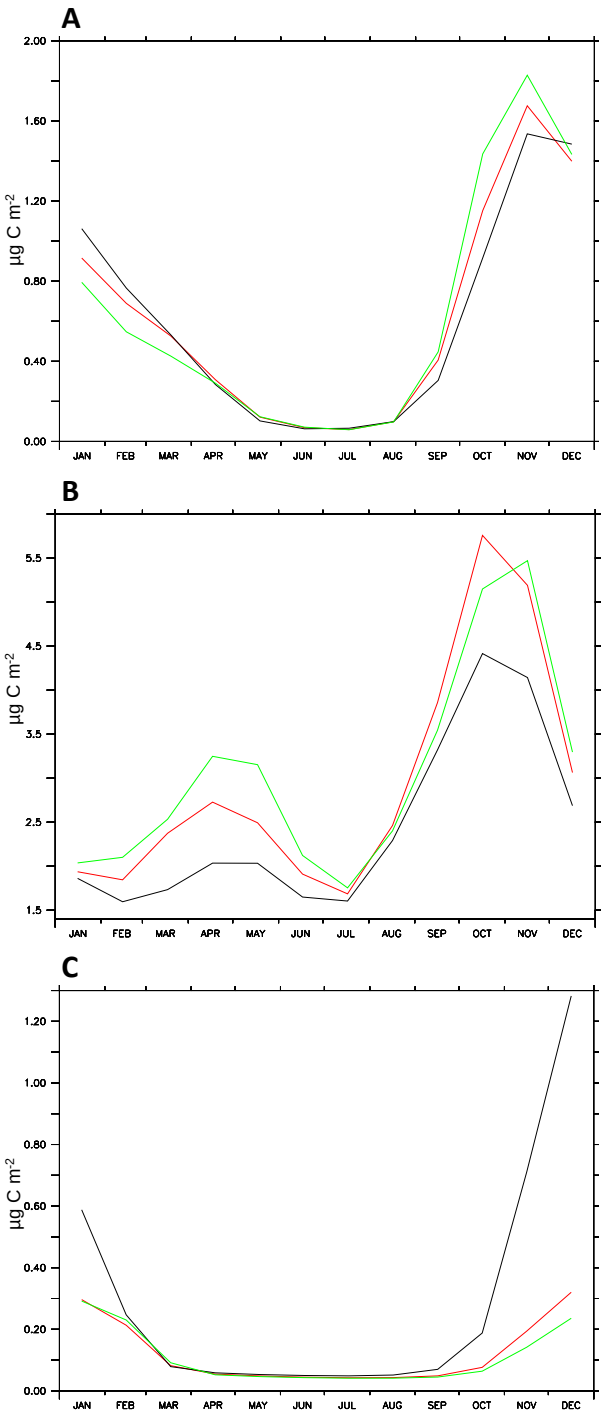

Fig. 4.6. Change in temperature dependence parameters: integrated concentrations over the year in SEP; Colours as in 4.4 ; A) Diatoms, B) mixed-phytoplankton, C) coccolithophores

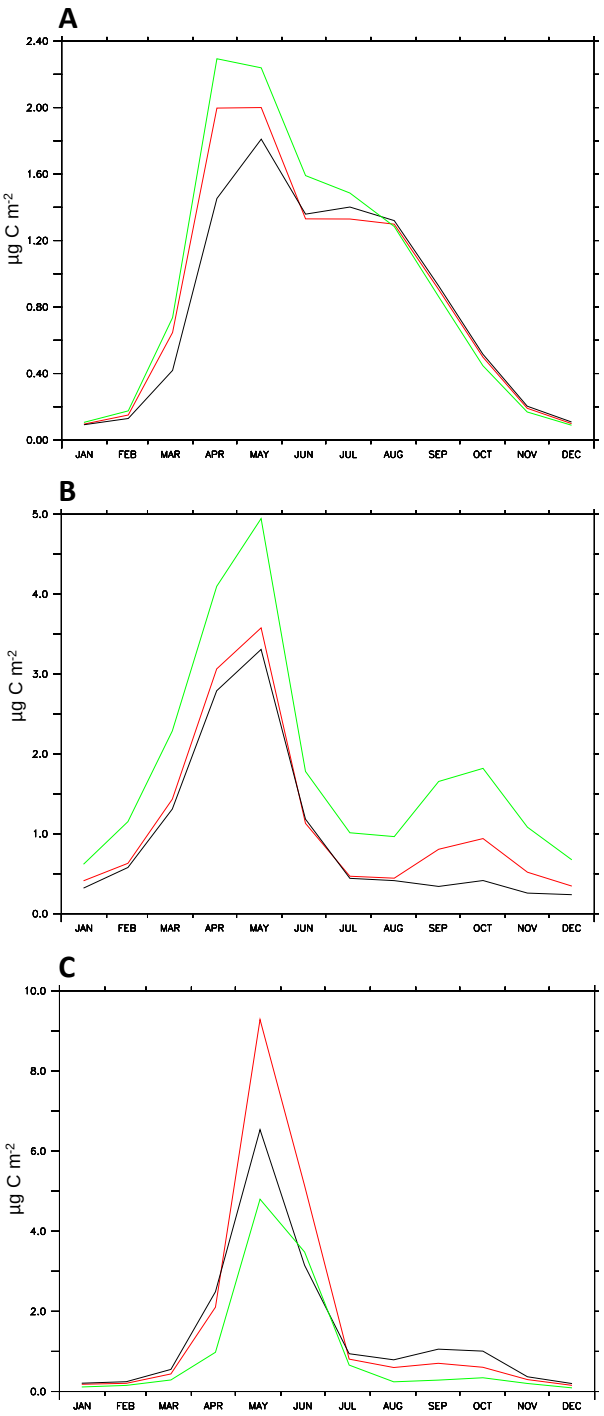

Fig. 4.7. Change in temperature dependence parameters: integrated concentrations over the year in NAt; Colours as in 4.4 ; A) Diatoms, B) mixed-phytoplankton, C) coccolithophores,

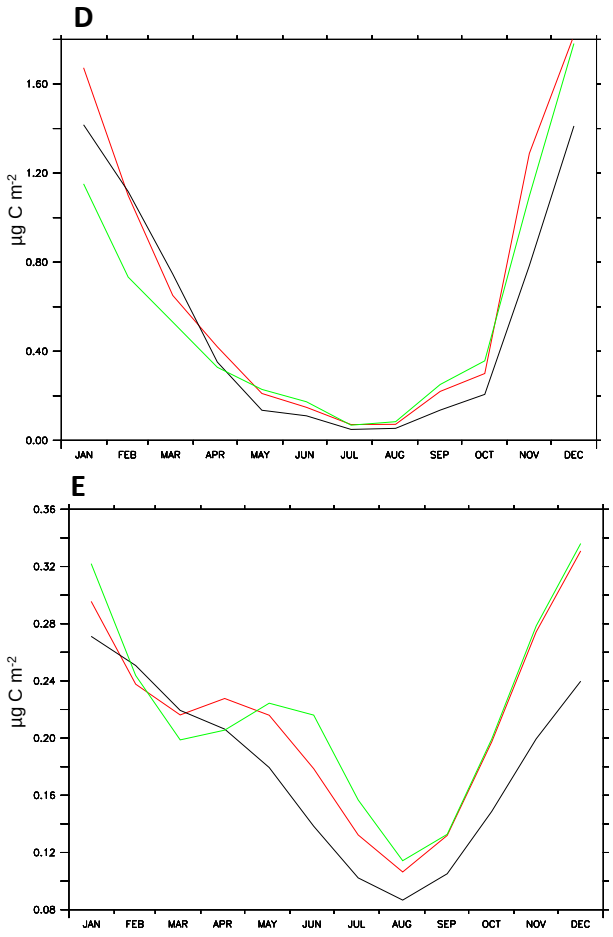

Fig. 4.6. D) proto-zooplankton, E) meso-zooplankton

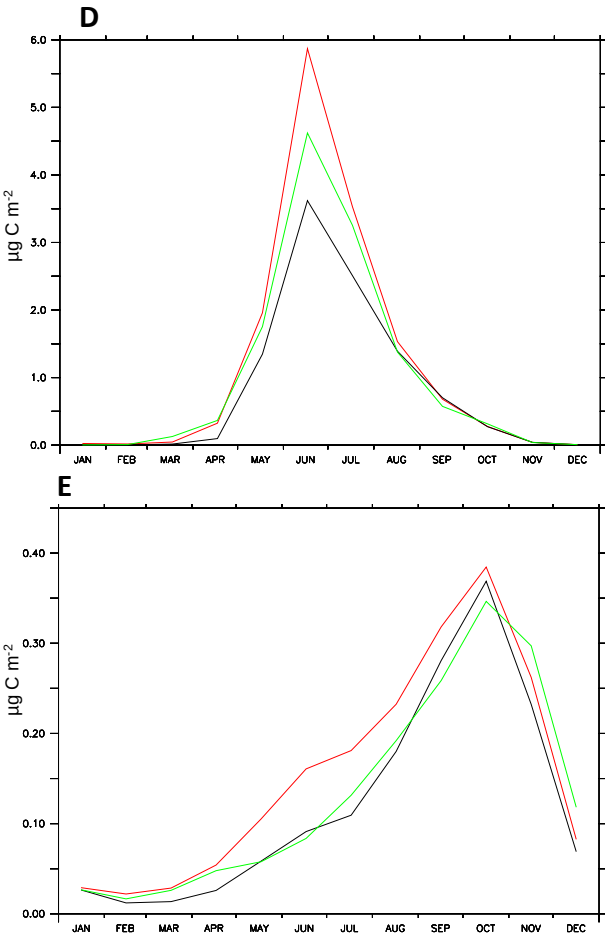

Fig. 4.7. D) proto-zooplankton, E) meso-zooplankton

It seems nutrients levels respond differently to phytoplankton concentration: in NAt, nutrients are lower when the phytoplankton biomass is lower (as in OPT). In SEP, nutrients are higher when diatoms and mixed-phytoplankton biomasses are lower, whereas coccolithophore biomass is higher.

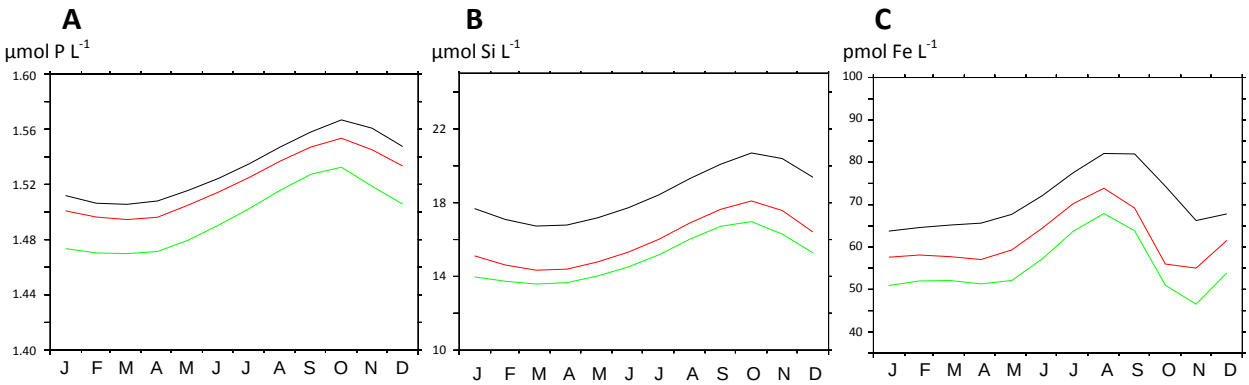

Fig. 4.8: (A) Phosphate, (B) silicate and (C) iron concentration in SEP, averaged over the first 200m. Colours as in 4.4.

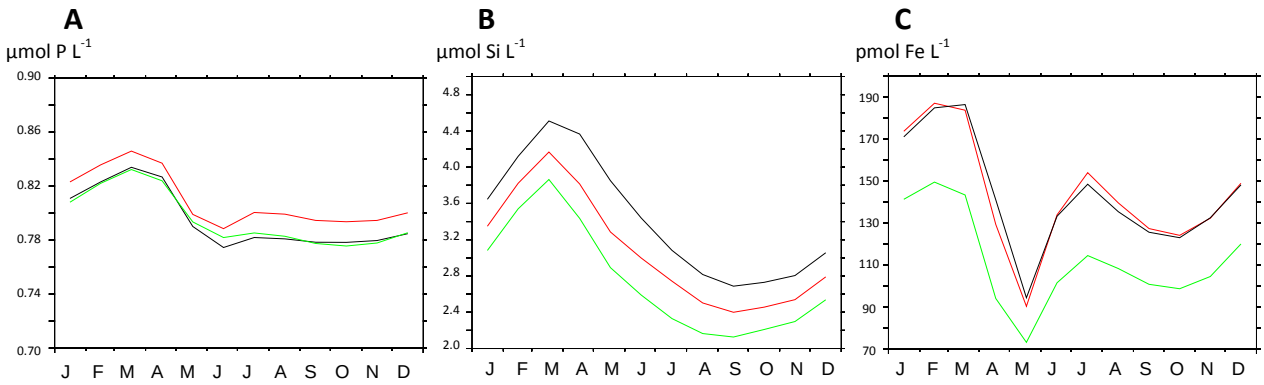

Fig. 4.9: (A) Phosphate, (B) silicate and (C) iron concentration in NAt, averaged over the first 200m layer. Colours as in 4.4.

4.3.3.2. Use of the maximum optimal function instead of Eppley curve (EPP to OPTm)

The optimal maximum function gives higher growth rates than does the Eppley curve. Diatom biomass increases in the simulation OPTm, relative to EPP, over all latitudes but mostly in the North hemisphere (+10 to 20%). In the Southern Ocean, the biomass peak shifts slightly southward (Fig. 4.5.A).

A map of the relative increase over the globe shows an increase of 10 to 20% in the Southern Ocean and an increase of 40-50% at mid-latitudes, with some areas showing a decrease of 10 to 20%. This picture corresponds very well to the changes in the growth curve: while the new function gives growth rates higher by 8 to 21% at 0 to 4°C, increase in biomass in polar areas are in the range of 10 to 20%. There is very slight or no increase at Equatorial latitudes.

The increase of diatom biomass in temperate waters indicates temperature is a limiting factor of growth. However, other factors limit phytoplankton growth. After the change in maximum growth rate parameters, the bloom in the Southern Ocean increases but does not occur earlier. Although the change of parameters allows a higher concentration, the light plays a bigger role in the bloom seasonality than the temperature.

We will first focus on the South East Pacific.

In SEP:

We observe the direct consequence of the change of temperature-dependence in the increase of diatom biomass during the bloom (September to November) in the simulation

OPTm, relative to EPP (Fig. 4.6.A). However, the decline is sharper and results in a lower post-bloom concentration. Changes of other PFTs biomass are of smaller amplitude than changes for OPT.

Coccolithophore production is lower than in EPP as well as, as a consequence, the proto-zooplankton production (Fig. 4.6). The meso-zooplankton production is similar to that in EPP but the spring bloom occurs a month later, probably due to the late bloom of mixed-phytoplankton.

Nutrients, iron and silicate concentration are lower than in EPP (Fig.4.8).

Let us examine the changes in the North Atlantic, another region largely affected by the change in diatom growth parameters.

In NAt:

Growing faster at low temperatures, diatoms become more concentrated in the northern latitudes (60-80°N) where they compete with coccolithophores (figure not included). The distribution of proto-zooplankton shows it grazes mainly on coccolithophores, hence their decrease in OPTm. Nevertheless, proto-zooplankton abundance is not as low as in OPT: they graze also on diatoms and mixed-phytoplankton.

Mixed-phytoplankton biomass increases through all the year, by up to 40% (Fig. 4.7.B). On the contrary, meso-zooplankton biomass decreases by approximately 10% (Fig. 4.7.E).

Meso-zooplankton biomass decreases in the North Sea due to the lower biomass of proto-zooplankton. Nevertheless, the grazing on diatoms in northern latitudes up to Iceland increases, as well as grazing on mixed-phytoplankton off the coast of New-Foundland. In addition to the shift northward of diatoms, we observe a similar shift of mixed-phytoplankton and meso-zooplankton populations.

The nutrient concentration is similar to that for EPP, whereas iron and silicate concentrations decrease (Fig.4.9). Iron concentration decreases more at northern latitudes.

4.3.4 Changes in photosynthetic parameters

In this section we describe changes of PFT production after a change of photosynthetic parameters. Phytoplankton cells in the upper mixed layer are exposed to various light

intensities depending on their depth. Moreover, light-limitation is exacerbated during the phytoplankton bloom, because of cell-shading. Light penetration through sea-ice is very limited.

A higher light-limited photosynthetic rate means diatom photosynthetic production will be higher at low light intensity. We expect to see consequences of an increase of alpha on the diatom abundance at the bottom of the euphotic layer and at high latitudes.

4.3.4.1 From OPT to Alp: change in alpha

The doubling of the light-limited photosynthesis rate causes an increase of the global diatom primary production, from 0.213 Pg C yr^{-1} in simulation OPT to 0.250 Pg C yr^{-1} in Alp (Table 4.3).

One large effect is a shift of the maximum diatom production about 40m deeper (Fig.4.10). Diatom biomass increases at all latitudes except in the Southern Ocean where we observe instead a shift of the biomass peak southward (Fig. 4.11.A). Moreover, we observe in the Southern Ocean the shift of the bloom one month earlier than in OPT (Fig. 4.12.A).

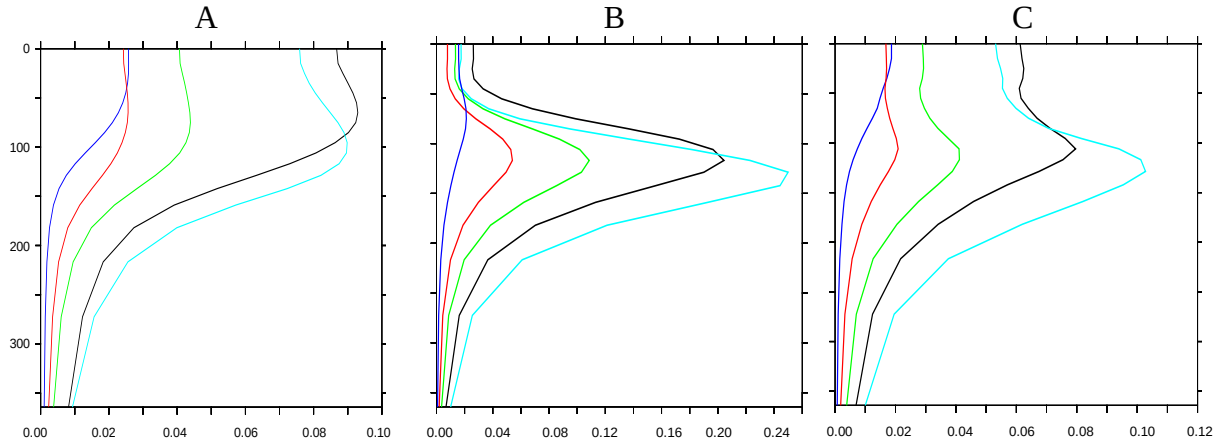

Fig. 4.10. Change in photosynthesis parameters: annual average concentration of chlorophyll as a function of depth. A) South-hemisphere, B) Equator, C) North-hemisphere; OPT, black; Alp, light-blue; Tht, blue; AT1, green; AT2, red.

The total primary production increases very slightly. The meso-zooplankton global production increases, relative to OPT, by 15%, while coccolithophores and proto-zooplankton global production decrease by 17% (Table 4.3).

We observe two changes of the Southern Ocean bloom in chlorophyll : not only does it start a month earlier, but also, the biomass concentration in winter increases by two-fold.

Plots of PFTs biomass per latitude show a net difference between productions in the North-hemisphere and in the South-hemisphere (Fig. 4.11). We detail those changes below.

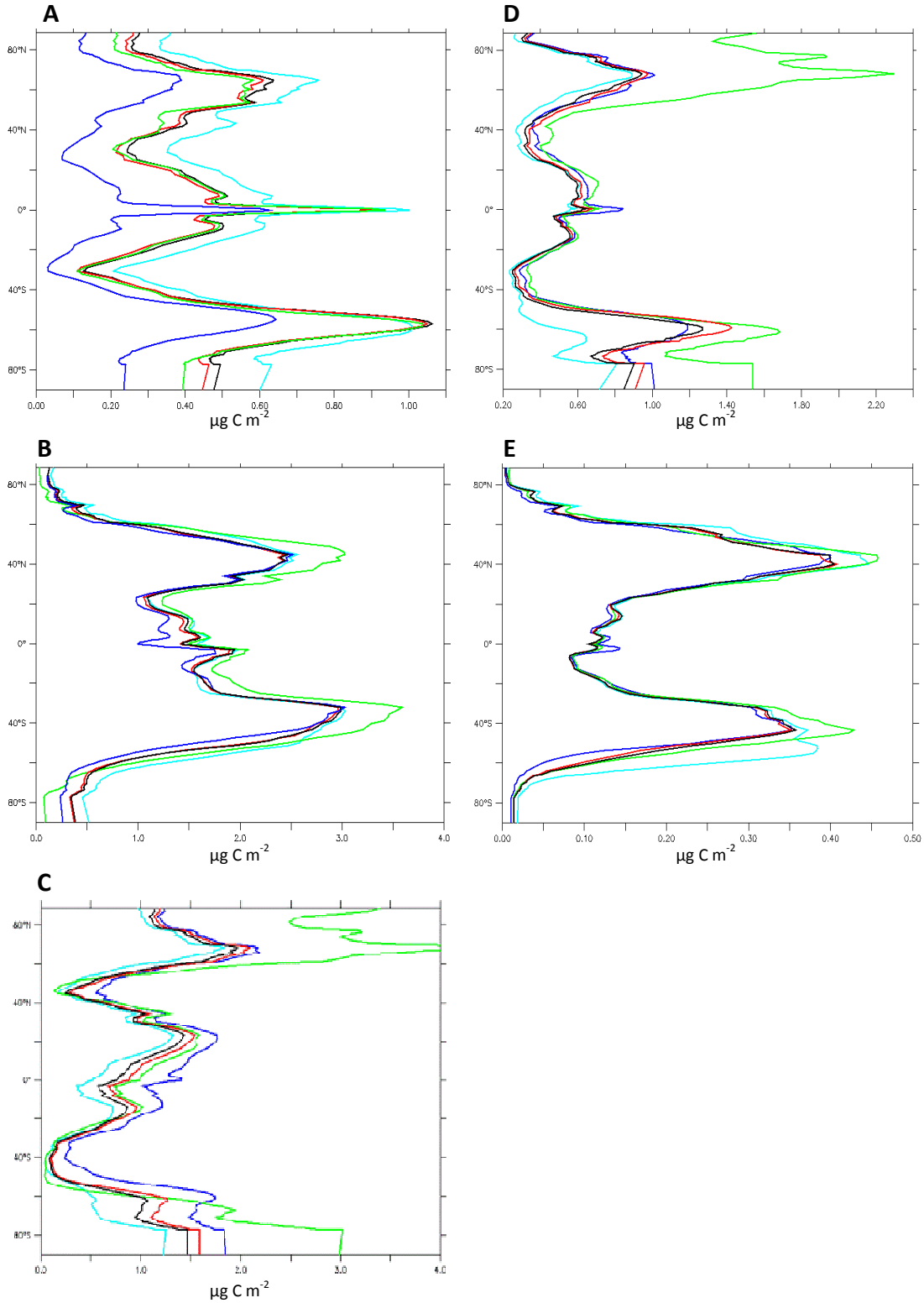

Fig. 4.11. Changes in photosynthetic parameters: vertically-integrated, zonal and annual average PFT concentrations as a function of latitude A) diatoms, B) mixed-phytoplankton, C) coccolithophores, D) proto-zooplankton and E) meso-zooplankton; colours as in 4.10: OPT, black; Alp, light-blue; Tht, blue; AT1, green; AT2, red.

In SEP:

A better photosynthetic activity at low light enables an early diatom development. First, the increase of diatom production affects directly the coccolithophores by competing for nutrients and iron: their biomass decreases more than two-fold (Fig. 4.12.C). The increase of diatom production influences also the meso-zooplankton. As for the diatoms, the bloom of meso-zooplankton starts a month earlier (Fig. 4.12.B); the peak of biomass not only increases but also shifts southward from 40°S to 50°S. The meso-zooplankton biomass doubles, relative to OPT, in January, leading to a higher grazing rate.

The decline of coccolithophores causes the decrease of proto-zooplankton, that are also maintained at a low density by grazing by meso-zooplankton.

The production of mixed-phytoplankton increases, mainly during the autumn bloom. They probably benefit from the lower grazing pressure by the proto-zooplankton from December to April.

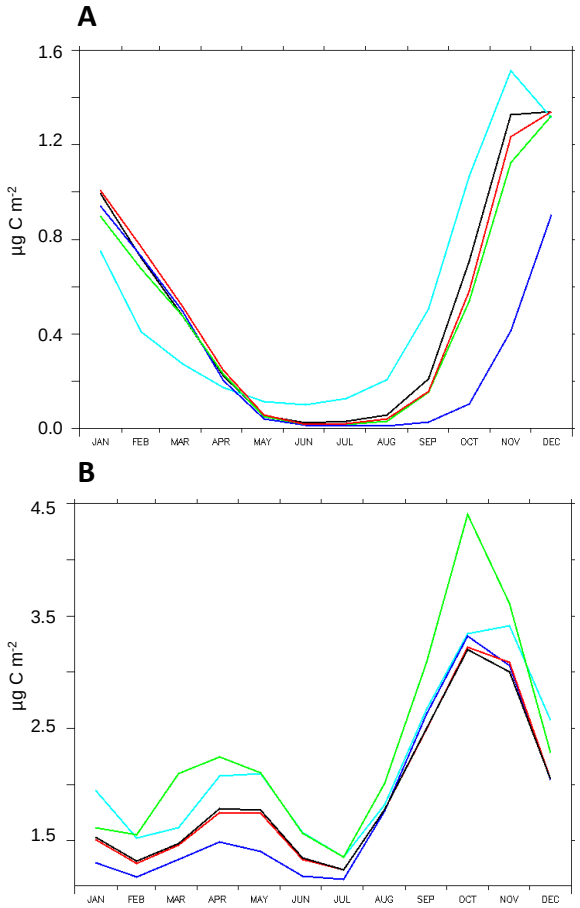

Fig. 4.12. Change in photosynthesis parameters: integrated concentrations over the year in SEP; Colours as in 4.10 ; A) diatoms, B) mixed-phytoplankton,

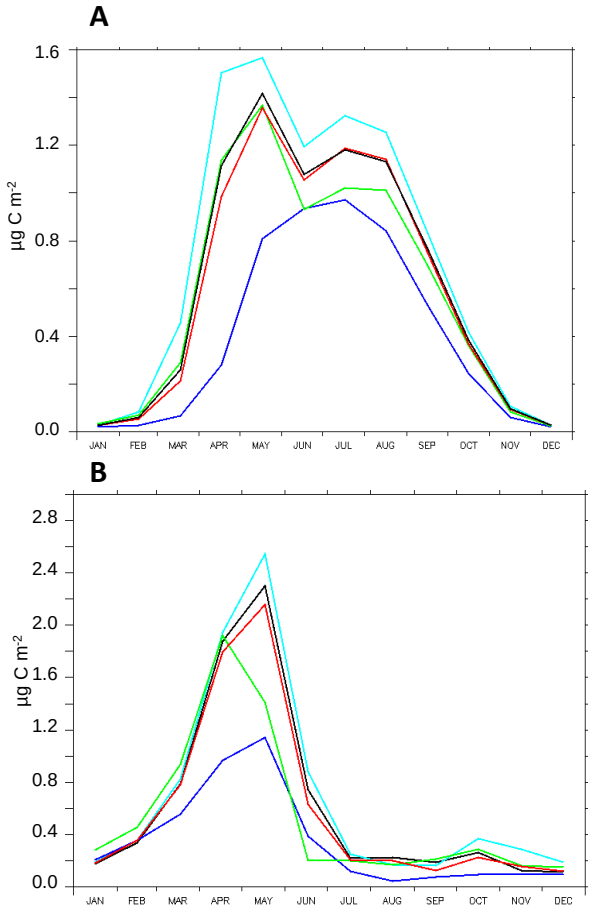

Fig. 4.13. Change in photosynthesis parameters: integrated concentrations over the year in NAt; Colours as in 4.10 ; A) diatoms, B) mixed-phytoplankton,

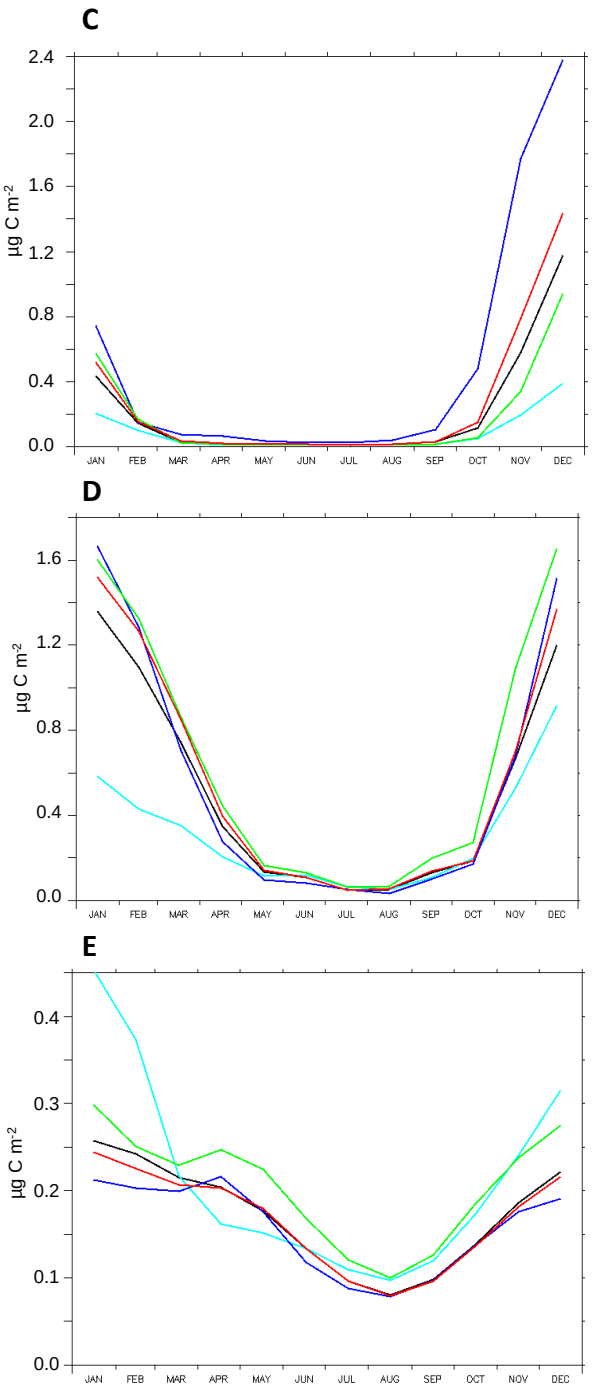

Fig. 4.12. C) coccolithophores, D) proto-zooplankton, E) meso-zooplankton

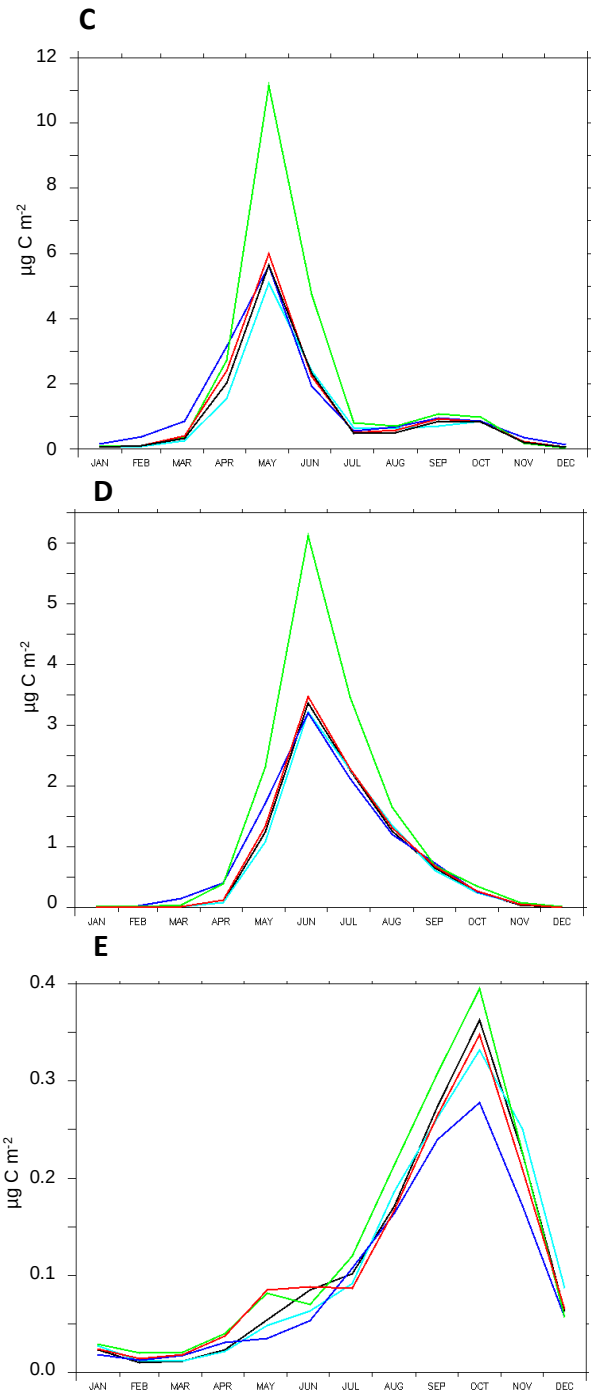

Fig.4.13 C) coccolithophores, D) proto-zooplankton, E) meso-zooplankton

Nutrients and iron concentrations decrease over the year (figure not shown). The silicate concentration is influenced by diatom growth: although the level is slightly lower in Alp than in OPT, the silicate concentration increases during the bloom development. It starts diminishing in October, while the diatom bloom reaches its peak in November. Although silicate concentration increases in February, diatoms grow only from August, showing that other physical or chemical factors limit their growth between February and August.

In NAt:

As expected, the diatom production is higher in Alp than in OPT. Diatom concentration increases mainly below 100 m.

Unlike in the Southern Ocean, effects on other PFTs are very limited (Fig. 4.13). The increase in diatom biomass leads to a small decrease of the coccolithophore biomass. However, it does not enhance the meso-zooplankton production. Each PFT grows in distinctly separated areas, therefore decreasing the level of connection and interdependence.

Nutrient concentrations decrease slightly over all latitudes, but this decrease is very small at 43°-50°N. Silicate concentration decreases homogenously over the latitudes. The iron concentration decreases as well, but to a lesser extent at 40°-50°N. Although the conditions seem more favourable below 50°N, the larger increase of mixed-phytoplankton occurs at 50°-55°N.

4.3.4.2 From OPT to Tht: change in θ_m

In the simulation Tht, θ_m decreases by two-fold. The cellular chlorophyll content is maximum under light-limitation. Therefore a decrease of θ_m will affect mainly cells under light-limitation. The greater the light intensity, the less cells will be affected. Less chlorophyll diminishes the photosynthetic capacity. As a consequence, we expect a change of diatom production at the bottom of the euphotic layer, at high latitudes, in turbid coastal waters or in a phytoplankton bloom, where cells shade each other. One consequence of a lower chlorophyll content could be a smaller need for iron as well as an increase of other phytoplankton types (no cell-shading).

As expected, diatom production in Tht is highly impacted: the global diatom production decreases by 43%. Changes are widespread over the globe: the production decreases by 20 to 60% in the highly-productive areas. The Chlorophyll production drops as well.

The increase in coccolithophore biomass is restricted to polar waters, where the biomass doubles (Fig.4.11).

In SEP:

Diatom production decreases, relative to OPT, during the bloom. Not only the biomass is about 30% lower, but the peak occurs later, in January instead of December in OPT (Fig.4.12. A).

This allows coccolithophores to reach a higher density (Fig. 4.12.C). They also extend further southward. The meso-zooplankton is affected by the decrease in diatom biomass during the spring bloom, however this is also a consequence of changes in coccolithophore growth.

Despite higher concentrations of proto-zooplankton, coccolithophore and mixed-phytoplankton, the meso-zooplankton concentration during the summer is lower than in OPT (Fig. 4.12.D). In addition, despite higher coccolithophore concentration, the proto-zooplankton biomass does not increase much. It could be affected by the grazing of meso-zooplankton.

in NAt:

As in the SEP, diatom biomass in NAt decreases (Fig.4.13.A). The density does not peak in spring but rather remains constant through the summer. The overall impact is a decrease of other PFTs biomass, particularly that of mixed-phytoplankton. The mixed-phytoplankton production peak drops by two-fold (Fig. 4.13.B). This is likely to be due to grazing by meso-zooplankton, as a replacement for diatoms. Although the coccolithophore production is higher during the spring, the concentration peak in May does not differ from that in OPT; proto-zooplankton production follows the trend of the coccolithophores; the meso-zooplankton is affected by the decrease of diatom and mixed-phytoplankton concentrations in spring and during the autumn, and by the decrease of proto-zooplankton density during the summer.

To summarise, a change in diatom biomass has major consequences on other phytoplankton types in the Southern Ocean. Proto-zooplankton responses follow that of coccolithophores. Meso-zooplankton seems to be more flexible than proto-zooplankton regarding feeding and habitat, which would explain why changes have a smaller effect on the former. More precisely, the meso-zooplankton has a flexible grazing strategy, being able to graze on mixed-phytoplankton when diatoms are missing. However, the meso-zooplankton is geographically separated from the coccolithophores. PFTs distribution in the North Atlantic is very much distinct, linked to the physical conditions.

4.3.4.3 From OPT to AT1: changes in both α^{Chl} and θ_m

In the previous section we performed two simulations to observe the effects of each parameter, α^{Chl} and θ_m, separately. However, experimental results from Chapter 3 show α^{Chl} and θ_m are not independent and an increase in the former is associated with a decrease of the latter. This means parameter values as in simulations Apl and tht are unlikely to occur. Therefore we focus now on the change of both parameters, as measured in our PI curve experiments. Effects on plankton production will be estimated by comparing simulation outputs with model as found by Buitenhuis and Geider (2010) and as found in experiments from this study (average for cold-water species).

First α^{Chl} and θ_m are modified to represent values as in temperate species (simulation AT1): while α^{Chl} increases by two-fold, θ_m decreases, in the same proportion. The increase of α^{Chl}, which means that, for the same amount of chlorophyll, phytoplankton cells can photosynthesise more organic matter, is balanced by the decrease in θ_m, which means a lower cellular Chlorophyll content. Therefore the product (α^{Chl} x θ_m), that represents the photosynthesis rate by carbon content under light-limitation, is similar in both simulations.

As we described previously, changes of α^{Chl} and then of θ_m had some opposite effects –the shift of diatom Chlorophyll peak in the water column, and the shift in time of the start of the bloom- which we can expect will cancel each other when considering changes of both parameters. Nevertheless, the two simulations had also non-opposite effects, such as changes in other PFT biomass and changes in carbon export. The value of (α^{Chl} x θ_m) being greater in AT1, we expect a higher diatoms carbon biomass in AT1 and, on the contrary, a decrease in diatom chlorophyll biomass.

Globally:

The changes of both α^{Chl} and θ_m in the simulation AT1 create a small decrease (-5%), relative to the simulation OPT, of the diatom production, occurring mostly above 40°N (Fig. 4.11). It induces increases of larger amplitude of all other PFTs biomasses, mostly at high latitudes for coccolithophores and proto-zooplankton and at mid-latitudes for mixed-

phytoplankton and meso-zooplankton. These changes are associated with a large increase of iron concentrations above 40°N (figure not shown).

Diatom production also varies over depth. After the change of α^{Chl} and θ_m, the maximum diatom concentration is about 20m deeper. However, the effect on diatom chlorophyll concentration is more pronounced: we observe a global two-fold decrease, while the maximum chlorophyll depth does not vary (Fig.4.10).

The export of carbon decreases (-0.8%) but the primary production increases. This means some organic matter is recycled in the mixing layer. The production of small (POC) and large particulate organic carbon (GOC) decrease by 22% and 2%, respectively.

We review below the changes of PFTs in SEP and in NAt.

In SEP:

Compared to OPT, the diatom biomass shows a very weak variation. The peak biomass is not only slightly lower, but it occurs one month later and further south. However, other PFTs biomasses are subjected to high variations (Fig. 4.12).

Silicate, nutrient and iron concentrations do not vary, compared to the simulation OPT. The drop of diatom production in AT1 enables mixed-phytoplankton to reach higher concentrations. This benefits the meso-zooplankton during the spring bloom. Unlike in previous simulations where a decline of diatom biomass allowed better growth of coccolithophores, we do not observe an increase of coccolithophores biomass during the spring in the simulation AT1.

During its growth in November and December, the proto-zooplankton is likely to feed on mixed-phytoplankton and coccolithophores, leading to the decrease of both populations. As it grows at the same latitudes (55°-65°S) as the meso-zooplankton, proto-zooplankton is a prey of the latter in October to December. From January, the proto-zooplankton moves southward to 65°-75°S where it is out of reach of the meso-zooplankton. There it feeds mainly on coccolithophores.

In NAt:

Changes of α^{Chl} and θ_m have different consequences in the North Atlantic than in SEP. The diatom decrease in simulation AT1 leads to a slight decrease, relative to OPT, of mixed-phytoplankton biomass and to a large increase of coccolithophore biomass (Fig. 4.13).

The change of diatom photosynthesis parameters has a large effect on coccolithophore and proto-zooplankton productions: their peak biomass increase by about 100 and 50%, respectively. Both populations increase northward, where diatoms and mixed-phytoplankton biomass decrease. Except a drop of concentration in June, due to lower diatoms and mixed-phytoplankton concentrations, meso-zooplankton production is higher in AT1.

First of all, nutrient and silicate concentrations increase slightly in AT1, compared to OPT. The iron concentration increases above 50°N. Therefore, phytoplankton in the North Atlantic should not be more limited by nutrients than in OPT.

Although the diatom bloom reaches the same maximum concentration in AT1 as in OPT, the biomass decreases more quickly. Diatoms compete with coccolithophores in high latitudes. However, diatoms are less competitive in the simulation AT1, allowing coccolithophores to grow.

We were not able to establish the relationship between the changes in Alp and tht in diatoms, with respect to the other changes observed. Nutrients and Iron concentration are not very much involved, but rather the interactions between PFTs.

4.3.5 Changes in both α^{Chl} and θ_m to higher values (AT2)

PI curve experiments resulted in a range of α^{Chl} and θ_m values. Low α^{Chl} values were measured in cold-water species and were associated with high θ_m values. Consequences of the change of the original model parameters to those ones were tested in simulations Alp, Tht and AT1 described above. In the following section we describe the simulation AT2 where values for both photosynthetic parameters α^{Chl} and θ_m are changed to match experimental results on temperate species. In this case, high α^{Chl} values are associated with low θ_m values. Outputs of the simulation are compared with those for OPT.

A high α^{Chl} value means photosynthesis performs well at low light intensity. However, a low θ_m value means a low Chlorophyll content at low light, thus decreasing the photosynthesis efficiency. Therefore, the combination of a high α^{Chl} value and a low θ_m value (AT2) may cancel these effects. More exactly, the product α^{Chl} x θ_m for AT2 (0.55) is smaller than that for AT1 (0.42). This means lower carbon assimilation per carbon content.

globally:

In general, the change of α^{Chl} and θ_m has few consequences on plankton biomass. The global decrease of diatom concentration is smaller than in AT1 (-4%). The most affected PFTs are coccolithophores and proto-zooplankton, whose biomasses increase by 9% and 7%, respectively; on the contrary, meso-zooplankton biomass does not change significantly.

Although diatom biomass, in carbon, does not show big changes, the biomass in chlorophyll decreases by a third. This was expected, as the maximum Chl:C ratio is three-fold smaller in AT2 than in OPT (Fig.4.10).

in SEP:

It appears that the very small decrease of diatoms observed in AT2 during the bloom affects mostly the coccolithophores. Nutrient and silicate concentrations are higher than in OPT. The only major change in AT2 is the diatom chlorophyll concentration, which is three-fold smaller than in OPT (Fig. 4.12.A). A high chlorophyll concentration can act as shade for the other phytoplankton cells. Therefore, cells with low chlorophyll content would allow other photosynthetic cells to grow alongside. This would explain the increase of coccolithophore production in AT2.

The photosynthetically active radiation (PAR) increases slightly in AT2, particularly between 10 and 80 m deep. On the contrary, it decreases at 35-40°S and at 80°S (data not shown).

The increase in coccolithophore production in the simulation AT2 leads to a slight increase in proto-zooplankton from November to February (Fig. 4.12). Despite more proto-zooplankton and diatoms from January, the meso-zooplankton biomass decreases. This reduces the grazing pressure on diatoms. A higher diatom biomass from January helps meso-zooplankton to recover its biomass in April.

Difference of diatom abundance between AT1 and AT2 are very small. In both simulations the production drops, relative to OPT, during the bloom. However, consequences for coccolithophore production differ: relative to OPT, it is lower in AT1 whereas it is higher in AT2. Changes of other PFT production differ as well between AT1 and AT2: biomasses are higher than in OPT for AT1, while lower or equal for AT2.

In NAt:

In the North Atlantic, the diatom production is significantly lower in AT2 than in OPT during March and April (Fig. 4.13.A). It induces a small increase of the coccolithophore biomass, as well as of the proto-zooplankton biomass. Mixed-phytoplankton biomass decreases. The meso-zooplankton production is influenced by other PFTs biomasses.

Figure 4.13 shows the difference in photosynthetically active radiation (PAR) between simulations OPT and AT2. The PAR decreases over the water column by absorption by pigments, like photosynthetic pigment from phytoplankton. The amount of light reaching the water column is higher in AT2. Since the phytoplankton biomass is nearly equal in both simulations, the increase of PAR is due to a lower absorption, which could be in this case a lower absorption by diatom chlorophyll.

4.3.6 Change in respiration rate

Change in the respiration affects the growth efficiency. A two-fold increase of R_d, from 0.10 d^{-1} in AT1 to 0.18 d^{-1} in the simulation RD, is expected to cause a decrease in the diatom biomass.

Globally:

Unexpectedly, we observe a 4% increase of the global diatom biomass in the simulation RD, from 0.202 Pg C in AT1 to 0.210 Pg C in RD (table 4.3). Most of the increase occurs in the Northern hemisphere (Fig 4.14). The production changes also over depth: we note at low latitudes a slight shift of the biomass from the surface water (0-100m) to the deeper layer (data not shown). At high latitudes, there is a small shift northward of the biomass.

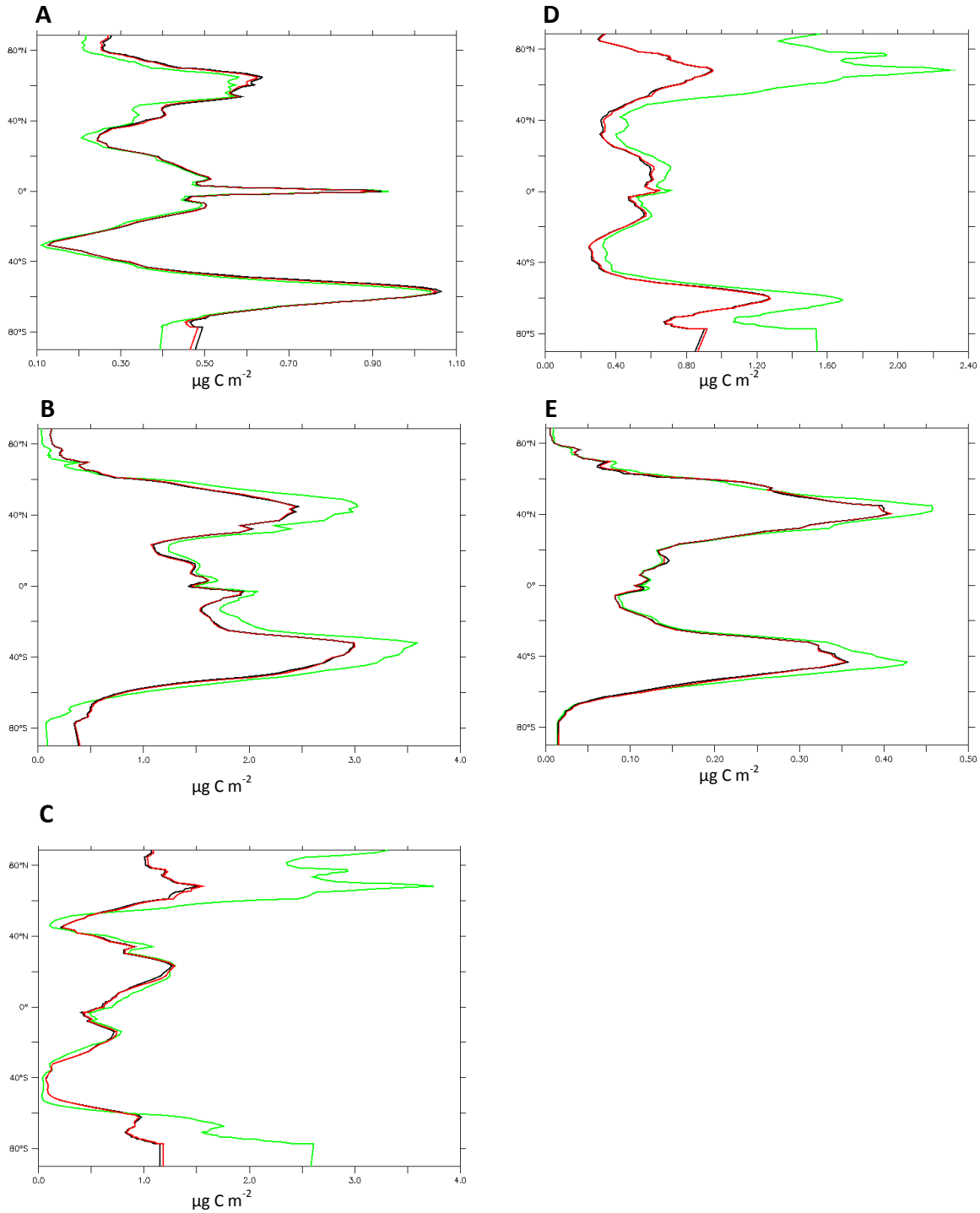

Fig. 4.14: Change of Rd: integrated annual concentrations as a function of latitude A) diatoms, B) mixed-phytoplankton, C) coccolithophores, D) proto-zooplankton and E) meso-zooplankton. OPT, black; AT1, green; RD, red.

The production of other PFTs decrease by 10 to 20%. The decrease of the zooplankton is higher at high-latitudes, whereas coccolithophores and mixed-phytoplankton biomasses are higher, at those latitudes, in RD than in AT1 (Fig. 4.14).

In SEP as in NAt, the diatom production increases slightly during the bloom. Diatom chlorophyll content varies like the carbon content. In both areas, the consequence is a drop of the meso-zooplankton and proto-zooplankton biomasses.

In SEP:

Diatom production during the bloom is a bit higher in RD than in AT1 (Fig. 4.14). mixed-phytoplankton production decreases by 25% while the coccolithophore production increases during the bloom. Meso-zooplankton biomass decreases in RD by about 15% relative to AT1. It is affected by the drop in mixed-phytoplankton biomass during the spring and of proto-zooplankton during the summer.

We suppose that the increase of diatom biomass is not caused by a better physiological fit but by a decrease of grazing by meso-zooplankton.

Contrary to other simulations where an increase of coccolithophore biomass was associated with an increase in proto-zooplankton, here the increase of coccolithophores is associated with a decrease of proto-zooplankton.

In NAt:

The diatom biomass increases in RD, relative to AT1, during the summer bloom (Fig. 4.14). The mixed-phytoplankton reaches its maximum density a month later than in AT1; moreover, the maximum density is higher. On the contrary, coccolithophore biomass drops in RD by nearly 50%. This affects the proto-zooplankton, whose biomass decreases in the same proportion.

The meso-zooplankton sees its biomass decreasing in RD from July to October. This could be linked to the lower proto-zooplankton biomass.

Proto-zooplankton feed more on POC than in the AT1 simulation.

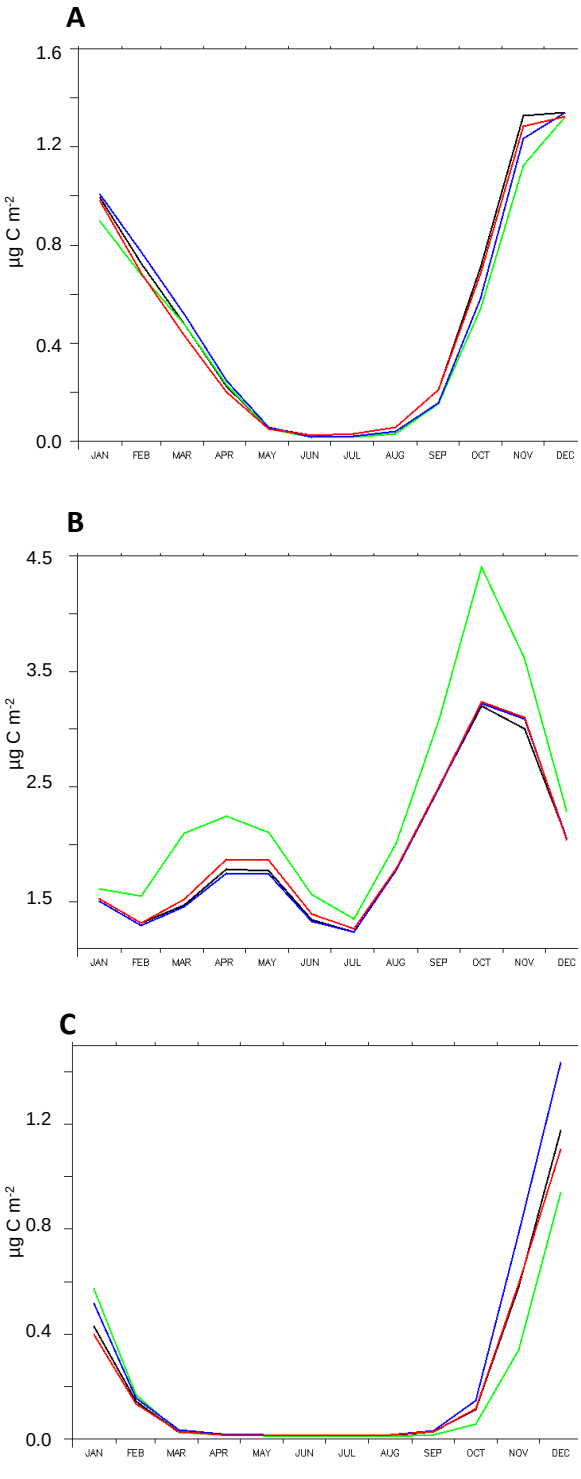

Fig. 4.15. Change in R_d: integrated concentrations over the year in SEP; OPT, black, AT1, green, AT2, blue, RD, red; A) diatoms, B) mixed-phytoplankton, C) coccolithophores,

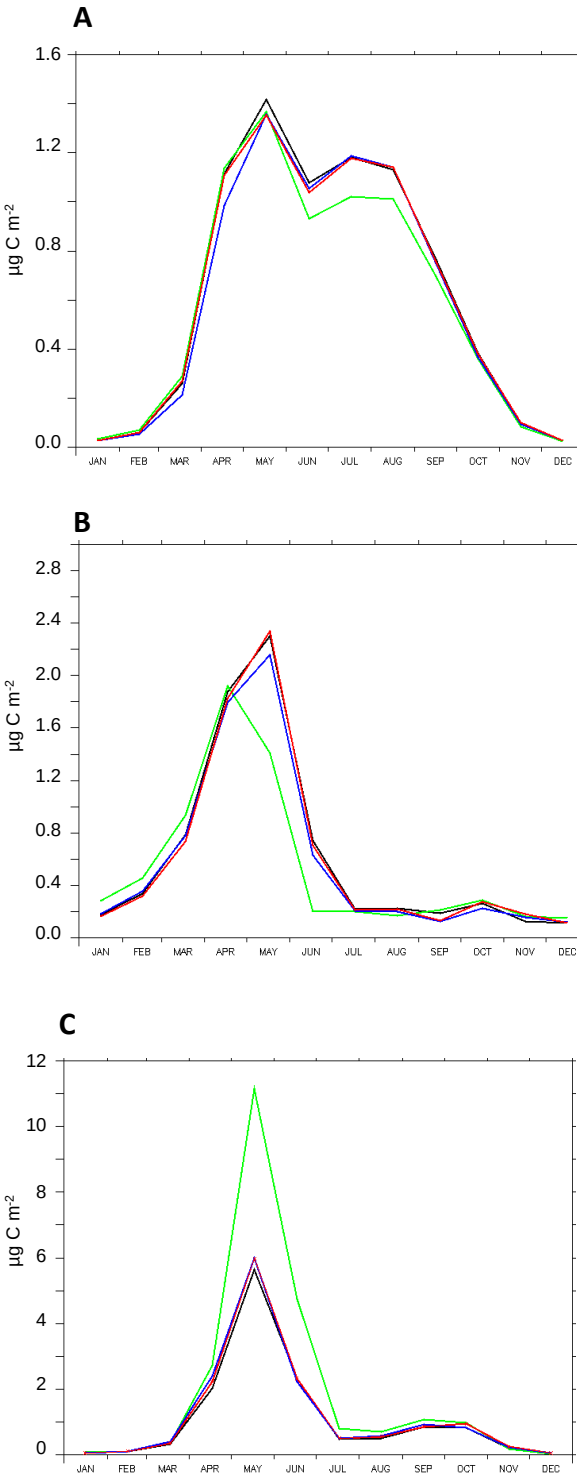

Fig. 4.16. Change in R_d: integrated concentrations over the year in NAt; Colours as in 4.12 ; A) diatoms, B) mixed-phytoplankton, C) coccolithophores,

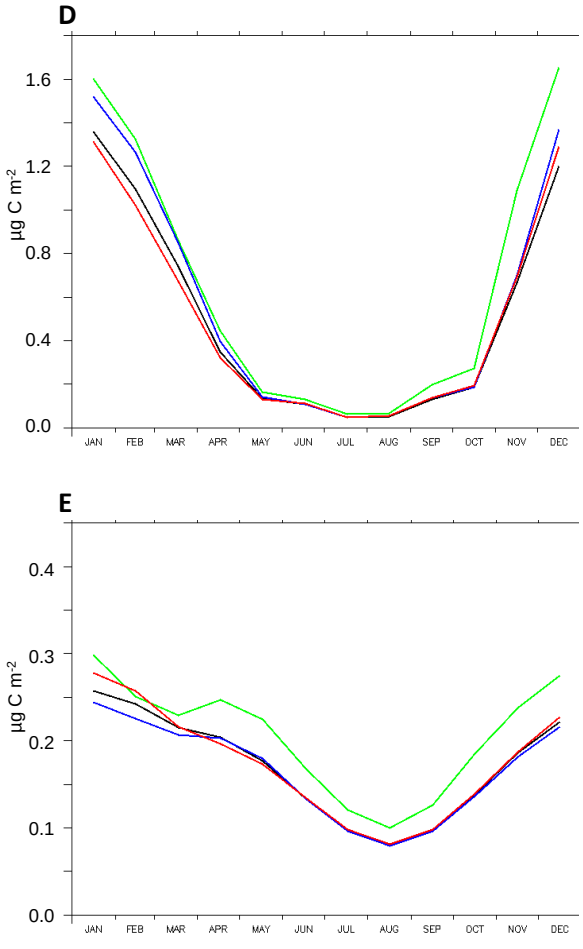

Fig. 4.15. Change in R_d, D) proto-zooplankton, E) meso-zooplankton.

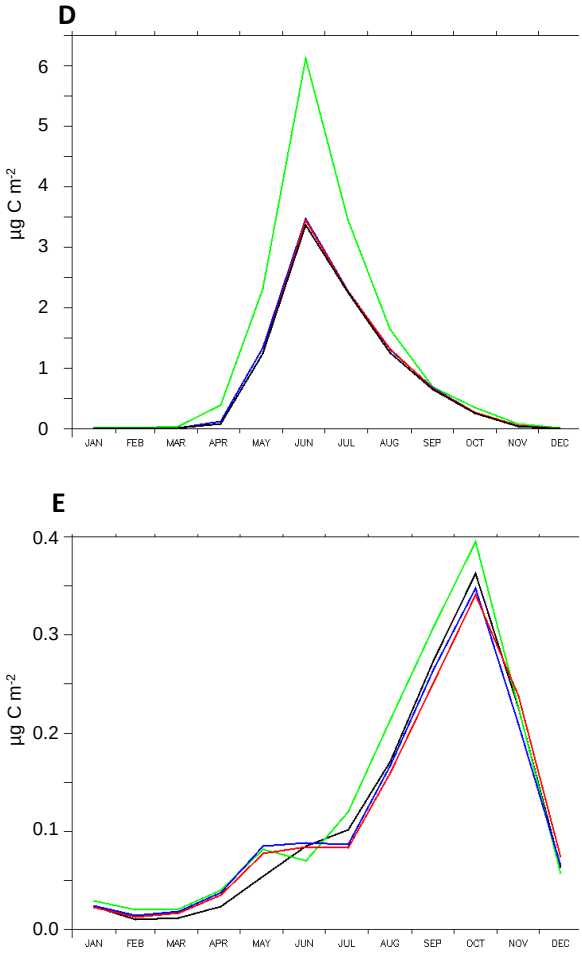

Fig. 4.16. Change in R_d, D) proto-zooplankton, E) meso-zooplankton.

4.3.7 Comparisons with observational data

We will now investigate which simulation represents best the marine ecosystem. For this we compare the model outputs to field data. The MareDAT network contains data from the literature or from field campaigns on diatoms, coccolithophores, proto- and meso-zooplankton. abundance over the global ocean. For each simulation, we calculated the residual sum of square (RSS) between the modelled PFT biomasses and the observations. The program compares, for each cell of the grid, the model output and the observational data if any. The simulation with the lowest RSS, RSSmin, is considered as fitting the best to the model. For every other simulation we calculated RSS/ RSSmin. If this ratio is higher than the 95% confidence interval, then we have proved a significant difference between models.

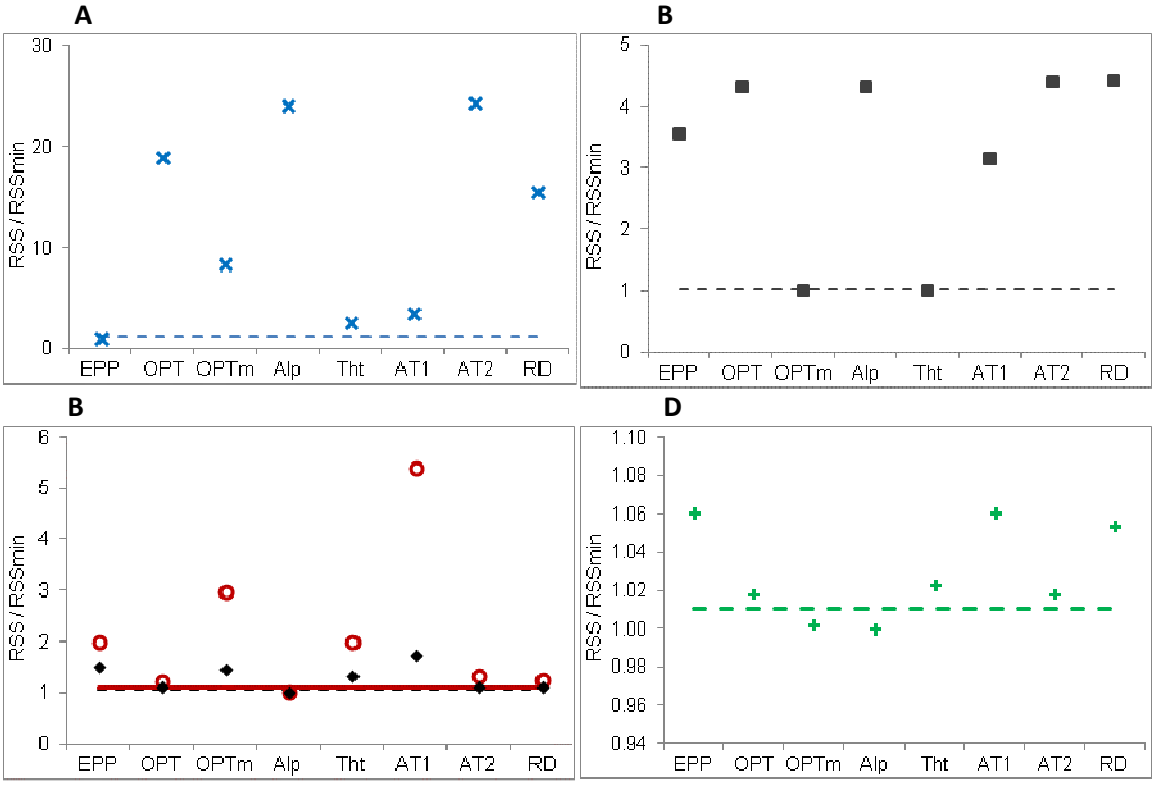

Fig. 4.17: Correlations between model simulations and observations of (A) diatoms, (B) meso-zooplankton, (C) coccolithophores (circles), proto-zooplankton (diamonds) and (D) total chlorophyll; lines are 95% confidence intervals.

It is difficult to select the simulation showing closest plankton abundance to the observations. Regarding diatoms, the best fit is OPT, Alp and AT2; meso-zooplankton is well represented in the model, except in OPTm and Tht. For coccolithophores, the best simulation is EPP, OPTm and AT1. Figure 1.17.D shows the comparison of total chlorophyll with the World Ocean Atlas 2005 data. The simulations the more realistic would be EPP, AT1 or RD.

4.4 DISCUSSION

Biological outputs of the PlankTOM5.3 model were compared for different simulations. Parameter values for temperature dependence, photosynthesis and dark respiration were successively changed, enabling us to study independently the impact of each of them on community structure and global biogeochemical outputs (primary production, export and chlorophyll). The range of parameter values corresponds to physiological data taken from laboratory experiments.

Global primary production in the original simulation (EPP) is 47.99 Pg C yr^{-1} (Table 4.3). Except for the simulation OPTm, all simulations give significantly higher estimates of the primary production, up to 50.44 Pg C yr^{-1}. All values are within the range of previous estimates from observations (45.9 Pg C yr^{-1}, Behrenfield and Falkowski, 1997) or models (59 ± 7 Pg C yr^{-1}, Buitenhuis and Le Quéré, *submitted*). Estimations for carbon export at 100 m, ranging from 8.50 to 10.05 Pg C yr^{-1} (Table 4.4), are in the same order than the estimate by Falkowski *et al.* (2003) of 11.1 Pg C yr^{-1}.

We can summarise our study in three successive experiments:

- the maximum growth rate and temperature dependence (4.4.1),
- the photosynthesis parameters (4.4.2),
- the respiration rate, or loss rate (4.4.3).

It is important to note that the simulations Alp and Tht do not have equivalence *in situ*. While we modified in AT1 both photosynthetic parameters α^{Chl} and θ_m as observed in laboratory experiments, only α^{Chl} (θ_m) was modified in Alp (Tht). This aims to understand their specific influence on the ecosystem. However, when comparing our results to field data, we will consider only the simulations EPP, OPT, OPTm, AT1, AT2 and RD.

First of all, the simulations OPT, OPTm, AT1, AT2 and RD present some common outputs. Changes of diatom parameters affect their abundance and/ or their distribution. Moreover, we observed changes in other PFT production, whose amplitude are at least as big as that of diatom abundance. In all experiments, changes of diatom biomass are bigger in the North-hemisphere than in the South. Changes of pPFT productions at high latitudes are equal or larger than at the Equator. Changes of zPFTs abundance are larger at high latitudes, while concentrations at the Equator are very much stable. We did not record any change of PFT distribution over depth, other than that of diatoms. Finally, outputs of the three experiments are within the same range of values.

Some PFTs are more affected by the changes of parameters than others. The mixed-phytoplankton is the PFT presenting the biggest standard error (12.4%) among the six simulations listed above, whereas diatoms present the smallest error (5.6%) (Table 4.3). The largest diatom production is found in the simulation OPTm, which produces also the largest

production of mixed-phytoplankton and meso-zooplankton. On the contrary, the production for those three PFTs is the smallest in the simulation AT2. The largest productions of coccolithophores and proto-zooplankton are obtained in AT1, in which the diatom production is also one of the smallest. These results resume a trend observed in all simulations: the association of the production of coccolithophores with proto-zooplankton and of mixed-phytoplankton and diatoms with meso-zooplankton.

Then, we have found regular differences in the community composition between North and South hemisphere. Diatoms are one of the most abundant phytoplankton groups in the Southern Ocean and the North-Atlantic. Hence consequences of diatom parameter changes are particularly important in those areas. We focused our analysis on those two areas and will develop this aspect further in the discussion. The way PFTs production varies among experiments helps us to estimate the importance of biological forcing versus physical forcing.

4.4.1 Maximum growth rate and temperature dependence

We tested two growth rate functions, representing the average (OPT) and maximal (OPTm) range for diatoms. Here we will discuss the differences between simulations EPP, OPT and OPTm. Although some modellers may use the maximal function (OPTm), we have chosen, as explained in chapter 2, to use the average (OPT). Therefore, OPT and OPTm represent the extreme functions for the representation of diatom growth rate. Testing the model with OPTm will provide us with an estimate of the sensitivity of the model to high diatom growth rates. In other words, outputs from OPT and OPTm will represent the corresponding deviation of the model due to plankton diversity.

As expected, the highest diatom production is obtained with OPTm. Although biomasses obtained in EPP and OPT are not significantly different, they lead to large differences in mixed-phytoplankton and proto-zooplankton production. It is worth noting that the small diatom biomass in OPT leads to the higher proportion of diatoms within the phytoplankton (15.7%). On the contrary, the proportion is the lowest in EPP (14%).

While growth rates are about 50% lower with the equation OPT than in OPTm, diatom production simulated by PlankTOM5.3 does not differ that much: global diatom production in OPT is 9% lower than in OPTm. When changing from OPTm to OPT, the biggest impacts are

on mixed-phytoplankton (+23%), coccolithophores (-13%) and meso-zooplankton (+14%). Proto-zooplankton biomass varies by only 2%. We can then consider the global production ranging between 0.213 to 0.235 Pg C per year for diatoms, 0.809 to 1.044 Pg C per year for mixed-phytoplankton, 0.297 to 0.336 Pg C per year for coccolithophores, 0.190 to 0.193 Pg C per year for proto-zooplankton and 0.068 to 0.079 Pg C per year for meso-zooplankton. The export would be 9.05 to 10.05 Pg C per year.

Furthermore, changes of plankton community composition differ between areas. The change of growth rate vs. temperature function brings much larger changes of diatom production in the North hemisphere than in the South (Fig.4.5). This is also the case for coccolithophores and proto-zooplankton when concentrations are averaged over longitude. Nevertheless, results for particular areas such as SEP or NAt can be different.

In SEP, the low diatom production in OPT (12% lower than in OPTm) enables the growth of coccolithophores to increase by six-fold, whereas in NAt, even though diatom production falls by 22%, coccolithophores growth increases by about 30% only.

In NAt, the biggest effect of growth parameter change is on mixed-phytoplankton, whereas meso-zooplankton biomass does not vary much.

Mixed-phytoplankton and meso-zooplankton biomasses increase as well. Nutrient concentration varies, showing the influence of phytoplankton on nutrient levels in the Southern Ocean.

A change of temperature is expected to make a larger difference in a polar environment than at the Equator. As shown in Fig. 4.1, the relative increase of diatom growth rate between the functions EPP and OPT and between OPT and OPTm is higher at low temperature than at high temperature. More precisely, the difference between OPT and OPTm varies from 48% at 15°C to 55% at extreme temperature. Our hypothesis is that the temperature is one of the limiting factors in polar waters. Actually, our simulation of PlankTOM5.3 shows the role of the temperature in cold water is not the expected one: the variation of diatom abundance from EPP to OPTm is minimum in the Southern Ocean. On the contrary, the largest changes occur between 50°S and 65°N. In the Southern Ocean, the diatom biomass shifts along the latitude, growing southward in OPTm.

However, the simulation OPTm cannot be compared to a temperature rise. While a change of temperature would affect all PFTs as well as physical parameters, the changes from EPP and OPT to OPTm affects directly only diatoms. Nevertheless, it is not excluded that the same phenomena can be observed with a rise of the temperature.

4.4.2 Photosynthesis: from OPT to AT1

The changes in α^{Chl} and in θ_m should be considered together, as it is unlikely that only one of those parameters would change. Nevertheless, studying distinct effects of changes in α^{Chl} and in θ_m, as we did in simulations Alp and Tht, respectively, gave us information about the importance of light-limited photosynthesis and chlorophyll content. We will briefly discuss those experiments before focusing on simulations AT1 and AT2.

The large changes in phytoplankton and zooplankton production are consequences of the complex interconnection between PFTs. Responses of PFTs differ between SEP and NAt.

For instance, the change in α^{Chl} has a major effect on several PFTs in the Southern Ocean, whereas it does not create any big changes in NAt. The difference between SEP and NAt does not reside in the diatom concentration, but in the start of the bloom: biomass increases one month earlier in SEP in the simulation Alp. Variations between simulations OPT and Alp shows phytoplankton in SEP ecosystem is highly limited by the light intensity. The high α^{Chl} value in Alp enables diatoms to photosynthesise more efficiently and therefore grow earlier.

The decrease of diatom chlorophyll content would affect their capacity for photosynthesis but also the light absorption by the cells. During blooms, light-shading by cells decreases the light penetration in the water column, preventing deeper cells from growing. A decrease of Chlorophyll content in diatom cells would enable other plankton to grow at the same time, as long as they are not limited by nutrients or trace metals. In the simulation Tht, the low θ_m affects the light absorbance in the water column. Less Chlorophyll in diatoms means more light can reach other phytoplankton cells. It appears that diatom chlorophyll concentration influences mostly the mixed-phytoplankton production.

The results of PFTs to those changes underline the strong interconnection between PFTs in SEP: competition for nutrients between diatoms and coccolithophores; dependence of meso-zooplankton on diatoms during the spring bloom and on proto-zooplankton and/ or coccolithophores in autumn; grazing of proto-zooplankton on mixed-phytoplankton in autumn.

The timing of the diatom bloom has a large impact on mixed-phytoplankton and coccolithophores. The late bloom of diatoms in the simulation Tht allows mixed-phytoplankton to grow first, consuming the available iron.

On the contrary, PFTs in the North Atlantic are geographically separated and affect less each other. Mixed-phytoplankton, unlike diatoms, grow in non-turbulent waters; coccolithophores and proto-zooplankton develop at northern latitudes along the Greenland East coast, while diatoms grow in open and deeper waters of the Atlantic.

Let us consider now the simulations AT1 and AT2, where both photosynthetic parameters were modified according to experimental results.

In the simulation AT1, although diatom carbon biomass changes very slightly compared to the simulation OPT, the chlorophyll content drops by two-fold. This has major consequences on other PFTs: mixed-phytoplankton and coccolithophores global biomass increase, as well as proto-zooplankton biomass. We also observed an increase of the iron concentration from 40°N northward.

The difference between carbon and Chlorophyll content is bigger in AT2. Diatom carbon content barely varies, but the chlorophyll content drops by about a third. While chlorophyll content is lower than in AT1, effects on other PFTs are very weak or inexistant, in SEP as in NAt. We are not able to explain the different responses of the plankton community between the simulations AT1 and AT2, particularly why the change from OPT to AT2 has fewer effects on other PFTs than the change to AT1.

The change of diatom photosynthetic parameters does not significantly affect nutrients and iron concentration.

Diatom biomass varies from 0.202 Pg C per year in AT1 to 0.213 Pg C per year in OPT. This small variation does not mean the difference in parameters should be under-estimated. As we discussed, effects on other PFTs are far bigger. Hence, every PFT biomass should be taken into account when choosing a parameter value.

However, modellers considering modifying α^{Chl} and θ_m as in AT1 and AT2 should also review the photosynthesis parameters for other PFTs. It has been shown different group of phytoplankton differ by their photosynthesis parameters. According to Parson *et al.* (1984),

green algae perform best at low light intensity, whereas dinoflagellates do best at high light intensities. Diatoms are situated in between. Therefore, a change in diatom parameters should be associated with a change of mixed-phytoplankton and/ or coccolithophores parameters. The present experiments do not aim to give the direction of each PFT, but rather to evaluate the relative importance of biomass changes.

We can compare the model outputs of AT1 and AT2 to the range of PFT productions determined above from OPT and OPTm. Diatom biomass is lower in AT1 and AT2 than in OPT. Coccolithophores and proto-zooplankton biomasses are above the range obtained in OPT and OPTm, whereas meso-zooplankton biomass is within.

Overall, global primary production increases in AT1 and AT2, while the export decreases.

4.4.3 Dark respiration: from AT1 to RD

Here, the R_d enters in the formulation of the loss rate. As R_d value doubles in RD, we would have expected a decrease of the diatom biomass. On the contrary, the diatom biomass increases from 0.202 Pg C per year in AT1 to 0.210 Pg C per year in RD. As for the change of temperature dependence, the change in diatom loss parameter has a bigger effect in the north hemisphere (Fig 4.14). This is also the case for the coccolithophores and proto-zooplankton.

While diatoms, mixed-phytoplankton and meso-zooplankton biomass are the most affected by the change in growth parameters, coccolithophores and proto-zooplankton biomass vary more with the change of diatom loss parameters (+13 and 17%, respectively).

However, productions in SEP and NAt show very limited changes.

4.4.4 Distribution of PFTs

Although the aim of this chapter is not to provide a deep comparison of each PFT distribution to available data, we will review the main outputs of our simulations on PlankTOM5.3. Comparison between simulations can help us identify incoherent predictions.

Diatoms are mainly present in polar water, in the North Atlantic and North Pacific and at the Equator. Mixed-phytoplankton is predicted in mid-latitudes. In the SEP as in NAt, diatoms are particularly present where the mixed-layer depth (MLD) exceeds 200m. Diatoms can grow

in turbulent water. As they can survive in darkness, they can be mixed below the MLD. On the contrary, coccolithophores grow along the coast, in stratified waters, where the MLD is less than 150m. PFTs distribution is largely dictated by physical characteristics, such as currents and MLD. At the Equator, zooplankton productions are very stable, whereas mixed-phytoplankton biomass varies between OPT and OPTm.

The general trends of PFTs distribution in EPP are close to observations. This is particularly true for diatoms, for example, that grow in high latitudes and in nutrient-rich waters from upwelling (Uitz *et al.*, 2006). However, the simulation EPP may not reflect accurately the coccolithophores distribution. If observations showed coccolithophores blooms in northern North Atlantic and Sub-Arctic Pacific (Holligan *et al.*, 1993; Brown and Yoder, 1994), field studies (Findlay and Giraudeau, 2000) and sediment record (McIntyre and Bé, 1967) do not highlight their presence south of the polar front in the Southern Ocean.

We observed significant changes in the ocean. Although the coccolithophores global production is equal in EPP and OPT, their distribution over latitude differs. The biomass is much higher in OPT than in EPP in the Southern Ocean, whereas lower in polar and sub-polar Northern latitudes. Therefore, the comparison of our simulations should be not only quantitative but also qualitative. The variation of the five PFT production among the simulations could provide some criteria of selection. For instance, the proto-zooplankton production follows in our experiments the same pattern as that of coccolithophores: their density is higher in OPT than in EPP in the Southern Ocean and lower in polar and sub-polar Northern latitudes. The correlations confirm the similar trend of proto-zooplankton and coccolithophore production: the correlation between model and data is the best in OPTm and AT1.

However, we cannot draw conclusions from the correlations with MareDAT observation data or with Chlorophyll data. There may be some bias in our method. We compared, for each cell of the grid, the model output and the observational data if any. If the same densities are found in the same area but in different cells, then the correlation will not take into account this similarity. It is possible our simulations are very close to observations, but not accurate enough for it to be noticed.

4.4.5 Role of diatoms in carbon export

The carbon export in the model PlankTOM5.3 is driven by the sinking of faecal pellets from zooplankton and of aggregated organic matter. Diatoms play a role in both pathways. They are the main source of food for the mesozooplankton. The silica contained in the cell wall contributes to the higher density of aggregates and faecal pellets.

The outputs of the eight simulations of PlankTOM5.3 show that carbon export is correlated with diatom production as well as to aggregated organic matter (GOC). Nevertheless, the complexity of the model means this correlation can be the result of many factors. Therefore, we do not give the diatom production as a direct explanation to the carbon export.

This study highlights the unpredictability of the marine ecosystem responses to a change in diatom parameterisation. The simulation outputs show how some groups of phytoplankton can dominate as soon as conditions are favourable. The variability of the mixed-phytoplankton biomass through our simulations shows it is composed of opportunistic organisms able to grow in a wide range of conditions. Although the model parameters set up diatoms and proto-zooplankton (mixed-phytoplankton) as preferential prey for the meso-zooplankton (proto-zooplankton), these preferences were not obvious in some simulations.

PFTs respond differently to the changes imposed. Global biomass data show that diatoms, mixed-phytoplankton and meso-zooplankton were more influenced by changes of temperature dependence, whereas coccolithophores and proto-zooplankton show a bigger response to changes in photosynthesis parameters (Table 4.3).

CHAPTER 5

CONCLUSION

This study took us from very specific laboratory physiological experiments through to the modelling of global primary production. It forms part of a larger project of cooperation between experimenters and modellers. Modellers of the marine ecosystem face the constant trade-off between the representation of major PFTs and solving the complexity in marine ecosystems. Individual species within each PFT can be very different. This highlights the challenge faced by modellers to expand the ecosystem representation to take in some of the biological complexity. On the other hand, physiologists face the difficulty to simplify the physiological data to define the ecological niches of PFTs or taxonomic groups.

In chapter 1 we introduced what has been the environmental cost of our countries' industrialisation and modernisation and what is now threatening the human population. Climate change is driven by anthropogenic carbon dioxide emissions, of which 90% comes from fossil fuel combustion. A part of this carbon remains in the atmosphere, while the rest is absorbed by the oceans or by the vegetation on land. However, the absorption by the oceans is decreasing, from 33% 50 years ago to 27% nowadays (Le Quéré, 2010).

The absorption of carbon by the oceans has consequences on chemical properties, like pH or the depth of calcite saturation, as well as on organisms. Scientists are only beginning to understand the effects of ocean acidification on organisms. While it is relatively easy to study physiological effects on individual species *in vitro*, it is much more difficult to estimate the effects within an ecosystem. By simulating physical, chemical and biological phenomena in the ocean, modelling is a way to estimate and predict the consequences of climate change on marine organisms, and therefore on the marine ecosystem.

Because of its photosynthetic activity - phytoplankton plays an important role in absorbing atmospheric carbon and exporting it to the deep-ocean. PlankTOM5 is one of the models simulating marine primary production where plankton is represented by functional groups that are each characterised by a specific biochemical metabolism. In the model PlankTOM5 phytoplankton is divided into coccolithophores, mixed-phytoplankton and diatoms, the latter being the subject of this study.

This work aims to constrain the parameters for diatom growth dependence on temperature and light with experimental data and to evaluate the sensitivity of model outputs on those parameters.

Chapter 2 is an in-depth review of the growth functions essential to phytoplankton modelling, i.e. the maximum growth of diatoms as a function of temperature. Although Eppley's (1972) curve has been widely used, no statistical study specifically concerning diatoms had been done until now.

Eppley (1972) compiled a database of growth rates from different groups, including eukaryotic and prokaryotic cells. An exponential curve was fitted graphically on the upper edge of the data points. Bissinger et al. (2008) compiled a bigger database of phytoplankton growth rates and applied a quantile regression to obtain a curve fitted at the 99^{th} quantile. The curve was graphically very similar to Eppley's (1972). Both authors assumed an exponential increase of the growth rate. Acknowledging this might not be the case at high temperature (Behrenfeld and Falkowski, 1997), Bissinger *et al.* applied the same method to a sub-set of growth rates up to 29°C. Although the curve obtained was not significantly different to the one fitted to the whole database, the author recommends not using this function above 29°C.

Diatom growth rate varies widely, in particular with cell size (Sarthou *et al.*, 2005). For each temperature, growth rates vary from about a factor of 5 up to one order of magnitude (Figure 2.1). This results in a large range of growth rates for each temperature, leaving many possible mathematical functions to represent the data. As a consequence, defining parameters of growth fitting to any species is challenging. Nevertheless, diatom growth rates differ in some aspects from that of other groups. The maximum rates are high, especially at low temperatures (Furnas, 1990). On the contrary, their growth rates at high temperatures are not as high as those of blue-green algae, which were included in Eppley's database.

We aim to provide modellers with a function representing the relatively high growth rates of diatoms, while giving realistic growth rates at high temperatures.

We intend to implement in PlankTOM5.3 the average diatom growth rate. In other words, we will not use a curve fitted to the upper edge of our experimental growth rates data, but to the average. We use for this a least minimum square cost-function, fitted to the average data.

The comparison of three functions (linear, exponential and optimal) shows that the optimal function (Schoemann *et al.*, 2005) fits the best to the average dataset, from -2°C to 37°C. It is also the best fit if we exclude growth rates obtained at supra-optimal temperature.

When considering rates up to 31°C only, the exponential function fits as well as the optimal one. However, we require, for modelling purposes, a function usable over 31, from 2°C to 37°C, which would not overestimate growth rates at high temperatures. Therefore we suggest the use of an optimal function (5), instead of Eppley's curve, to represent the diatom growth in models.

To compare our data to Eppley's and Bissinger's, we fit an exponential and an optimal function, by the quantile regression method, on the 99^{th} quantile of our database, as in Bissinger et al. (2008). The exponential curve is higher than Eppley's curve but is not significantly different from Bissinger's. The exponential curve gives growth rates such as $4.5d^{-1}$ at 28°C, which is very high. If the maximal growth rate is to be represented in a model, we recommend using the optimal curve.

In the experiments detailed in chapter 3, four diatom species were incubated at different light intensities. In consequence cells adjusted their metabolism and chemical content to the light intensity. A cell exposed to low light will synthesise a high amount of chlorophyll, in order to increase light absorption. This results in a high Chlorophyll: carbon ratio (θ). On the contrary, cells exposed to high light intensity have a reduced θ. This is clearly demonstrated in figure 3.1, where θ for the four species decreases with the acclimation light intensity.

During PI curve experiments, cells are subjected to increasing light intensities. The oxygen production, normalised to the cellular chlorophyll content, informs us on their light-limited photosynthetic efficiency (α^{Chl}). Because the photosynthetic efficiency is expressed per chlorophyll content, we would expect α^{Chl} not to vary with acclimation light intensity (Geider et al., 1985). It depends on the light absorption efficiency (in meter square per chlorophyll) and on the maximum quantum efficiency of the photosynthesis (in oxygen produced per photon), both parameters that are constant for the same species (Geider et al., 1985; Kolber et al., 1988). Deviation of α^{Chl} in our experiments comes from cumulated errors in cell counting, chlorophyll analysis and oxygen measurements. However, our experiments show more variations of α^{Chl} in cold-water species *Chaetoceros brevis* and *Thalassiosira antarctica*, of unknown origin. Although the light-limited photosynthetic efficiency per cell

confirm results from previous studies, low chlorophyll content in our species lead to higher α^{Chl} than reported in the literature.

The oxygen production normalised to the cellular carbon content informs us on the maximum photosynthetic rate (P_m). It is directly related to the growth rate, i.e. to the carbon assimilation and the respiration rate. Cells exposed at high-light intensity reach their maximum photosynthesis rate (P_m). Deviations of P_m in our experiments could come from error in measurements of respiration rate,

Regarding the application of our results into the photosynthesis model, we are particularly interested in the relation between α^{Chl} and θ_m. As explained above, we found lower θ_m values for higher α^{Chl} values, compared to the literature (Fig.B.2). However, the ratio α^{Chl} over θ_m is similar to other studies (Geider et al. 1997).

In the iron-light co-limitation model (Buitenhuis and Geider, 2010), cellular ratio (Fe:C and Chl:C) and growth rates are defined as a function of the light intensity and the iron availability. There are two ways of calibrating the model parameters. As in Buitenhuis and Geider (2010) we used data on growth rate and Chl:C ratio obtained at different light intensities to optimise the model values for α^{Chl}, θ_m and μ_m (annexe II). Independently from that, we also calculated directly the photosynthetic parameters P_m and α^{Chl} from PI curves, as well as the cellular content in carbon and chlorophyll. The second method can be used as a validation of the optimisation. The difference between the parameters that were obtained by parameter optimisation and the parameters that were obtained by fitting PI-curves to the measurements are discussed in terms of the difference between measured and observed Chl:C ratio.

The optimisation gives different values for α^{Chl}, P_m and θ_m. The difference could come from errors in our measurements and/ or deviations from badly constrained parameters in the model. Optimised values for P_m are closer to our species' growth rate than the P_m from the PI curves. A possible error could be an under-estimate of the growth rate, for instance if the cultures were not acclimated enough time to the conditions of growth; error in carbon analyses; error in calibration of the Oxygraph, leading to wrong oxygen evolution rates.

The various photosynthesis parameters obtained among species can be grouped in two sets of parameters, which are included in the model, in two different simulations (AT1 and AT2). Simulation of the model will show how these differences influence the marine ecosystem.

In the chapter 4, we ran eight simulations of the model PlankTOM5.3, differing in the parameter values for diatom maximum growth rate, photosynthetic parameters and/ or respiration rate. A comparison of the outputs, such as PFT biomasses, primary production and carbon export gives an estimate of the sensitivity of the model to the diatom parameters.

We first experimented on the function defining the diatom temperature-dependence. As justified in Chapter 2, Eppley's curve (1972) is replaced by an optimal function fitted at the average growth rate (simulation OPT). Although the global diatom production is not significantly different, the change is big enough to create a global increase of mixed-phytoplankton and meso-zooplankton biomass, as well as an increase in the North hemisphere of the coccolithophores and proto-zooplankton biomass. To simulate a maximum diatom growth, we also ran the simulation OPTm using an optimal curve fitted at the upper-edge of the plot. The global diatom production is significantly higher, but mixed-phytoplankton and meso-zooplankton biomasses do not change as much as they do in the simulation OPT. The parameters as in OPT were kept in the following runs.

In the second series of experiments we modified the parameters α^{Chl} and/ or θ_m. In the simulation Alp, α^{Chl} was doubled, creating an increase of the diatom biomass and a deepening of the maximum chlorophyll depth. It mainly advantages the meso-zooplankton. In the simulation Tht, the value for θ_m was halved. As a consequence, the diatom biomass decreases by 43% and the maximum chlorophyll depth becomes shallower. In the simulation AT1, α^{Chl} was doubled and θ_m was halved, representing our observations on cold-water species. This creates a 50% decrease of the diatoms chlorophyll biomass which benefits mostly to mixed-phytoplankton, coccolithophores and proto-zooplankton. The primary production increases, while the export decreases. In the simulation AT2, α^{Chl} was multiplied by three and θ_m was divided by three, to fit our observations on temperate species. Compared to OPT, the diatom carbon biomass is only slightly lower (-4%), but the chlorophyll biomass drops by about 70%. Changes to other PFTs are small or non-significant., giving advantage to coccolithophores and proto-zooplankton. There is no change to carbon export.

In the last simulation (RD) we use the temperature-dependence as in OPT and the photosynthetic parameters as in AT1. The respiration rate is doubled and outputs are

compared to the simulation AT1. Unexpectedly, the diatom carbon production increases, whereas the biomass of the four other PFTs decreases. The global primary production decreases while the export increases.

The changes in PFTs production in SEP and NAt inform us on the interconnection between PFTs. In SEP, small changes in diatom production can lead to very large development of coccolithophores. Proto- and meso-zooplankton feed on various PFTs at different times of the year.

In NAt, coccolithophores and proto-zooplankton are very much restricted to the Northern latitudes along Greenland coast. Coccolithophores are the main prey for proto-zooplankton. Mixed-phytoplankton and meso-zooplankton are more opportunists and grow in various places, depending on the location of food. The meso-zooplankton production is stable, a sign of a wide range of prey. Diatoms are represented on a large area from Canada to Europe.

So, how good is the model PlankTOM5.3?

If we look at the primary production, outputs of the different simulations range from 47.28 (for OPT) to 50.44 Pg C yr^{-1} (for AT1) with a standard deviation of 2%. This is in agreement with previous estimates of primary production by satellite algorithms which extend from 38 to 67 Pg C yr^{-1} (Behrenfield and Falkowski, 1997). Variation from the change in temperature dependence is +1.34%, between OPT and OPTm, whereas that caused by the change of photosynthesis parameters is +3.70% (between OPT and AT1). The change in respiration rate leads to a variation of -2.9% (between AT1 and RD). Relative to the range from satellite algorithm estimates, the primary productions by the different simulations are then very close to each others. Because of this small range, primary production could not be used as a criterion to choose the best model for representing the marine ecosystem.

Moreover, as we explained above, the primary production cannot be used on itself to validate a model. Effectively, similar global productions can hide large differences at regional level as, for instance, between the North and South hemisphere.

Therefore, other parameters like PFT production or ecosystem composition need to be taken into account. The general trend of PFT distributions is coherent with observation data. A dataset of field data on plankton abundance is the ideal tool to validate a model. We used

the MareDAT data to compare the outputs of each simulation. No simulation appears better than others. At least we can identify the worst, which would be the simulation Tht. Simulations OPT, Alp, AT1 and AT2 give the best correlation for two PFTs.

Despite the large effort of data collection by the network MareDAT, the number of field data is still limited and carbon estimates are prone to high uncertainty (Fig.5.1).

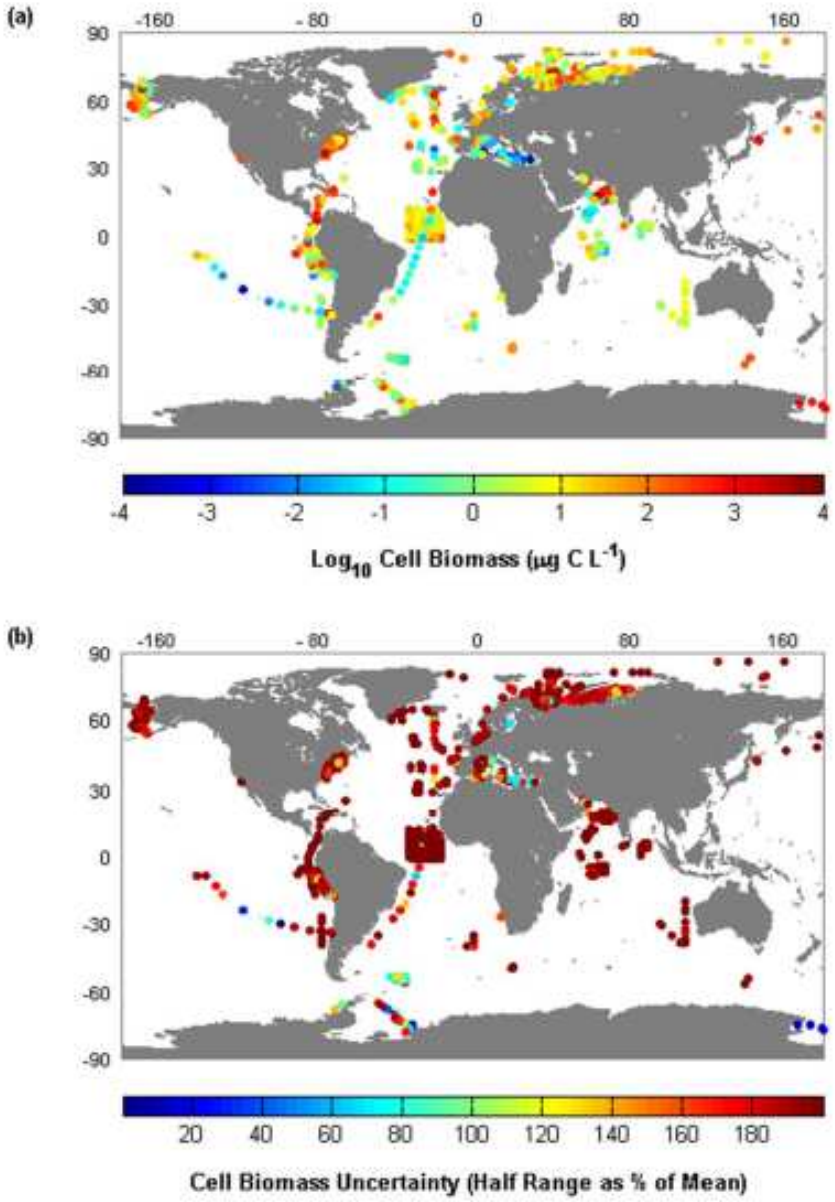

Fig. 5.1: Mean surface diatom carbon biomass (a) and uncertainty in cell biomass, in % of the mean (b). Figures reproduced from Leblanc et al., 2012.

How to validate the model with few field data? Satellite observations of the ocean content in chlorophyll are another tool to validate model outputs. Outputs for each simulation were

compared, by correlation, with Chlorophyll concentration from the World Ocean Data 2005. The best correlations are obtained with simulation EPP, AT1 and Rd.

This work brings more information on diatom growth and representation in a DGOM. The next step in the building of PlankTOM5.3 is to improve the parameters for other PFTs. Data are still missing in terms of PFTs abundance and distribution. A comparison of the model at local or regional level of the community composition over the year could help identify incoherence. For instance, is the bloom of coccolithophores in Fig. 4.6 C realistic? The results of the simulations could be studied deeper. The fact that coccolithophores respond by very large variation after a change of diatom growth parameter may indicate the parameters of coccolithophore growth need improvements.

The validation of the model would require more field data on cell abundance, carbon content per cell and PFT dominance over the year. Another way to validate the model outputs would be to compare the relative abundance of the different PFTs, i.e. the dominant phytoplankton. This information has been obtained from satellite observations of the ocean surface (Alvain et al. 2008). This method would give an overview of the model output and would allow the identification of areas of misrepresentation.

We can expect the model outputs to be sensitive to every parameter of the model. Are they more or less sensitive to diatom growth parameters? The same study on other PFTs could answer this question.

The study presented in Chapter 4 could be done using the model PlankTOM10, which includes ten PFTs. The mixed-phytoplankton is replaced by four PFTs: pico- and nanophytoplankton, N_2-fixers and DMSp-producers. The heterotrophs also include two more PFTs: macrozooplankton and picoheterotrophs (*Bacteria* and *Archaea*). It would be interesting to study the effects of changes of diatom photosynthesis parameters on the nine other PFTs. This could reveal some features such as competition and grazing preference. As diatoms have an important role in the Southern Ocean ecosystem, the comparison of biomass production, PFTs succession and carbon export in different simulations would help us to evaluate the model.

Much research is being done to identify the main drivers of the marine ecosystem. Sinha *et al*. (2010) compared the behaviour of the same model run within two different physical models. They showed a strong sensitivity of the DGOM PlankTOM5.2 to the ocean general circulation in which it is implemented. Anderson *et al*. (2010) studied the sensitivity of

PlankTOM 5.2 to the grazing formulation;. More recently, Sailley *et al*. (2013) compared food web structures of four DGOMs, differing in the number and characterisation of PFTs.

Although models are built to represent an intended ecosystem, the complexity of the marine ecosystem is such that modellers cannot predict the effects of environmental changes. In the same way, small changes of parameters can cause unexpected deviation of plankton abundance or distribution.

The PlankTOM models are under continuous development. The latest version, PlankTOM 10, includes ten PFTs, which have specific ecological functions (Le Quéré et al., 2005). A rigorous parameterisation of their growth and photosynthesis would allow a realistic representation across the ocean. However, improvements can also be made in the modeling of the nutrient assimilation, photosynthesis and organic matter recycling. Climate change is likely to bring changes in oceanic nutrient supplies (Laruelle et al., 2009). PlankTOM5.3 includes a constant cellular O: C: N: P ratio and variable Fe:C and Si:C ratios. As mentioned in the introduction chapter, some BGC models allow for variable cellular ratios, such as variable N:C ratio (Moore et al., 2002a, 200b). In the context of climate change and the effects of changes in nutrients supply, a good representation of the phytoplankton content is necessary to describe the consequences on other plankton species and higher trophic levels. The observational results that define the main controlling factors of cellular elemental ratios are still being made (e.g. Toseland *et al.*, 2013), so that these model developments largely remain to be implemented in the future.

BIBLIOGRAPHY

Alldredge, A. L. and C. C. Gotschalk (1989). "Direct observations of the mass flocculation of diatom blooms: Characteristics, settling velocities and formation of diatom aggregates." Deep Sea Research Part A, Oceanographic Research Papers **36**(2): 159-171.

Allen, J. I., J. R. Siddorn, J. C. Blackford and F. J. Gilbert (2004). "Turbulence as a control on the microbial loop in a temperate seasonally stratified marine systems model." Journal of Sea Research **52**(1): 1-20.

Alvain, S., C. Moulin, Y. Dandonneau and H. Loisel (2008). "Seasonal distribution and succession of dominant phytoplankton groups in the global ocean: A satellite view." Global Biogeochemical Cycles **22** (3): 3001.

Anderson, T. R. and I. J. Totterdell (2004). "Modelling the response of the biological pump to climate change." The ocean carbon cycle and climate M. a. O. Follows, T. Dordrecht, NATO Science Series. **IV:** 65-96.

Anning, T., G. Harris and R. J. Geider (2001). "Thermal acclimation in the marine diatom *Chaetoceros calcitrans* (bacillariophyceae)." European Journal of Phycology **36**(3): 233-241.

Antoine, D., J.-M. André and A. Morel (1996). "Oceanic primary production 2. Estimation at global scale from satellite (coastal zone color scanner) chlorophyll." Global Biogeochemical Cycles **10**: 57-69.

Armstrong, R. A. (1994). "Grazing limitation and nutrient limitation in marine ecosystems: steady state solutions of an ecosystem model with multiple food chains." Limnology and Oceanography **39**(3): 597-608.

Armstrong, R. A., C. Lee, J. I. Hedges, S. Honjo and S. G. Wakeham (2002). "A new, mechanistic model for organic carbon fluxes in the ocean based on the quantitative association of POC with ballast minerals." Deep-Sea Research Part II **49**(1): 219-236.

Aumont, O., S. Belviso and P. Monfray (2002). "Dimethylsulfoniopropionate (dmsp) and dimethylsulfide (dms) sea surface distributions simulated from a global three-dimensional ocean carbon cycle model." Journal of Geophysical Research **107**(4): 1-19.

Aumont, O., E. Maier-Reimer, S. Blain and P. Monfray (2003). "An ecosystem model of the global ocean including Fe, Si, P colimitations." Global Biogeochemical Cycles **17**(2).

Aumont, O. and L. Bopp (2006). "Globalizing results from ocean *in situ* iron fertilization studies." Global Biogeochemical Cycles **20**: n/a.

Beardall, J., Morris, Ian (1976). "The concept of light intensity adaptation in marine phytoplankton: Some experiments with *Phaeodactylum tricomutum*." Marine Biology **37**: 377-387.

Behrenfeld, M. J. and J. P. G. Falkowski (1997). "Photosynthetic rates derived from satellite-based chlorophyll concentrations." Limnology and Oceanography **42**: 1-20.

Behrenfeld, M. J., E. Boss, D. A. Siegel and D. M. Shea (2005). "Carbon-based ocean

productivity and phytoplankton physiology from space." Global Biogeochemical Cycles **19**(1): GB1006.

Bissinger, J. E., D. J. S. Montagnes, J. Sharples and D. Atkinson (2008). "Predicting marine phytoplankton maximum growth rates from temperature: Improving on the Eppley curve using quantile regression." Limnology and Oceanography **53**(2): 487-493.

Blasco, D., T. T. Packard and P. C. Garfield (1982). "Size dependence of growth rate, respiratory electron transport system activity, and chemical composition in marine diatoms in the laboratory." Journal of Phycology **18**(1): 58-63.

Boyd, P. W., A. J. Watson, C. S. Law, E. R. Abraham, T. Trull, R. Murdoch, D. C. E. Bakker, A. R. Bowie, K. O. Buesseler, H. Chang, M. Charette, P. Croot, K. Downing, R. Frew, M. Gall, M. Hadfield, M. Hall, M. Harvey, G. Jameson, J. Laroche, M. Liddicoat, R. Ling, M. T. Maldonado, R. M. Mckay, S. Nodder, S. Pickmere, R. Pridmore, S. Rintoul, K. Safi, P. Sutton, R. Strzepek, K. Tanneberger, S. Turner, A. Waite and J. Zeldis (2000). "A mesoscale phytoplankton bloom in the polar Southern Ocean stimulated by iron fertilization." Nature **407**(6805): 695.

Brand, L. E. and R. R. L. Guillard (1981). "The effects of continuous light and light intensity on the reproduction rates of twenty-two species of marine phytoplankton." Journal of Experimental Marine Biology and Ecology **50**: 119-132.

Brzezinski, M. A. (1985). "The Si:C:N ratio of marine diatoms - interspecific variability and the effect of some environmental variables." Journal of Phycology **21**(3): 347-357.

Brown, C. W. and J. A. Yoder (1994). "Coccolithophorid blooms in the global ocean." Journal of Geophysical Research **99**: 7467-7482.

Bucciarelli, E., P. Pondaven and G. Sarthou (2010). "Effects of an iron-light co-limitation on the elemental composition (Si, C, N) of the marine diatoms *Thalassiosira oceanica* and *Ditylum brightwellii*." Biogeosciences **7**(2): 657-669.

Buesseler, K., L. Ball, J. Andrews, C. Benitez-Nelson, R. Belastock, F. Chai and Y. Chao (1998). "Upper ocean export of particulate organic carbon in the Arabian sea derived from thorium-234." Deep-Sea Research Part II-Topical Studies in Oceanography **45**(10-11): 2461-2487.

Buesseler, K. O. (1998). "The decoupling of production and particulate export in the surface ocean." Global Biogeochemical Cycles **12**: 297-310.

Buitenhuis, E. T. and C. Le Quere (*submitted*) "Combined constraints on ocean primary production and phytoplankton biomass from observations and a model." Global Biogeochemical Cycles doi:10.1029/2010BG004006.

Buitenhuis, E. T., R. B. Rivkin, S. Sailley and C. Le Quere (2010) "Biogeochemical fluxes through microzooplankton." Global Biogeochemical Cycles **24**.

Buitenhuis, E., C. Le Quere, O. Aumont, G. Beaugrand, A. Bunker, A. Hirst, T. Ikeda, T. O'brien, S. Piontkovski and D. Straile (2006). "Biogeochemical fluxes through mesozooplankton." Global Biogeochemical Cycles **20**(2).

Buitenhuis, E. T. and R. J. Geider (2010). "A model of phytoplankton acclimation to iron-light colimitation." Limnology and Oceanography **55**(2): 714-724.

Burkhardt, S. and U. Riebesell (1997). "Co_2 availability affects elemental composition (C:N:P) of the marine diatom *Skeletonema costatum*." Marine Ecology Progress Series **155**: 67-76.

Burkhardt, S., I. Zondervan and U. Riebesell (1999). "Effect of CO_2 concentration on C: N: P ratio in marine phytoplankton: A species comparison." Limnology and Oceanography **44**(3): 683-690.

Burnham, K. P. and D. R. Anderson (2002). "Model selection and inference: A practical information-theoretic approach." New York; London: Springer 2002.

Cannon, D., J. W. G. Lund and J. Sieminska (1961). "The growth of *Tabellaria flocculosa* (roth) kutz var flocculosa (roth) knuds under natural conditions of light and temperature." Journal of Ecology **49**(2): 277-287.

Castenholtz, R. W. (1964). "The effect of day length and light intensity on the growth of littoral marine diatoms in culture." Physiologia Plantarum **17**: 951-963.

Castenholz, R. W. (1969). "Thermophilic blue-green algae and the thermal environment." Bact. Rev. **33**: 476-504.

Claquin, P., I. Probert, S. Lefebvre and B. Veron (2008). "Effects of temperature on photosynthetic parameters and tep production in eight species of marine microalgae." Aquatic Microbial Ecology **51**(1): 1-11.

Crutzen, P. J. and E. F. Stoermer (2000). "The anthropocene." IGBP Newsletter **41**: 12-13.

Curl, H. J. and G. C. Mcleod (1961). "The physiologival ecology of a marine diatom *Skeletonema costatum*." Journal of Marine Research **19**(1): 70-88.

Dunstan, W. M. (1973). "A comparison of the photosynthesis- light intensity relationship in phylogenetically different marine microalgae." Journal of Experimental Marine Biology and Ecology **13**: 181-187.

Durbin, E. G. (1974). "Studies on the autoecology of the marine diatom *Thalassiosira nordenskioldii* cleve. I. The influence of daylenght, light intensity and temperature on growth." Journal of Phycology **10**: 220-225.

Egge, J. K. and A. Jacobsen (1997). "Influence of silicate on particulate carbon production in phytoplankton." Marine Ecology-Progress Series **147**(1-3): 219-230.

El-Sabaawi, R. and P. J. Harrison (2006). "Interactive effects of irradiance and temperature on the photosynthetic physiology of the pennate diatom *Pseudo-nitzschia granii* (bacillariophyceae) from the northeast subarctic Pacific." Journal of Phycology **42**(4): 778-785.

Eppley, R. W. and P. R. Sloan (1966). "Growth rates of marine phytoplankton: Correlation with light absorption by cell chlorophyll *a*." Physiologia Plantarum **19**(1): 47-59.

Eppley, R. W. (1972). "Temperature and phytoplankton growth at sea." Fishery Bulletin **70**(4): 1063-1085.

Eppley, R. W. (1980). "Primary productivity in the sea". Nature, **286**(5769):109-110.

Etheridge, D. M., L. P. Steele, R. L. Langenfelds and R. J. Francey (1996). "Natural and anthropogenic changes in atmospheric CO_2 over the last 1000 years from air in antarctic ice and firn." Journal of Geophysical Research. **101**: 4115-4128.

Falkowski, J. P. G. (1977). "The adenylate energy charge in marine phytoplantkon: The effect of temperature on the physiological state of *Skeletonema costatum* (grev.) cleve." Journal of Experimental Marine Biology and Ecology **27**(1): 37-45.

Falkowski, P. G. (1981). "Light shade adaptation and assimilation numbers." Journal of Plankton Research **3**(2): 203-216.

Falkowski, J. P. G., Z. Dubinsky and K. Wyman (1985). "Growth-irradiance relationships

in phytoplankton." Limnology and Oceanography **30**(2): 311-321.

Falkowski, P. G., J. A. Raven (1997). Aquatic Photosynthesis. Oxford, Blackwell Science.

Fasham, M. J. R. (1995). "Variations in the seasonal cycle of biological production in subarctic oceans: A model sensitivity analysis." Deep Sea Research Part I. Oceanographic Research Papers **1995**(42): 7.

Fawley, W. M. (1984). "Effects of light intensity and temperature interactions on growth characteristics of *Phaeodactylum tricornutum* (bacillariophyceae)." Journal of Phycology **20**(1): 67-72.

Findlay, C. S. and J. Giraudeau (2000). "Extant calcareous nannoplankton in the australian sector of the Southern Ocean (austral summers 1994 and 1995)." Marine Micropaleontology **40**(4): 417-439.

Flynn, K. J. (2001). "A mechanistic model for describing dynamic multi-nutrient, light, temperature interactions in phytoplankton." Journal of Plankton Research.

Francois, R., S. Honjo, R. Krishfield and S. Manganini (2002). "Factors controlling the flux of organic carbon to the bathypelagic zone of the ocean." Global Biogeochemical Cycles **16**(4): 1087.

Furnas, M. (1978). "Influence of temperature and cell size on the division rate and chemical content of the diatom *Chaetoceros curvisetum* cleve." Journal of Experimental Marine Biology and Ecology **34**(2): 97-109.

Furnas, M. J. (1990). "*In situ* growth rates of marine phytoplankton: Approaches to measurement, community and species growth rates." Journal of Plankton research **12**(6): 1117-1151.

Gallagher, J. (1982). "Physiological variation and electrophoretic banding patterns of genetically different seasonal populations of *Skeletonema costatum* (bacillariophyceae)." Journal of Phycology **18**: 148-162.

Gao, Y., S. G. Jason and R. S. Alberte (2000). "Temperature dependence of nitrate reductase activity in marine phytoplankton: Biochemical analysis and ecological implications." Journal of Phycology **36**(2): 304-313.

Geider, R. J., B. A. Osborne and J. A. Raven (1985). "Light dependence of growth and photosynthesis in *Phaeodactylum tricornutum* (bacillariophyceae)." Journal of Phycology **21**(4): 609-619.

Geider, R. J. and B. A. Osborne (1989). "Respiration and microbial growth: A review of the quantitative relationship between dark respiration and growth." New Phytology **112**: 327-341.

Geider, R. J. (1993). "Quantitative phytoplankton physiology - implications for primary production and phytoplankton growth." Measurement of Primary Production from the Molecular to the Global Scale **197**: 52-62.

Geider, R. J., H. I. Macintyre and T. M. Kana (1997). "Dynamic model of phytoplankton growth and acclimation:Responses of the balanced growth rate and the chlorophyll a:Carbon ratio to light, nutrient-limitation and temperature." Marine Ecology Progress Series **148**: 187-200.

Geider, R. J., H. L. Macintyre and T. M. Kana (1998). "A dynamic regulatory model of phytoplanktonic acclimation to light, nutrients, and temperature." Limnology and Oceanography **43**(4): 679-694.

Gilstad, M. and E. Sakshaug (1990). "Growth rates of ten diatom species from the barents

sea at different irradiances and day lengths." Marine Ecology Progress Series **64**(1-2): 169-173.

Goldman, J. C. and E. Carpenter (1974). "Kinetic approach to effect of temperature on algal growth." Limnology and Oceanography **19**(5): 756-766.

Goldman, J. C., D. A. Hansell and M. R. Dennett (1992). "Chemical characterization of three large oceanic diatoms: Potential impact on the water column chemistry." Marine Ecology Progress Series. **88**: 257-270.

Greene, R. M., R. J. Geider and P. G. Falkowski (1991). "Effect of iron limitation on photosynthesis in a marine diatom." Limnology and Oceanography **36**(8): 1772-1782.

Gregg, W. W., P. Ginoux, P. S. Schopf and N. W. Casey (2003). "Phytoplankton and iron: Validation of a global three-dimensional ocean biogeochemical model." Deep Sea Research Part II: Topical Studies in Oceanography **50**(22-26): 3143-3169.

Guillard, R. R. L. and J. H. Ryther (1962). "Studies of marine planktonic diatoms, i. *Cyclotella nana* hustedt and *Detonula confervacea* (cleve) gran." Canadian Journal of Microbiology **8**: 229-239.

Harrison, P. J., H. Conway, R. Holmes and C. Davis (1977). "Marine diatoms grown in chemostats under silicate or ammonium limitation. III. Cellular chemical composition and morphology of *Chaetoceros debilis*, *Skeletonema costatum*, and *Thalassiosira gravida*." Marine Biology **43**(1): 19-31.

Harrison, P. J., R. E. Waters and F. J. R. Taylor (1980). "A broad spectrum artificial sea water medium for coastal and open ocean phytoplankton." Journal of Phycology **16**(1): 28-35.

Harrison, G. I. and F. M. M. Morel (1986). "Response of the Marine Diatom *Thalassiosira weissflogii* to iron stress" Limnology and Oceanography. **31**: 989-997.

Hartey, H. O. (1950). "The use of range in analysis of variance." Biometrika **39**: 422-424.

Hegseth, E. N. (1989). "Photoadaptation in marine arctic diatoms." Polar Biology **9**(8): 479-486.

Henley, W. J. (1993). "Measurement and interpretation of photosynthetic light-response curves in algae in the context of photoinhibition and diel changes." Journal of phycology **29**: 729-739.

Hessen, D. O., E. Leu, P. J. Færøvig and S. Falk Petersen (2008). "Light and spectral properties as determinants of C:N:P-ratios in phytoplankton." Deep Sea Research Part II: Topical Studies in Oceanography **55**(20-21): 2169-2175.

Hitchcock, G. L. (1980). "Diel variation in chlorophyll a, carbohydrate and protein content of the marine diatom *Skeletonema costatum*." Marine Biology **57**: 271-278.

Holligan, A. T., E. Fernandez, J. Aiken, W. Balch, P. Boyd, P. Burkill, M. Finch, S. B. Groom, G. Malin, K. Muller, D. A. Purdie, C. Robinson, C. Trees, S. M. Turner and P. Van Der Wal (1993). "A biogeochemical study of the coccolithophore, *Emiliania huxleyi*, in the North Atlantic." Global Biogeochemical Cycles **7**(4): 879-900.

Hood, R. R., E. A. Laws, R. A. Armstrong, N. R. Bates, C. W. Brown, C. A. Carlson, F. Chai, S. C. Doney, P. G. Falkowski, R. A. Feely, M. a. M. Friedrichs, M. R. Landry, J. Keith Moore, D. M. Nelson, T. L. Richardson, B. Salihoglu, M. Schartau, D. A. Toole and J. D. Wiggert (2006). "Pelagic functional group modeling: Progress, challenges and prospects." Deep Sea Research Part II: Topical Studies in

Oceanography **53**(5–7): 459-512.

Hoogenho, H. and J. Amesz (1965). "Growth rates of photosynthetic microorganisms in laboratory cultures." Archiv Fur Mikrobiologie **50**(1): 10.

Hoppe, H. G., P. Breithaupt, K. Walther, R. Koppe, S. Bleck, U. Sommer and K. Jurgens (2008). "Climate warming in winter affects the coupling between phytoplankton and bacteria during the spring bloom: A mesocosm study." Aquatic Microbial Ecology **51**(2): 105-115.

Hulburt, E. M. and R. R. L. Guillard (1968). "The relationship of the distribution of the diatom *Skeletonema tropicum* to temperature." Ecology **49**(2): 337-339.

Indermühle, A., T. F. Stocker, F. Joos, H. Fischer, H. J. Smith, M. Wahlen, C. O. Deck, D. Mastroianni, J. Tschumi, T. Blunier, R. Meyer and C. O. Stauffer (1999). "Holocene carbon-cycle dynamics based on co2 trapped in ice at taylor dome, antarctica." Nature **398**(6723): 121-126.

Iversen, M. H. and H. Ploug (2010). "Ballast minerals and the sinking carbon flux in the ocean: Carbon-specific respiration rates and sinking velocity of marine snow aggregates." Biogeosciences **7**(9): 2613-2624.

Jassby, A. D. and T. Platt (1976). "Mathematical formulation of relationship between photosynthesis and light for phytoplankton." Limnology and Oceanography **21**(4): 540-547.

Jørgensen, E. G. (1968). "The adaptation of plankton algae. Ii. Aspects of the temperature adaptation of *skeletonema costatum*." Physiologia Plantarum **21**: 423-427.

Kain, J. M. and G. E. Fogg (1958). "Studies on the growth of marine phytoplankton .1. *Asterionella japonica* gran." Journal of the Marine Biological Association of the United Kingdom **37**(2): 397-413.

Kana, T. M., J. L. Watts and P. M. Glibert (1985). "Diel periodicity in the photosynthetic capacity of coastal and offshore phytoplankton assemblages." Marine Ecology-Progress Series **25**(2): 131-139.

Karsten, U., R. Schumann, S. Rothe, I. Jung and L. Medlin (2006). "Temperature and light requirements for growth of two diatom species (bacillariophyceae) isolated from an arctic macroalga." Polar Biology **29**(6): 476-486.

Kiefer, D. A. and B. G. Mitchell (1983). "A simple, steady state description of phytoplankton growth based on absorption cross section and quantum efficiency." Limnology and Oceanography **28**(4): 770-776.

Klaas, C. and D. E. Archer (2002). "Association of sinking organic matter with various types of mineral ballast in the deep sea: Implications for the rain ratio." Global Biogeochemical Cycles **16**(4): 1116.

Klunder, M. B., P. Laan, R. Middag, H. J. W. De Baar and J. C. van Ooijen (2011). "Dissolved iron in the Southern Ocean (Atlantic sector)." Deep Sea Research Part II: Topical Studies In Oceanography **58**(25-26): 2678-2694.

Koenker, R. and G. Bassett (1978). "Regression quantiles." Econometrica **46**(1): 33-50.

Kolber, Z., J. Zehr and P. Falkowski (1988). "Effects of growth irradiance and nitrogen limitation on photosynthetic energy conversion in photosystem II." Plant Physiology **88**(3): 923-929.

Kooijman, S. A. L. M. (2000). "Dynamic energy and mass budgets in biological systems." Cambridge, Cambridge University Press.

Krawiec, R. W. (1982). "Autecology and clonal variability of the marine centric diatom *Thalassiosira rotula* (bacillariophyceae) in response to light, temperature and salinity." Marine Biology **69**(1): 79-89.

Kudo, I., M. Miyamoto, Y. Noiri and Y. Maita (2000). "Combined effects of temperature and iron on the growth and physiology of the marine diatom *Phaeodactylum tricornutum* (bacillariophyceae)." Journal of Phycology **36**(6): 1096-1102.

Lancelot, C. E., E. Hannon, S. Becquevort, C. Veth and H. J. W. De Baar (2000). "Modeling phytoplankton blooms and carbon export production in the southern ocean: Dominant control by light and iron in the Atlantic sector in austral spring 1992." Deep Sea Research Part I: Oceanographic Research Papers **47**(9): 1621-1662.

Lancelot, C. E., Y. Spitz, N. Gypens, K. Ruddick, S. Becquevort, V. Rousseau, G. Lacroix and G. Billen (2005). "Modelling diatom and *phaeocystis* blooms and nutrient cycles in the southern bight of the north sea: The miro model." Marine Ecology Progress Series **289**: 63-78.

Langdon, C. (1988). "On the causes of interspecific differences in the growth-irradiance relationship for phytoplankton . II. A general review." Journal of Plankton Research **10**(6): 1291-1312.

Laws, E. A. and T. T. Bannister (1980). "Nutrient-limited and light-limited growth of *Thalassiosira fluviatilis* in continuous culture, with implications for phytoplankton growth in the ocean." Limnology and Oceanography **25**(3): 457-473.

Laws, E. A. (1991). "Photosynthetic quotients, new production and net community production in the open ocean." Deep Sea Research Part I: Oceanographic Research Papers **38**(1): 143-167.

Le Quere, C., S. P. Harrison, I. C. Prentice, E. T. Buitenhuis, O. Aumont, L. Bopp, H. Claustre, L. C. Da Cunha, R. J. Geider, X. Giraud, C. Klaas, K. E. Kohfeld, L. Legendre, M. Manizza, T. Platt, R. B. Rivkin, S. Sathyendranath, J. Uitz, A. J. Watson and D. Wolf-Gladrow (2005). "Ecosystem dynamics based on plankton functional types for global ocean biogeochemistry models." Global Change Biology **11**(11): 2016-2040.

Le Quéré, C., C. Rödenbeck, E. T. Buitenhuis, T. J. Conway, R. Langenfelds, A. Gomez, C. Labuschagne, M. Ramonet, T. Nakazawa, N. Metzl, N. Gillett, M. Heimann (2007) "Saturation of the southern ocean CO_2 sink due to recent climate change." Science **316**: 1735-1738.

Le Quéré, C. (2010). "Trends in the land and ocean uptake." Current opinion in Environmental Sustainability **2**(4): 219-224.

Leblanc, K., J. Aristegui, L. Armand, P. Assmy, B. Beker, A. Bode, E. Breton, V. Cornet, J. Gibson, M.-P. Gosselin, E. Kopczynska, H. Marshall, J. Peloquin, S. Piontkovski, A. J. Poulton, B. Quéguiner, B. Schiebel, R. Shipe, J. Stefels, M. A. Van Leeuwe, M. Varela, C. Widdicombe and M. Yallop (2012). "A global diatom database – abundance, biovolume and biomass in the world ocean." Earth System Science Data Discussions **5**(1): 147-185.

Lewin, J. C. (1957). "Silicon metabolism in diatoms .4. Growth and frustule formation in *Navicula pelliculosa*." Canadian Journal of Microbiology **3**(3): 427-&.

Li, W. K. W. and I. Morris (1982). "Temperature adaptation in *Phaeodactylum tricornutum* bohlin: Photosynthetic rate compensation and capacity." Journal of Experimental

Marine Biology and Ecology **58**: 135-150.

Lund, J. W. G. (1949). "Studies on *Asterionella* .1. The origin and nature of the cells producing seasonal maxima." Journal of Ecology **37**(2): 389-419.

Maldonado, M. T. and N. M. Price (1996). "Influence of n substrate on fe requirements of marine centric diatoms." Marine Ecology Progress Series **141**: 161-172.

Marland, G., T. A. Boden and R. J. Andres (2000). "Global, regional and national co_2 emissions." Trends: A Compendium of Data on Global Change. U. S. D. O. E. Carbon Dioxide Information Analysis Center. Oak Ridge, USA.

Mcginnis, K. M., T. A. Dempster and M. R. Sommerfeld (1997). "Characterization of the growth and lipid content of the diatom *Chaetoceros muelleri*." Journal of Applied Phycology **9**(1): 19-24.

McIntyre, A. and A. W. H. Bé (1967). "Modern coccolithophoridae of the atlantic ocean. I. Placoliths and cyrtoliths." Deep-Sea Research and Oceanographic Abstracts **14**(5): 561-597.

Merico, A., T. Tyrrel, E. J. Lessard, T. Oguz, P. J. Stabeno, S. I. Zeeman and T. E. Whitledge (2004). "Modelling phytoplankton succession on the bering sea shelf: Role of climate influences and trophic interactions in generating *Emiliania huxley*i blooms 1997-2000." Deep Sea Research Part I: Oceanographic Research Papers **51**(12): 1803-1826.

Monnin, E., A. Indermuhle, A. Dallenbach, J. Fluckiger, B. Stauffer, T. F. Stocker, D. Raynaud and J.-M. Barnola (2001). "Atmospheric CO_2 concentrations over the last glacial termination." Science **291**(5501): 112.

Monod, J. (1949). "The growth of bacterial cultures." Annual Review of Microbiology **3**(1): 371-394.

Montagnes, D. J. S. and D. J. Franklin (2001). "Effect of temperature on diatom volume, growth rate, and carbon and nitrogen content: Reconsidering some paradigms." Limnology and Oceanography **46**(8): 2008-2018.

Montagnes, D. J. S., S. A. Kimmance and D. Atkinson (2003). "Using Q_{10}: Can growth rates increase linearly with temperature?" Aquatic Microbial Ecology **32**: 307-313.

Moore, J. K., S. C. Doney, D. M. Glover and I. Y. Fung (2002a). "Iron cycling and nutrient-limitation patterns in surface waters of the world ocean." Deep Sea Research Part II: Topical Studies in Oceanography **49**(3): 463-507.

Moore, J. K., S. C. Doney, J. A. Kleypas, D. M. Glover and I. Y. Fung (2002b). "An intermediate complexity marine ecosystem model for the global domain." Deep Sea Research Part II: Topical Studies in Oceanography **49**(1): 403-462.

Mortain-Bertrand, A., C. Descolas-Gros and H. Jupin (1987). "Stimulating effect of light-to-dark transitions on carbon assimilation by a marine diatom." Journal of Experimental Marine Biology and Ecology **112**(1): 11-26.

Mortain-Bertrand, A., C. Descolas-Gros and H. Jupin (1988). "Growth, photosynthesis and carbon metabolism in the temperate marine diatom *Skeletonema costatum* adapted to low temperature and low photon-flux density." Marine Biology **100**: 135-141.

Muggli, D. L., M. Lecourt and P. J. Harrison (1996). "Effects of iron and nitrogen source on the sinking rate, physiology and metal composition of an oceanic diatom from the subarctic Pacific." Marine Ecology Progress Series **132**: 215-227.

Najjar, R. G., J. L. Sarmiento and J. R. Toggweiler (1992). "Downward transport and fate

of organic matter in the ocean: Simulations with a general circulation model." Global Biogeochemical Cycles **6**: 45-76.

Nelson, D. M., P. Treguer, M. A. Brzezinski, A. Leynaert and B. Queguiner (1995). "Production and dissolution of biogenic silica in the ocean - revised global estimates, comparison with regional data and relationship to biogenic sedimentation." Global Biogeochemical Cycles **9**(3): 359-372.

Nishikawa, T. and M. Yamaguchi (2006). "Effect of temperature on light-limited growth of the harmful diatom *Eucampia zodiacus* ehrenberg, a causative organism in the discoloration of *Porphyra thalli*." Harmful Algae **5**(2): 141-147.

Nobili R., C. Robinson, E. Buitenhuis and C. Castellani (2013). "Food quality regulates the metabolism and reproduction of *Temora longicornis*." Biogeosciences Discussions **10**(2): 3203.

Olascoaga, M. J., N. Idrisi and A. Romanou (2005). "Biophysical isopycnic-coordinate modelling of plankton dynamics in the Arabian sea." Ocean Modelling **8**(1–2): 55-80.

Paasche, E. (1968). "Marine plankton algae grown with light-dark cycles. Ii. *Ditylum brightwellii* and *Nitzschia turgidula*." Physiologia Plantarum **21**: 66-77.

Paasche, E. and I. Ostergren (1980). "The annual cycle of plankton diatom growth and silica production in the inner Oslofjord." Limnology and Oceanography **25**(3): 481-494.

Parsons T., M. Takahashi and B. Hargrave (1984). "Biological oceanographic processes." New York: Pergamon.

Pearson, P. N. and M. R. Palmer (2000). "Atmospheric carbon dioxide concentrations over the past 60 million years." Nature **406**(6797): 695-699.

Petit, J. R., J. Jouzel, D. Raynaud, N. I. Barkov, J. M. Barnola, I. Basile, M. Bender, J. Chappellaz, M. Davis, G. Delaygue, M. Delmotte, V. M. Kotlyakov, M. Legrand, V. Y. Lipenkov, C. Lorius, L. Pepin, C. Ritz, E. Saltzman and M. Stievenard (1999). "Climate and atmospheric history of the past 420,000 years from the Vostok ice core, antarctica." Nature **399**(6735): 429-436.

Prentice, I. C., G. D. Farquhar, M. J. R. Fasham, M. L. Goulden, M. Heimann, V. J. Jaramillo, H. S. Kheshgi, C. Le Quéré, R. J. Scholes, D. W. R. Wallace, J. T. Houghton, Y. Ding, D. J. Griggs, M. Noguer, P. J. Van Der Linden, X. Dai, K. Maskell and C. A. Johnson (2001). "The carbon cycle and atmospheric carbon dioxide." Climate change 2001: The Scientific Basis. J. T. H. E. Al. Cambridge**:** 183-237.

Putt, M. and B. B. Prezelin (1985). "Observations of diel patterns of photosynthesis in cyanobacteria and nanoplankton in the Santa Barbara channel during el-nino." Journal of Plankton Research **7**(6): 779-790.

Ramaswany, V., O. Boucher, J. Haigh, D. Hauglustaine, J. M. Haywood, G. Myhre, T. Nakajima, G. Y. Shi and S. Solomon (2001). "Radiative forcing of climate change." Climate Change 2001: The scientific Basis. H. J.T. and E. Al. Cambridge, Cambridge University Press**:** 349-416.

Raven, J. A. and J. Beardall (1981). "Respiration and photo-respiration." Canadian Bulletin of Fisheries and Aquatic Sciences (210): 55-82.

Raven, J. A. and R. J. Geider (1988). "Temperature and algal growth." New Phytologist

110(4): 441-461.

Rivkin, R. B. and M. Putt (1987). "Photosynthesis and cell division by Antarctic microalgae: Comparison of benthic, planktonic and ice algae." Journal of Phycology **23**: 223-229.

Ryther, J. H. (1954). "The ratio of photosynthesis to respiration in marine plankton algae and its effect upon the measurement of productivity." Deep Sea Research **2**(2): 134-139.

Sabine, C. L., R. A. Feely, N. Gruber, R. M. Key, K. Lee, J. L. Bullister, R. Wanninkhof, C. S. Wong, D. W. R. Wallace, B. Tilbrook, F. J. Millero, T.-H. Peng, A. Kozyr, T. Ono and A. F. Rios (2004). "The oceanic sink for anthropogenic CO_2." Science **305**(5682): 367-371.

Sailley, S. F., M. Vogt, S. C. Doney, M. N. Aita and L. Bopp (2013). "Comparing food web structures and dynamics across a suite of global marine ecosystem models." Ecological Modelling **261**: 43-57.

Sakshaug, E. and O. Holm-Hansen (1977). "Chemical composition of *Skeletonema costatum* (grev.) cleve and *Pavlova* (*monochrysis*) *lutheri* (droop) green as a function of nitrate-, phosphate-, and iron-limited growth." Journal of Experimental Marine Biology and Ecology **29**(1): 1-34.

Sakshaug, E. and K. Andresen (1986). "Effect of light regime upon growth-rate and chemical composition of a clone of *Skeletonema costatum* from the Trondheim's fjord, Norway." Journal of Plankton Research **8**(4): 619-637.

Sakshaug, E. and K. Andreden (1989). "A steady state description of growth and light absorption in the marine planktonic diatom *Skeletonema costatum*." Limnology and Oceanography **34**(1): 7.

Sakshaug, E., G. Johnsen, K. Andresen and M. Vernet (1991). "Modeling of light-dependent algal photosynthesis and growth - experiments with the Barents sea diatoms *Thalassiosira nordenskioeldii* and *Chaetoceros furcellatus*." Deep Sea Research Part I: Oceanographic Research Papers **38**(4): 415-430.

Sarthou, G., K. R. Timmermans, S. Blain and P. Treguer (2005). "Growth physiology and fate of diatoms in the ocean: A review." Journal of Sea Research **53**(1-2): 25-42.

Sarthou, G., E. Bucciarelli, F. Chever, S. P. Hansard, M. Gonzalez-Davila, J. M. Santana-Casiano, F. Planchon and S. Speich (2011). "Labile Fe(II) concentrations in the Atlantic sector of the Southern Ocean along a transect from the subtropical domain to the Weddell Sea Gyre." Biogeosciences **8**(9): 2461-2479.

Schlitzer, R. (2004). "Export production in the equatorial and north pacific derived from dissolved oxygen, nutrient and carbon data." Journal of Oceanography **60**(1): 53-62.

Schoemann, V., S. Becquevort, J. Stefels, V. Rousseau and C. E. Lancelot (2005). "*Phaeocystis* blooms in the global ocean and their controlling mechanisms: A review." Journal of Sea Research **53**(1): 43-66.

Schone (1982). "The influence of light and temperature on the growth rates of six phytoplankton species from the upwelling area off northwest Africa." Rapport Proces-verbal de la Réunion Cons. int. Explor. Mer. **180**: 246-253.

Sinha, B, E. T. Buitenhuis, C. Le Quéré and T. R. Anderson (2010). "Comparison of the emergent behaviour of a complex ecosystem model in two ocean general circulation models." Progress in Oceanography **84**: 204-224.

Smayda, T. J. (1969). "Experimental observations on influence of temperature, light, and salinity on cell division of marine diatom, *Detonula confervacea* (cleve) gran." Journal of Phycology **5**(2): 150.

Smith, E. L. (1936). "Photosynthesis in relation to light and carbon dioxide." Proceedings of the National Academy of Sciences **22**: 504-511.

Smith, H. J., H. Fischer, M. Wahlen, D. Mastroianni and B. Deck (1999). "Dual modes of the carbon cycle since the last glacial maximum." Nature **400**(6741): 248-250.

Soto, K. C. G., M. Zahr and J. Kuznar (2005). "Simultaneous enumeration of *Phaeodactylum tricornutum* (mlb292) and bacteria growing in mixed communities." Investigaciones Marinas **33**(2).

Sournia, A., M. Chretiennotdinet and M. Ricard (2001). "Marine-phytoplankton - how many species in the world ocean." Journal of Plankton Research **13**(5): 1093-1099.

Strzepek, R. F. and P. J. Harrison (2004). "Photosynthetic architecture differs in coastal and oceanic diatoms." Nature **431**(7009): 689-692.

Sunda, W. G. and S. A. Huntsman (1995). "Iron uptake and growth limitation in oceanic and coastal phytoplankton." Marine Chemistry **50**(1-4): 189-206.

Sunda, W. G. and S. A. Huntsman (1997). "Interrelated influence of iron, light and cell size on marine phytoplankton growth." Nature **390**(6658): 389-392.

Suzuki, Y. and M. Takahashi (1995). "Growth responses of several diatom species isolated from various environments to temperature." Journal of Phycology **31**: 880-888.

Swale, E. M. F. (1963). "Notes on *Stephanodiscus hantzschii* grun. In culture." Archiv Fur Mikrobiologie **45**(2): 210.

Terry, K. L., J. Hirata and E. A. Laws (1983). "Light-limited growth of two strains of the marine diatom *Phaeodactylum tricornutum* bohlin: Chemical composition, carbon partitioning and the diel periodicity of physiological processes." Journal of Experimental Marine Biology and Ecology **68**(3): 209-227.

Thomas, W. H. (1966). "Effects of temperature and illuminance on cell division rates of three species of tropical oceanic phytoplankton." Journal of Phycology **2**: 17-22.

Thompson, P. A., M.-X. Guo and P. J. Harrison (1992). "Effects of variation in temperature .I. On the biochemical composition of eight species of marine phytoplankton." Journal of Phycology **28**(4): 481-488.

Thompson, P. A. (1999). "The response of growth and biochemical composition to variations in day length, temperature and irradiance in the marine diatom *Thalassiosira pseudonana* (bacillariophyceae)." Journal of Phycology **35**(6): 1215-1223.

Timmermans, K. R., B. Van Der Wagt, M. J. W. Veldhuis, A. Maatman and H. J. W. De Baar (2005). "Physiological responses of three species of marine pico-phytoplankton to ammonium, phosphate, iron and light limitation." Journal of Sea Research **53**(1-2): 109-120.

Toseland, A., S. J. Daines, J. R. Clark, A. Kirkham, J. Strauss, C. Uhlig, T. M. Lenton, K. Valentin, G. A. Pearson, V. Moulton and T. Mock (2013). "The impact of temperature on marine phytoplankton resource allocation and metabolism." Nature Climate Change **3**: 979-984.

Tréguer, P., D. M. Nelson, A. J. Van Bennekom, D. J. Demaster, A. Leynaert and B. Queguiner (1995). "The silica balance in the world ocean: A re-estimate." Science

268(5209): 375-379.

Tréguer, P. and C. L. De La Rocha (2013). "The world ocean silica cycle." Annual Review of Marine Science **5**(1): 477-501.

Tyrrell, T. (1999). "The relative influences of nitrogen and phosphorus on oceanic primary production." Nature.

Uitz, J., H. Claustre, A. Morel and S. B. Hooker (2006). "Vertical distribution of phytoplankton communities in open ocean: An assessment based on surface chlorophyll." Journal of Geophysical Research - Oceans **111**(C8).

Uitz, J., H. Claustre, B. Gentili and D. Stramski (2010). "Phytoplankton class-specific primary production in the world's oceans: Seasonal and interannual variability from satellite observations." Global Biogeochemical Cycles **24**(3).

Van De Poll, W. H., M. A. Van Leeuwe, J. Roggeveld and A. G. J. Buma (2005). "Nutrient limitation and high irradiance acclimation reduce par and UV-induced viability loss in the Antarctic diatom *Chaetoceros brevis* (bacillariophyceae)." Journal of Phycology **41**: 840-850.

Van Den Berg, A. J., H. Ridderinkhof, R. Riegman, P. Ruardij and H. Lenhart (1996). "Influence of variability in water transport on phytoplankton biomass and composition in the southern north sea: A modelling approach (fyfy)." Continental Shelf Research **16**(7): 907-931.

Verity, P. G. (1982). "Effects of temperature, iradiance and daylenght on the marine diatoms *Leptocylindrus danicus* cleve. IV. Growth." Journal of Experimental Marine Biology and Ecology **60**: 209-222.

Vernon, L. P. (1960). "Spectrophotometric determination of chlorophylls and pheophytins in plant extracts." Analytical Chemistry **32**(9): 1144-1150.

Webb, W., M. Newton and D. Starr (1974). "Carbon dioxide exchange of *Alnus rubra*: A mathematical model." Oecologia **17**(4): 281-291.

Yoder, J. A. (1979). "Effect of temperature on light-limited growth and chemical composition of *Skeletonema costatum* (bacillariophyceae)." Journal of Phycology **15**: 362-370.

Web sites:

Energy Information Administration, U. S: http://www.eia.gov

CO_2Now: http://co2now.org

Study of the optimal growth temperature of four diatom species

Phaeodactylum tricornutum CCMP 632 and *Thalassiosira pseudonana* CCMP 1335 were obtained from the Provasoli culture centre (USA) *several years ago*. According to Provasoli culture centre, both range from 11 to 16°C. Both stock cultures are maintained in f/2 medium at 15°C.

Sub-cultures of polar diatoms *Chaetoceros brevis* and *Thalassiosira antarctica* were given by Klaas Timmermans (NIOZ, Netherlands). They are maintained in f/2 medium at 4°C.

In order to determinate the optimal growth temperature of the four species, at which we aim to grow them later on during photosynthesis experiments, we cultivated them in a temperature-gradient bar.

Materials and Methods

Temperature-gradient bar

The purpose-built temperature-gradient bar is a block of steel hollowed with 5 rows of 13 spaces for 25mm-diameter culture tubes. A water-cooling circulation at one extremity and a heating resistance at the other create a gradient of temperature along the rows. Light is provided from the bottom of the holes, each tube being lighted by seven white LEDs. Five dimmable voltmeters allow the control of the LEDs intensity of each row. This experiment was the first one since the apparatus was built.

Diatoms are grown in natural seawater enriched to f/2 concentrations, in 25 mm-diameter culture tubes. The light intensity in every row is 500 µmol photon. m^{-2}. sec^{-1}. First, cells are grown at the stock culture temperature of 15°C. After three to five days, cells are gradually transferred to lower and higher temperatures, until filling all the temperature gradient. For each temperature, cells are maintained in exponential growth through successive dilution every three or four days. Growth rates are calculated from daily fluorescence, measured directly in the culture tube (Turner, model 10-AU, kit 10-037R).

Use of fluorometry to calculate the growth rate.

Previous experiments were done on *C. brevis* to compare growth rate values obtained by different methods. Growth in duplicate cultures was followed during six days by fluorometry (Turner, model 10-AU, kit 10-037R) and by counting with a Coulter counter. The experiment

was repeated once. Comparison of cell density and absorbance shows a linearity when the absorbance is between 3 and 19, which corresponds in this experiment to a density of 45000 and 351000 cells/ml, respectively. Within this range, the difference in growth rates obtained by both methods is up to 3%.

Results

For *Phaeodactylum tricornutum*, the optimal temperature is between 16 and 20.5°C (Fig.A.1).

The temperature-gradient bar broke down after four weeks of experiments. Condensation caused by the cooling damaged the LEDs.

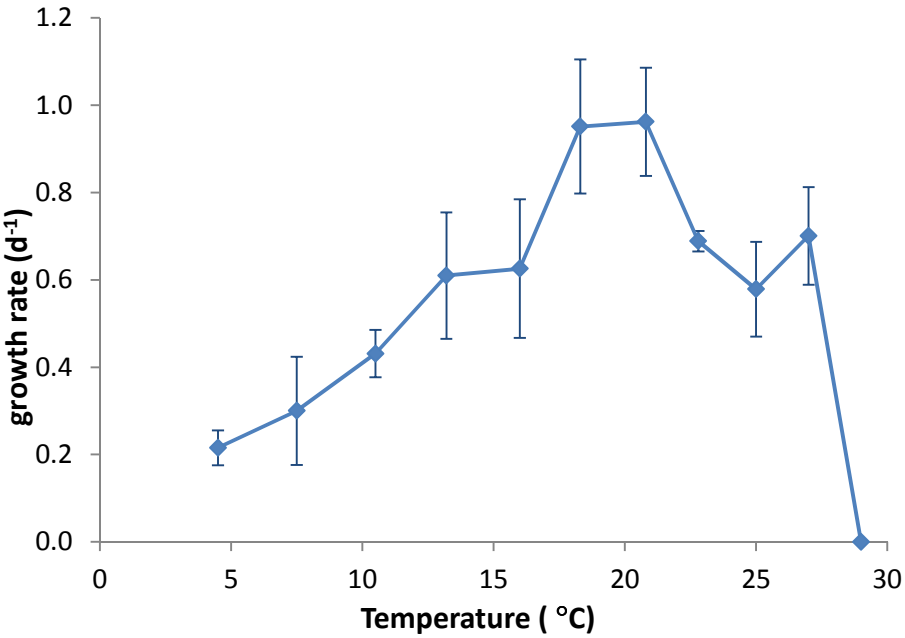

Fig. A.1. Growth rate of *Phaeodactylum tricornutum* at different temperatures. Errors bars represent standard deviation between growth rates of successive cultures.

For the cultures of *Thalassiosira pseudonana*, lights stopped working soon after the beginning of the experiment. As a consequence, we don't have any data for *T.pseudonana* growth rates.

According to our results, *C. brevis* grows well between 4.5 and 10.5°C (Fig.A.2), whereas *T. Antarctica* grows at its best rate at 7.5 and 10.5°C (Fig.A.3). Nevertheless, these data should be used carefully. Effectively, we cannot guaranty the light intensity was constant over time.

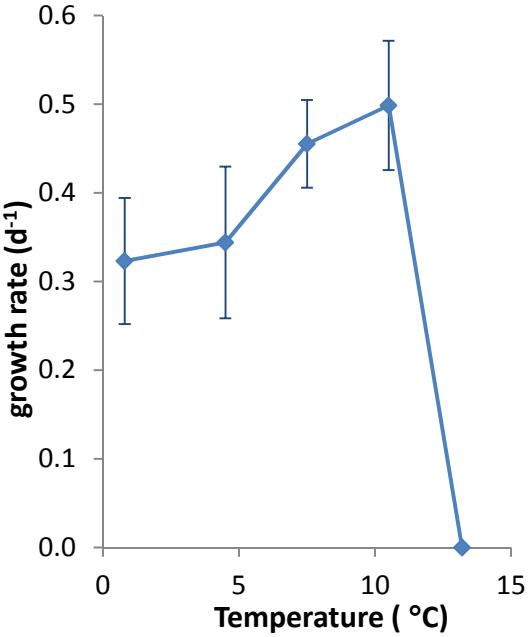

Fig. A.2. Growth rate of *Chaetoceros brevis* at different temperatures. Errors bars represent standard deviation between growth rates of successive cultures.

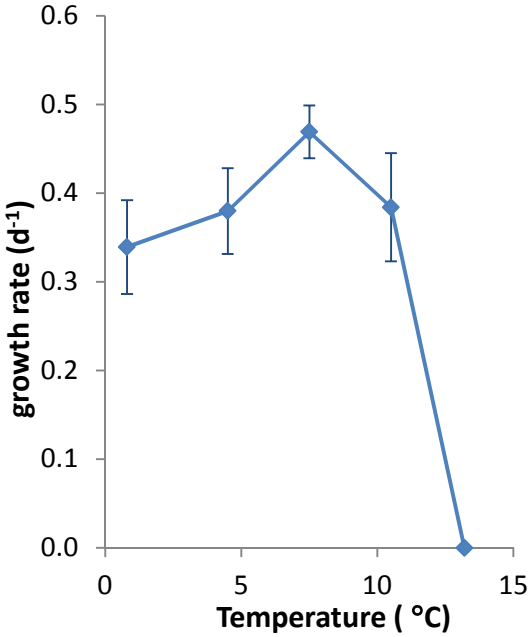

Fig. A.3. Growth rate of *Thalassiosira antarctica* at different temperatures. Errors bars represent standard deviation between growth rates of successive cultures.

Conclusion

The choice of the experimental temperature was a trade-off between the optimal growth temperature and temperatures of the laboratory's available incubators. The incubators' temperatures in the laboratory were 15, 17 and 22°C. We decided to grow the temperate species at 17°C.

The cold-room available to our research group was already set up at 4°C. As other researchers used it, a change in temperature would have disrupted several experiments. Moreover, although the optimal growth temperature of *C. brevis* and *T. Antarctica* may approach 10°C, the maximum temperature of polar waters is closer to 4°C. Therefore experiments at 4°C will be more representative of the field conditions.

Model optimization of the parameters

The photosynthesis is represented in PlankTOM5.3 by an iron-light-colimitation model (Buitenhuis and Geider, 2010). In this model, Fe:C and Chl:C ratio vary as a function of the light intensity and iron availability. Parameters of photosynthesis and iron uptake and the maximal growth rate function define the model. In Buitenhuis and Geider (2010), parameters were optimized using experimental values and a cost-function minimization. One of the outcomes of this paper is the lack of experimental data to both calibrate and validate the model.

In the present study we use the results from our light acclimation experiments (chapter 3) to optimize the model parameters. The obtained values will be compared to the parameter values measured during the PI curve experiments.

The calibration method is as in Buitenhuis and Geider (2010) except for a change in the cost function to: $CF=\Sigma$ (log (model - observation)^2). As our study did not take into account the iron concentration, parameters of iron uptake and iron cellular ratio were not optimized. The parameters optimized were then only those which did not involve iron concentration or growth in iron-limited conditions:

α^{Chl}_m light-limited photosynthetic rate

θ_m maximum chlorophyll: carbon ratio

μ_m maximum growth rate

The following independent variables were required to calibrate the model:

I acclimation light intensity

θ Chl:C ratio

μ growth rate

Therefore, we entered data on growth rate and Chl:C ratio obtained at different light intensity for the four diatoms. One calibration of the model was made for each species.

Parameter values estimated from the PI curves and those optimized by the model are presented in Fig.D, for the four species.

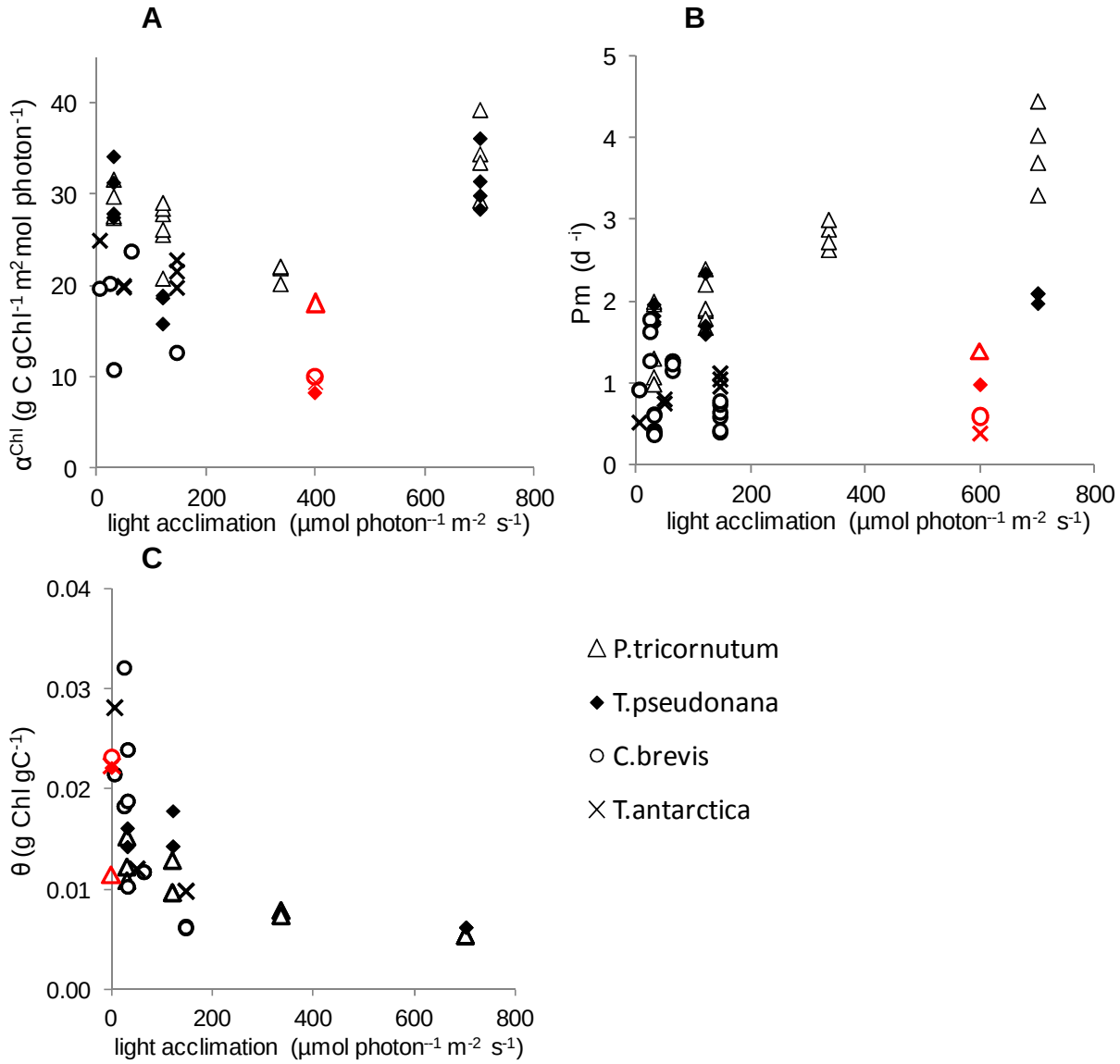

Fig. B.1: Parameters calculated from the PI curves (black symbols) and optimized by the model (red symbols) for *P.tricornutum* (triangles), *T.pseudonana* (diamonds), *C.brevis* (circles) and *T.antarctica* (crosses), A) α^{Chl}, B) P_m, C) θ and θ_m.

Since the method of fitting the model parameters to the independent variables is based on the steady-state solution to the photosynthesis model and does not use the oxygen evolution rates of the PI curve experiments, it serves as an alternative check of the photosynthetic parameter values. The two methods are not entirely independent, since the same measurements of Chl and C were used in both approaches.

The figure B.2 represents the optimised parameters α^{Chl} as a function of θ_m for the four species experimented here and for other diatoms cited by Buitenhuis & Geider (2010) (Fig.2 in Buitenhuis & Geider, 2010).

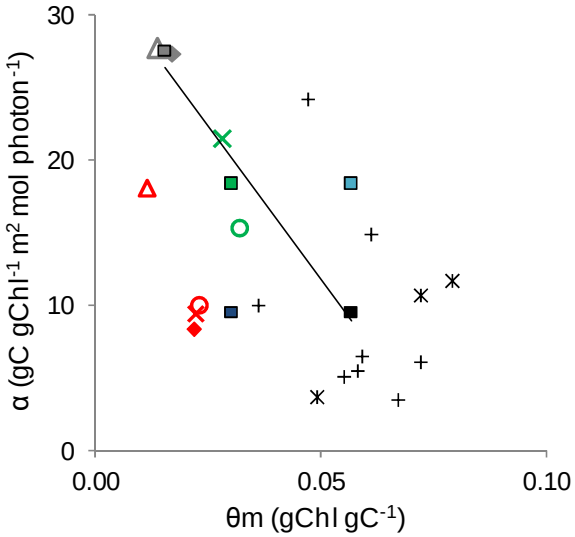

Fig. B.2: Light-limited photosynthetic rate as a function of the maximal Chl:C ratio, from PI curve experiments described in chapter 3 (symbols as in Fig.B.1; polar species, green; temperate species, grey), optimisation (red, symbols as in Fig.B.1), data compiled in Geider (1997) (black crosses) or optimisation (Buitenhuis and Geider, 2010; black asterisk); Green and grey squares represent average for polar and temperate species, respectively; Squares represent parameters used in PlankTOM5.3 (chapter 4): OPT, black; Alp, light-blue; Tht, blue; AT1, green; AT2, grey; line, regression line between black, green and grey squares.

Our experimental data widens the range of diatom photosynthesis parameters. The outputs of the optimisation are similar for the species *T.pseudonana*, *C.brevis* and *T.antarctica* (Fig.B.1). Optimised values for θ_m are close to our measurements (Fig.B.1.C). However, values for α^{Chl} and P_m are lower.